

## Graphene and related two-dimensional materials: Structure-property relationships for electronics and optoelectronics

Xinming Li,<sup>1,a),b)</sup> Li Tao,<sup>1,b)</sup> Zefeng Chen,<sup>1,b)</sup> Hui Fang,<sup>2</sup> Xuesong Li,<sup>3</sup> Xinran Wang,<sup>4</sup> Jian-Bin Xu,<sup>1,a)</sup> and Hongwei Zhu<sup>5,a)</sup>

<sup>1</sup>Department of Electronic Engineering, The Chinese University of Hong Kong, Hong Kong, China

<sup>2</sup>Department of Electrical and Computer Engineering, Northeastern University, Boston, Massachusetts 02115, USA

<sup>3</sup>State Key Laboratory of Electronic Thin Films and Integrated Devices and School of Microelectronics and Solid State Electronics, University of Electronic Science and Technology of China, Chengdu 610054, China

<sup>4</sup>National Laboratory of Solid State Microstructures, School of Electronic Science and Engineering, and Collaborative Innovation Center of Advanced Microstructures, Nanjing University, Nanjing 210093, China

<sup>5</sup>State Key Laboratory of New Ceramics and Fine Processing, School of Materials Science and Engineering, Tsinghua University, Beijing 100084, China

(Received 20 December 2016; accepted 3 May 2017; published online 6 June 2017)

The exfoliation and identification of the two-dimensional (2D) single atomic layer of carbon have opened the opportunity to explore graphene and related 2D materials due to their unique properties. 2D materials are regarded as one of the most exciting solutions for next generation electronics and optoelectronics in the technological evolution of semiconductor technology. In this review, we focus on the core concept of “structure-property relationships” to explain the state-of-the-art of 2D materials and summarize the unique electrical and light-matter interaction properties in 2D materials. Based on this, we discuss and analyze the structural properties of 2D materials, such as defects and dopants, the number of layers, composition, phase, strain, and other structural characteristics, which could significantly alter the properties of 2D materials and hence affect the performance of semiconductor devices. In particular, the building blocks principles and potential electronic and optoelectronic applications based on 2D materials are explained and illustrated. Indeed, 2D materials and related heterostructures offer the promise for challenging the existing technologies and providing the chance to have social impact. More efforts are expected to propel this exciting field forward. Published by AIP Publishing. [<http://dx.doi.org/10.1063/1.4983646>]

### TABLE OF CONTENTS

I. INTRODUCTION .....	2
A. Two-dimensional (2D) material family .....	2
B. 2D material tetrahedron .....	3
II. ELECTRONIC AND OPTICAL PROPERTIES ..	3
A. Electronic properties of graphene.....	3
1. Band structure .....	4
2. Electron optics .....	4
3. Electron transport .....	4
B. Light-matter interactions in graphene .....	5
C. Graphene plasmons .....	7
D. 2D semiconductors .....	7
1. Electronic properties .....	7
2. Optical properties .....	8
E. <i>h</i> -BN .....	9

III. SYNTHESIS AND PROCESSING .....	9
A. Top-down .....	9
B. Bottom-up .....	10
C. Transfer and assembly .....	11
IV. STRUCTURAL MODIFICATIONS .....	11
A. Defects .....	11
1. Point defects .....	11
2. Line defects .....	12
B. Dopants .....	13
1. Substitutional doping .....	13
2. Surface doping .....	14
C. Alloying .....	14
D. Phase transition .....	15
E. Number of layers .....	15
F. Strain .....	16
G. Corrugations .....	18
V. BUILDING BLOCKS .....	18
A. Schottky junction .....	19
1. Graphene-semiconductor contacts .....	19
2. Metal-2D semiconductor contacts .....	19
B. p-n junction .....	20
1. 2D-3D semiconductor heterostructures ..	20

<sup>a)</sup>Authors to whom correspondence should be addressed: xmli1015@gmail.com; jbxu@ee.cuhk.edu.hk; and hongweizhu@tsinghua.edu.cn

<sup>b)</sup>X. M. Li, L. Tao, and Z. F. Chen contributed equally to this work.

2. 2D-2D semiconductor vertical heterostructures .....	20
3. 2D-2D semiconductor lateral heterostructures .....	21
4. Homostructures .....	21
VI. DEVICES AND APPLICATIONS.....	22
A. Field effect transistors .....	22
B. Photodetectors .....	22
C. Photovoltaic devices .....	23
D. Light emission devices.....	24
E. Electro-optic modulators .....	24
VII. OUTLOOK: LEARN FROM THE HISTORY..	25

## I. INTRODUCTION

### A. Two-dimensional (2D) material family

Two-dimensional (2D) materials, normally referred to as the single layer materials, have become a central topic of research interest since the exfoliation of graphene in 2004.<sup>1</sup> In stark contrast to their bulk counterpart, what is more fascinating about 2D materials is the ultra-high specific surface areas which enables their energy band structures sensitive to external perturbations and matter. This all-surface nature of 2D materials makes them competitive for devices as described by Herbert Kroemer “The interface is the device.”<sup>2</sup> Research on 2D material based devices not only has contributed to the deeper understanding of the physics of these novel layered materials but also has provided a great platform for the potential opportunities in many fields ranging from electronics, optoelectronics to energy and sensing applications.

In 1959, Richard Feynman gave an inspiring and influential lecture entitled “There’s Plenty of Room at the Bottom.”<sup>3</sup> In his talk, Feynman envisioned a scientific breakthrough in the field of physics with his questions “What could we do with layered structures with just the right layers? What would the properties of materials be if we could really arrange the atoms the way we want them?” Feynman’s questions challenge scientists to manipulate and control things on the atomic scale. It was not until 2004, 45 years later, that the University of Manchester physicists Andre K. Geim, Konstantin S. Novoselov, and collaborators experimentally exfoliated and identified graphene, a 2D single atomic layer of carbon.<sup>1</sup> The history of research on graphene, however, can be traced back much further. As early as 1947, Philip Wallace calculated the band structure of this one-atom-thick crystal.<sup>4</sup> 15 years later, Hanns-Peter Boehm synthesized graphene flakes through reductions of graphene oxide (GO) dispersions.<sup>5</sup> Then, materials scientists tried to produce this one-layer graphite with exfoliation methods or thin-film growth technologies.<sup>6–8</sup> Indeed, “graphene” or “graphene layer” was officially defined to introduce this single atomic carbon layer of graphite structure by the International Union of Pure and Applied Chemistry in 1995.<sup>9</sup> Based on the earlier studies of ultrathin graphite, along with the rise of other carbon nanomaterials (such as fullerene and carbon nanotubes),<sup>10–12</sup> scientists and engineers devoted more interests and energies into this new fascinating material

to discover its remarkable science and potential for practical applications.

Graphene, with zero band-gap semimetal behavior, normally results in a low current on/off ratio in graphene-based field effect transistors (FETs). In recent years, various 2D materials beyond graphene have attracted considerable attention to the research community, including insulators [e.g., hexagonal boron nitride (*h*-BN) and transition metal oxides], topological insulators (e.g.,  $\text{Bi}_2\text{Te}_3$ ), semiconductors [e.g.,  $\text{MoS}_2$ ,  $\text{WSe}_2$ , and black phosphorus (BP)], metals (e.g.,  $\text{TiS}_2$ ), superconductors (e.g.,  $\text{NbSe}_2$ ), and charge density waves (e.g.,  $1\text{T-TaS}_2$  at low temperatures) (Fig. 1). With such rich choices and high tunability in 2D materials, next-generation devices with specific functions can be developed. Particularly, the weak van der Waals (vdW) interaction (as compared to the strong covalent bond interaction inside covalently bonded material structures) was made it possible to construct promising building blocks for future electronics and optoelectronics by stacking 2D materials with multi-dimensional materials to form van der Waals heterostructures (vdWHs).<sup>13–18</sup>

In general, the up-to-date 2D material family can be categorized into five types: (1) graphene with single-layer atoms arranging in hexagonal honeycomb lattices, its analogs, and elemental 2D materials, such as borophene, silicene, germanene, stanene, *h*-BN, and BP; (2) 2D Metal chalcogenides, such as three-atom-thick transitional metal dichalcogenides (TMDs) with a general stoichiometry formula  $\text{MX}_2$  (where M represents the transition metal: Mo, W, Ti, Nb, Re, Pt, etc., and X represents chalcogen elements: S, Se, or Te), III–VI and IV–VI families ( $\text{GaSe}$ ,  $\text{InSe}$ ,  $\text{GeSe}$ ,  $\text{SnS}$ ,  $\text{SnSe}$ ,  $\text{SnS}_2$ ,  $\text{SnSe}_2$ , etc.), and some others ( $\text{Bi}_2\text{Te}_3$ , etc.); (3) 2D transition metal carbides and/or nitrides (MXenes), a general stoichiometry formula  $\text{M}_{n+1}\text{X}_n$  (where M represents the transition metal: Mo, Ti, V, Cr, Nb, etc., X represents C and/or N, and n is 1, 2, or 3) with surface terminated by O, OH, or F atoms;

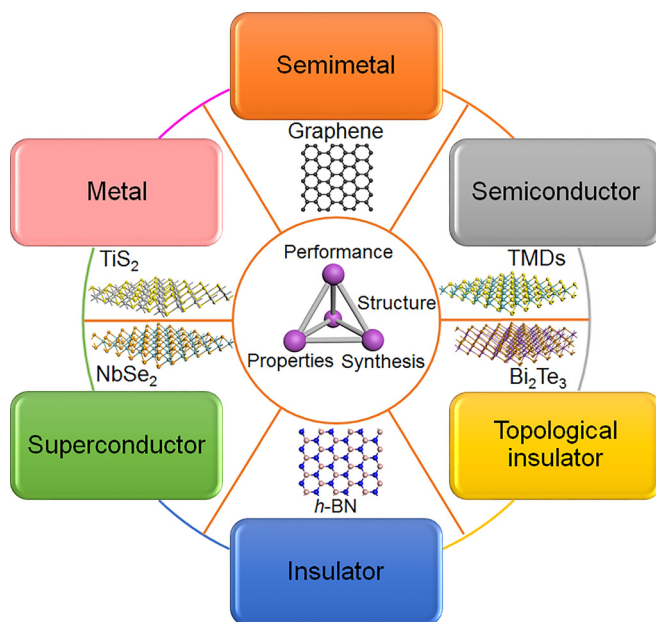


FIG. 1. 2D material family and tetrahedron.

(4) 2D oxides or hydroxides, such as titania nanosheets; (5) 2D organic materials, such as pentacene. Since limited information is known on the electronic and optoelectronic devices based on MXenes and 2D oxides or hydroxides, we do not emphasize on these 2D layered materials in this review. The research on 2D organic materials is also not included in this review due to the difference in the structural characteristics and research methods. Here, we will focus on the electronics and optoelectronics based on graphene, its analogs, and related 2D metal chalcogenides.

## B. 2D material tetrahedron

One important mission of materials science and engineering is to invent, design, develop, and achieve new materials. To materials scientists and engineers, 2D materials are similar to cocktails to a bartender or paintings to an artist. The breakthrough of 2D materials represents a significant moment and has drawn numerous interests in not only experimentally characterizing and understanding these high-crystal-quality and chemically stable materials but also manipulating and controlling these layered crystalline materials and integrating them into current devices and technologies. We herein raise several outstanding issues relevant to 2D materials based on traditional materials science tetrahedron.

- Properties: What are the most promising and novel properties of 2D materials? What are the interactions between them and external perturbations and matter?
- Synthesis and processing: What is the state-of-the-art technology in the synthesis and assembly of 2D materials and related heterostructures? How can we make them

compatible and integrated with the existing technologies and devices?

- Structure: What are the implications of unique structural properties in 2D materials for physical properties? How can one manipulate and control the structure of 2D materials for future electronic and optoelectronic applications?
- Performance: What are the principles of building blocks of 2D material-based devices? How do the contacts of 2D material-based devices function? What is the promise of 2D materials for next generation electronic and optoelectronic applications?

The structure-property relationship is a powerful concept in materials and related fields. In this review, we will summarize the basic structure-property relationships of graphene and related 2D materials and then present their potential applications in electronic and optoelectronic devices, with the aim to shed light on the above questions. With the rapid progress in this field, the answers are certainly prone to evolve as time and remain to be revisited in not-too-distant future.

## II. ELECTRONIC AND OPTICAL PROPERTIES

### A. Electronic properties of graphene

Graphene is made of a  $sp^2$  hybridized hexagonal honeycomb carbon structure with the carbon-carbon distance of  $1.42 \text{ \AA}$ ,<sup>19</sup> as shown in Fig. 2(a). Because of its unique electronic properties, such as zero bandgap, Dirac fermions behavior of its electrons and low density of states, many idiosyncratic physical phenomena were found in graphene. For example, the room temperature quantum Hall effect

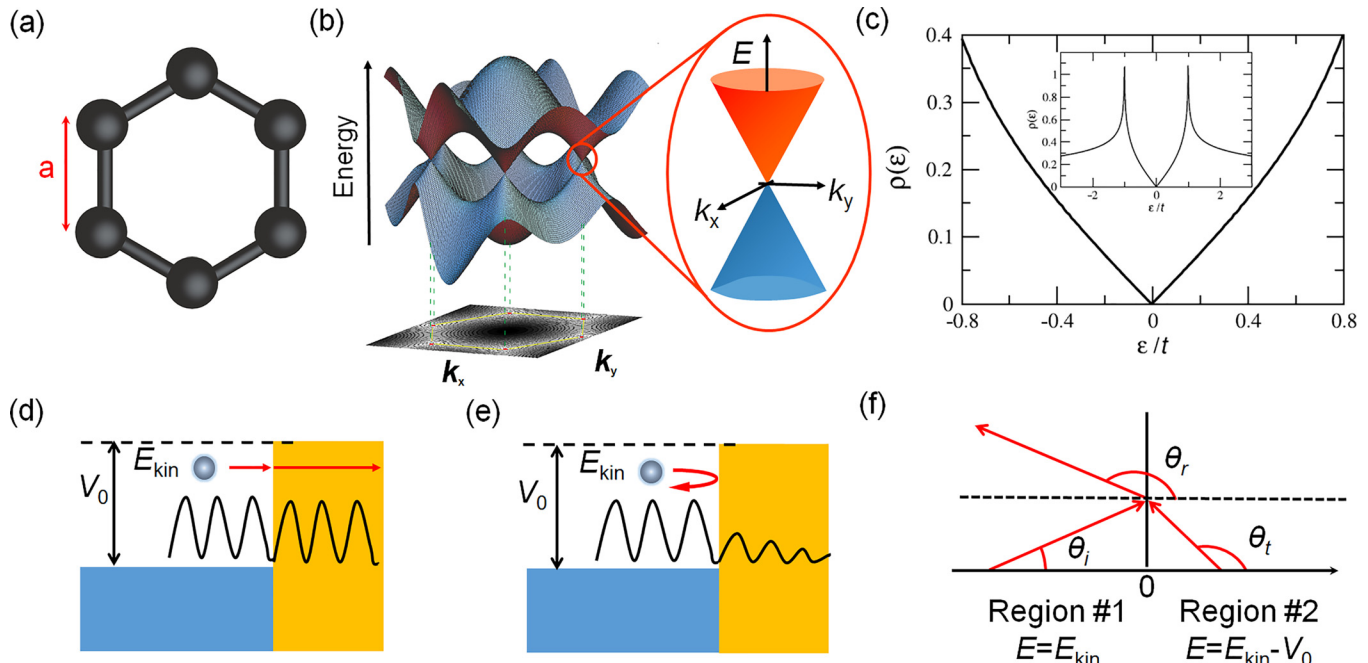


FIG. 2. (a) Honeycomb lattice of graphene. (b) Electronic dispersion in the honeycomb lattice. Left: energy spectrum  $E$  in units of  $t$  for finite values of  $t$  and  $t'$ . Right: zoom in of the energy bands close to one of the Dirac points, which shows cone-shaped valence and conduction bands meeting at the  $K$  points of the Brillouin zone.<sup>18</sup> Redrawn and reprinted with permission from Phys. Today **69**(9), 46 (2016). Copyright 2016 AIP Publishing LLC. (c) The density of states of graphene close to the Dirac point and the inset shows the full electron bandwidth.<sup>21</sup> Reprinted with permission from Sarma *et al.*, Rev. Mod. Phys. **83**, 407 (2011). Copyright 2011 American Physical Society. (d) Relativistic electrons inject into a barrier. (e) Nonrelativistic electrons inject into a barrier. (f) An electron with energy  $E = E_{\text{kin}}$  injects into a square potential step of height  $V_0$ , with an incident angle  $\theta_i$ , reflected angle  $\theta_r$ , and transmitted angle  $\theta_t$ .

observed in graphene originates from the behavior of massless fermions with ultrafast Fermi velocity.<sup>20</sup> Here, important electrical properties of graphene are reviewed.

## 1. Band structure

The band structure of graphene, calculated from a Tight-Binding approach, can be seen as a triangular lattice with a basis of two atoms per unit cell. The derived energy band structure has the following form:<sup>4,19</sup>

$$E_{\pm}(k) = \pm t\sqrt{3+f(k)} - t'f(k), \quad (1)$$

where  $f(k) = 2\cos(\sqrt{3}k_ya) + 4\cos((\sqrt{3}k_ya)/2)\cos((3k_xa)/2)$ , and  $t$  ( $\sim 2.7$  eV) and  $t'$  are the nearest-neighbor hopping energy (hopping between different sublattices) and the next nearest-neighbor hopping energy (hopping in the same sublattice), respectively.<sup>4</sup> The plus sign applies to the upper  $\pi^*$  and the minus sign applies to the lower  $\pi$  band.  $k_x$  and  $k_y$  are the momentum in  $x$  and  $y$  directions. If  $t'=0$ , the energy band structure is symmetric around zero energy. The band structure close to one of the Dirac points is shown at the  $K$  or  $K'$  point in the Brillouin zone [Fig. 2(b)].<sup>18</sup> The first order of the expanding of Eq. (1) is

$$E_{\pm}(k) = \pm v_F|k|, \quad \text{and} \quad v_F = 3at/2, \quad (2)$$

where  $k$  is the relative momentum (to the Dirac points).  $v_F$  is the Fermi velocity with a value of  $10^6$  m/s, which is 1/300 of the velocity of light. It can be seen that around zero energy, the energy  $E(k)$  is linear to the momentum  $k$  and  $v_F$  does not depend on the energy, which is different from the three-dimension system, in which  $E(k) \sim k^2/(2m)$  and  $v \sim k/m \sim \sqrt{2E/m}$ .

The density of states can be driven from the energy dispersion Eq. (1). In particular, near the Dirac point, the density of states in graphene is  $\rho(E) = (2A_c/\pi)(|E|/v_F)$ , where the unit cell area  $A_c = 3\sqrt{3}a^2/2$ . It shows that the density of states is linear to energy, and at the Dirac point, it is zero [Fig. 2(c)].<sup>19,21</sup> However, it is found that graphene's zero-field conductivity does not disappear even if the Fermi level is at the Dirac point. Instead, it exhibits values close to the conductivity quantum  $e^2/h$  per carrier type.<sup>20</sup> The minimum conductivity of graphene is governed not by the physics of the Dirac point singularity but by the carrier-density inhomogeneities induced by the potential of charged impurities.<sup>22,23</sup>

The dispersion relation shows that the conduction band and valence band intersect at Dirac points, which forms a band structure with a zero bandgap. This property makes graphene a promising material for broadband photodetectors, but it can lead to the low on/off ratio of the graphene-based FET.<sup>24</sup> The bandgap of graphene can be opened by three ways: tailoring into one-dimension (nanoribbons),<sup>25,26</sup> biasing bilayer graphene,<sup>27,28</sup> and applying strain to graphene.<sup>29</sup>

## 2. Electron optics

Near the Dirac point, carriers in graphene exhibit quasi-particle behavior of relativistic massless Dirac fermion with a pseudo-spin degree of freedom (chiral nature) originating

from graphene's two carbon sublattices. Because of this property, electrons in graphene with energies higher than  $2mc^2$  (the Dirac energy gap) can travel through the barrier with a probability of near 100% (Klein tunneling)<sup>30,31</sup> but not an exponential damping like non-relativistic electrons tunneling through the barrier [Figs. 2(d) and 2(e)]. As shown in Fig. 2(f), an electron with energy  $E > 0$  incident onto a potential step of height  $V_0$  with an incident angle  $\theta_i$ . We defined two regions:  $x < 0$ , electrons with a kinetic energy of  $E_{kin} = E$ ; and  $x > 0$ , electrons with a kinetic energy of  $E_{kin} = E - V_0$ . Assuming that the angles of reflection and transmission are  $\theta_r$  and  $\theta_t$ , the reflection wavefunction  $r$  and transmission wavefunction  $t$  are expressed as

$$r = -\frac{e^{i\theta_i} - sgn(E - V_0)e^{i\theta_t}}{e^{i\theta_r} - sgn(E - V_0)e^{i\theta_t}} \quad \text{and} \quad t = \frac{e^{i\theta_r} - e^{i\theta_i}}{e^{i\theta_r} - sgn(E - V_0)e^{i\theta_t}}. \quad (3)$$

The relations between  $\theta_r$ ,  $\theta_t$ , and  $\theta_i$  are

$$\theta_r = \pi - \theta_i \quad \text{and} \quad E \sin \theta_i = [sgn(E - V_0)](E - V_0) \sin \theta_t. \quad (4)$$

According to the conservation of one-dimensional current, we have

$$\cos \theta_i + |r|^2 \cos \theta_r = |t|^2 \cos \theta_t. \quad (5)$$

So the transmission probability  $T$  and reflection probability  $R$  are

$$T = \frac{sgn(E - V_0)|t|^2 \cos \theta_t}{\cos \theta_i} \quad \text{and} \quad R = -|r|^2 \frac{\cos \theta_r}{\cos \theta_i}. \quad (6)$$

Combining Eqs. (3) and (6), we can get the transmission and reflection probability of an electron tunneling in graphene. Considering a p-n junction, corresponding to  $0 < E < V_0$  and an electron with normal incidence ( $\theta_i = 0$ ),  $T$  equals 1, which means that the graphene p-n junction cannot block the injection of electrons and the rectifier effect does not exist. This Klein tunneling effect was confirmed using a set of metallic gates capacitively coupled to graphene to modulate the potential landscape.<sup>32</sup> If an electron injects into a p-n junction with incidence angle  $\theta_i \neq 0$ , the electron behavior is ruled by electronic Snell's law, including positive and negative refraction, and lens focusing.<sup>33-35</sup>

## 3. Electron transport

Graphene exhibits remarkable electron mobility at room temperature. According to the unique band structure, electrons in graphene can move with a  $v_F$  in the ballistic transport regime. The mobility of suspended exfoliated graphene is up to about  $200\,000 \text{ cm}^2 \text{ V}^{-1} \text{ s}^{-1}$ ,<sup>36</sup> without considering the charged impurities and ripples. When graphene is placed on the substrate, the carrier transport is limited by the scattering which can be classified into intrinsic and extrinsic scattering sources.<sup>37,38</sup> While the former one mainly includes longitudinal acoustic (LA) phonon scatterings,<sup>39</sup> the lattice defects and grains boundaries formed during the growth process,<sup>40</sup>

the latter one contains charged impurity scattering,<sup>41</sup> interfacial roughness,<sup>42</sup> remote interfacial phonon (RIP) scattering,<sup>37</sup> and wrinkles or cracks introduced during the growth and transfer processes,<sup>43</sup> which will be discussed in Sec. IV.

Recently, it was found, both theoretically and experimentally, that the electron sub-system in a pristine, intrinsic graphene film could behave like a viscous flow, rather than diffusion/drift related transport in conventional solids, due to its strong electron-electron interactions and weak electron-lattice interactions.<sup>44</sup> Such a hydrodynamic transport behavior could give rise to many unusual phenomena, such as the breaking of Wiedemann-Franz law,<sup>45</sup> the observation of negative local resistance due to the electron traveling against the electric field,<sup>46</sup> and so on.

## B. Light-matter interactions in graphene

With a remarkable naturally gapless band structure, graphene can absorb light of the broad spectrum ranging from ultraviolet and visible to infrared and terahertz (THz) spectral region, distinguished from other traditional semiconductors. However, doping always inevitably exists in graphene, which leads to the opening optical bandgap of  $2E_F$ . When graphene is excited by incident light with the photon energy  $\hbar\omega$ , there are two photoexcitation modes: interband transition and intraband transition [Fig. 3(a)].<sup>47,48</sup> If the photon energy  $\hbar\omega$  is higher than  $2E_F$ , one electron can be excited from the valence band to the conduction band and a hole is

left in the valence band, which is named interband transition. If the photon energy  $\hbar\omega$  is lower than  $2E_F$ , interband transition is not allowed and intraband transition dominates.

The light-graphene interaction is commonly described in terms of complex dynamic conductivity  $\sigma = \sigma_r + i\sigma_i = \sigma_{\text{inter}} + \sigma_{\text{intra}}$ . Here,  $\sigma_{\text{inter}}$  and  $\sigma_{\text{intra}}$  are the complex conductivities which are contributed from the interband and intraband transitions. Within the random-phase approximation (RPA),<sup>48–50</sup> the dynamical conductivity of graphene is

$$\sigma = \frac{e^2}{4\hbar} \left[ \theta(\omega - 2E_F/\hbar) - \frac{i}{2\pi} \ln \frac{(\omega + 2E_F/\hbar)^2}{(\omega - 2E_F/\hbar)^2} \right] + \frac{ie^2 k_B T}{\pi\hbar(\omega + i\tau^{-1})} \left[ \frac{E_F}{k_B T} + 2 \ln \left( e^{-\frac{E_F}{k_B T}} + 1 \right) \right]. \quad (7)$$

The first term represents the conductivity due to the interband transition. The step function  $\theta(\omega)$  conveys the condition for a photon exciting an electron from the valence band to the conduction band. The second term represents the intraband transition described by the free electron model or Drude model. For the fermi-Dirac statistics, if  $E_F \gg k_B T$ , the intraband conductivity becomes

$$\sigma_{\text{intra}} = \frac{ie^2 |E_F|}{\pi\hbar(\omega + i\tau^{-1})}. \quad (8)$$

The contribution of the carrier concentration is described by the Fermi energy  $n_0 = (E_F/\hbar v_F)^2/\pi$ . The electron-disorder

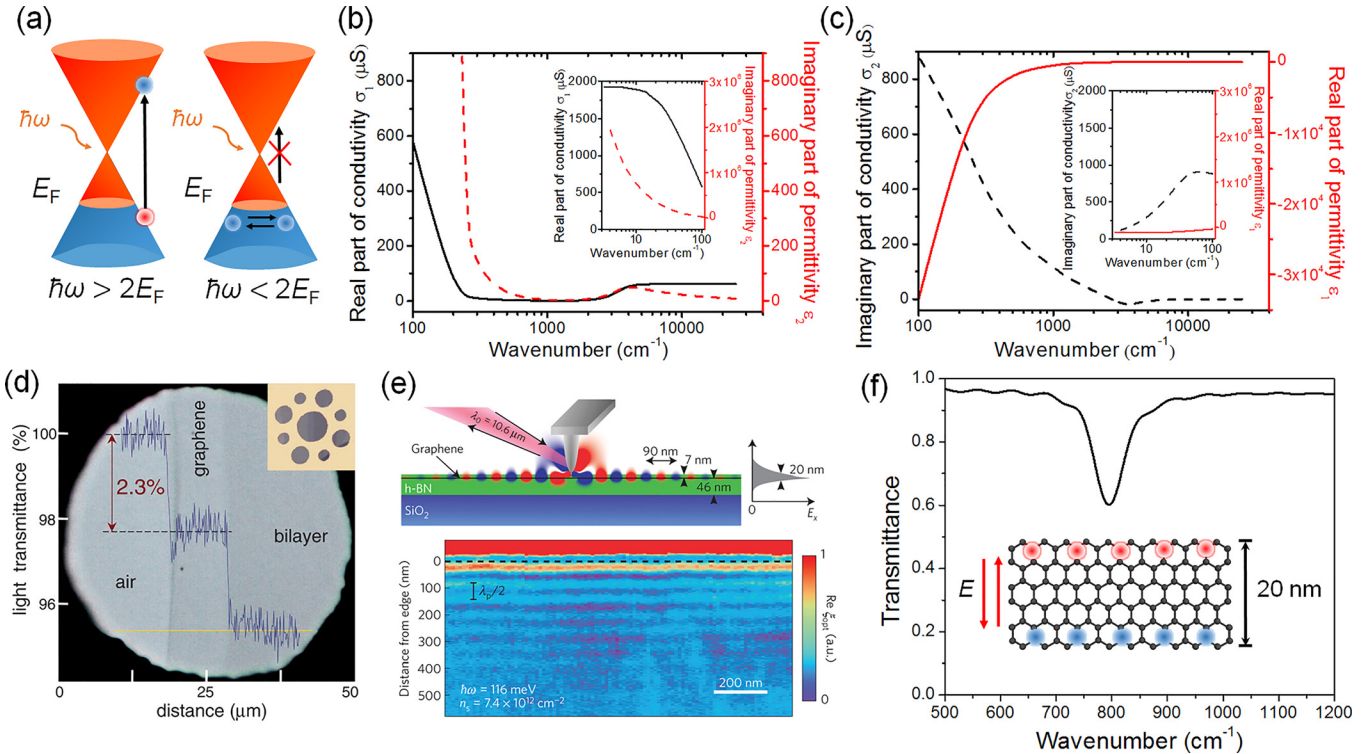


FIG. 3. (a) Interband (left) and intraband (right) transition of electrons in graphene. The real part (b) and the imaginary part (c) of conductivity (black line) and corresponding imaginary part (b) and real part (c) of permittivity (blue dash line) from visible to the far infrared region for graphene; the inset is the THz region. (d) Photograph image of graphene. The line shows the intensity of transmitted white light over graphene.<sup>51</sup> Reprinted with permission from Nair *et al.*, Science **320**, 1308 (2008). Copyright 2008 AAAS. (e) Propagating plasmonic wave excited by far infrared light through tip coupling and the experimental plasmonic wave in graphene.<sup>57</sup> Reprinted with permission from Woessner *et al.*, Nat. Mater. **14**, 421 (2015). Copyright 2015 Macmillan Publishers Limited. (f) Localized plasmonic resonance in nanopatterned graphene.

scattering processes are taken into account by the relaxation time  $\tau$ . The main mechanism of the carrier relaxation is provided by the long range scatterers and gives the collision rate  $\tau^{-1} = ev_F^2/E_F\mu_c$ , where  $\mu_c$  is the carrier mobility of graphene. As the conductivity is known, the permittivity of graphene can be calculated through  $\varepsilon = i\sigma/\omega$ , as well as the refraction index  $n = \sqrt{\varepsilon}$ . The calculated result of dynamic conductivity (real and imaginary part), permittivity of doped graphene, in the wavelength from the visible light region to the terahertz (THz) region, is shown in Figs. 3(b) and 3(c), respectively.

In the high-frequency region, corresponding to the visible and near infrared region, the dynamical conductivity is dominated by loss (real part) due to the interband transition. If the incident photon energy  $\hbar\omega > 2E_F$ , the real part of the first term becomes  $e^2/4\hbar$ , corresponding to a constant light absorption of 2.3% [Fig. 3(d)].<sup>51</sup> Normally, graphene is p-type doped with Fermi energy  $E_F$  around 0.3 eV.<sup>20</sup> Therefore, if the incident photon energy is higher than 0.6 eV, corresponding to the wavelength shorter than 2000 nm, the light will be absorbed due to interband transition [Fig. 3(b)]. By tuning the Fermi energy of graphene, including electrostatic gating or doping, the light absorption of graphene can be controlled. This property exhibits potential applications in dynamical optical devices, which will be discussed in Sec. VI E.

In the lower frequency region, such as infrared and THz region, the dynamical conductivity is dominated by the intra-band transition, which is described by Drude model. Both the Drude weight  $D = (e^2|E_F|)/\hbar = (v_F e^2 \sqrt{\pi n_0})/\hbar$  and the scattering rate  $\tau^{-1}$  are related to the carrier concentration and can be tuned by electrostatic gating or doping. If  $\omega > \tau^{-1}$ , the imaginary part of conductivity dominates and graphene

exhibits a negative permittivity with ohmic losses, which is ruled by  $\varepsilon = i\sigma/\omega$ . Therefore, it is possible to excite the plasmonic effect in this wavelength region, typically in the far infrared region, which will be shown in Sec. II C. It is worth mentioning that the expression of Drude weight D in graphene is also proportional to the Fermi velocity, which is different from the Drude model in metal (only related to carrier concentration). When  $\omega \ll \tau^{-1}$  (normally, the value of  $\tau^{-1}$  is in the order of  $10^{12}\text{--}10^{13}$  unit),<sup>52,53</sup> the real part of conductivity is much larger than the imaginary part. Therefore, graphene exhibits a metal-like reflection due to the high conductivity in the THz to microwave region.

Because of the atomic thickness of graphene, the strength of the light-matter interaction in graphene is limited. Therefore, photo-active substrates (optical nano/micro structures) are introduced for enhancing the light interaction, such as quantum dots, optical cavities, waveguides, plasmonic nanostructures, and photonic crystals. The strategy is generic and applicable for other 2D materials. In summary, the light-matter interactions of graphene can be divided into four different regions [Figs. 3(b) and 3(c)] and their related applications are summarized in Fig. 4:

- (1) From the visible region to the near infrared region, 2.3% of incident light is absorbed by graphene due to the interband transition.
- (2) In the middle infrared region, graphene becomes more transparent to light due to the suppression of interband transitions because of Pauli state blocking.
- (3) In the far infrared region, graphene can reflect and absorb the incident light. The reflection is because of the imaginary part of conductivity origin from the coupling between free carriers and electromagnetic wave

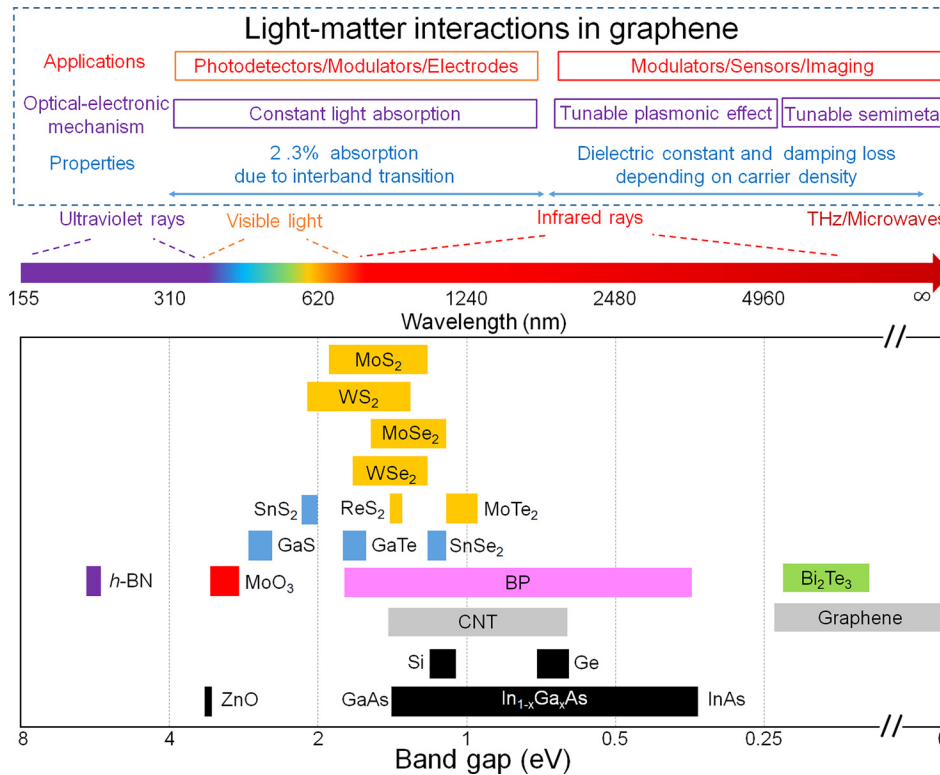


FIG. 4. Electromagnetic spectrum from ultraviolet rays to THz/microwaves and the corresponding light-matter interactions in graphene and the bandgap values for different 2D semiconductors and conventional semiconductors. The bandgap can be tuned over that range by changing the material's structure.

(EMW). The absorption is because of the ohmic loss of free carriers.

- (4) From the THz region to the microwave region, graphene exhibits high reflection like metal because of the high conductivity of graphene.

### C. Graphene plasmons

Plasmons, the collective oscillations of free electrons excited by EMW in noble metals, possess unique properties for photonic technologies. Doped graphene emerges as an alternative, unique 2D plasmonic material which displays a wide range of extraordinary properties.<sup>54–59</sup>

Considering that a doped graphene is surrounded by medias with dielectrics constants of  $\epsilon_1$  and  $\epsilon_2$  and the collective oscillations in graphene are excited by EMW of transverse magnetic (TM) mode, the dispersion relation can be simplified as<sup>50,54</sup>

$$K_{sp} = \epsilon_0 \frac{\epsilon_1 + \epsilon_2}{2} \frac{2i\omega}{\sigma(\omega, q)}, \quad (9)$$

where  $K_{sp}$  is a complex, where the real part represents the propagating plasmonic wave, and the imaginary part represents the decay. The value of  $K_{sp}$  can be retraced to the dynamical conductivity  $\sigma(\omega)$  of graphene. The plasmonic wave can be achieved in the far infrared region [Fig. 3(e)]<sup>57</sup> as the significant imaginary conductivity and relatively small Ohmic loss (real part) [Figs. 3(b) and 3(c)]. Graphene plasmons exhibit some unique properties due to the special energy band structure of graphene: (1) Deep subwavelength effect, which means that the plasmonic wavelength  $\lambda_{sp}$  in graphene is extremely shorter than that in free space  $\lambda_0$ , as shown in function  $\lambda_{sp}/\lambda_0 = (4\alpha/(\epsilon_1 + \epsilon_2))(E_F/\hbar\omega)$ , where  $\alpha$  ( $\approx 1/137$ ) is the fine-structure constant. In the infrared frequency,  $E_F/\hbar\omega$  is on the order of 1, so the localized plasmonic wavelength is two orders smaller than  $\lambda_0$ .<sup>55–57</sup> (2) Long distance in-plane propagation, which means that the graphene plasmonic propagation distance ( $1/(\text{Im}[K_{sp}])$ ) can reach up to 100 plasmonic wavelengths.<sup>55,56</sup> (3) High tunability of the plamonic effect. As the dispersion relation is dependent on the Fermi energy of graphene, the plasmons on graphene can be controlled, e.g., by electrostatic gating, doping, and optical pumping.<sup>55–58</sup>

Localized plasmons in graphene nano/micro patterns can be directly excited by EMW [Fig. 3(f)], which is another kind of plasmonic mode paralleling to the propagating surface plasmon.<sup>60–63</sup> Without considering the interaction of nearby patterns, the localized plasmon frequency for a nano-pattern can be seen as a damped oscillator, and the effective optical conductivity is given by the following functions:<sup>64</sup>

$$\omega_{pl} = \sqrt{\frac{3D}{8\epsilon\epsilon_m d}} \quad \text{and} \quad \sigma(\omega) = i \frac{fD}{\pi} \frac{\omega}{(\omega^2 - \omega_p^2) + i\Gamma\omega}, \quad (10)$$

where  $d$  is the pattern size,  $\epsilon_m$  is the media dielectric constant,  $\epsilon$  is the vacuum permittivity,  $\Gamma$  is the damping frequency  $\tau^{-1}$ , and  $f$  is the fill factor of the graphene area over the total area. Drude weight is proportional to the Fermi

energy of graphene and thus the localized plasmon mode in graphene can be controlled by electrostatic gating or doping.

### D. 2D semiconductors

#### 1. Electronic properties

Apart from semi-metallic graphene, 2D semiconductors with finite bandgaps, such as TMDs, BP, and III–VI layered materials, are particularly interesting for semiconductor physics and devices.

The diversity and variability of band structures of 2D TMDs which cover the range from semiconducting to metallic make this kind of 2D materials a powerful candidate for building functional devices. The band structures of 2D TMDs differ a lot from their bulk crystals. As the material becomes thinner from the bulk to the monolayer, the band structure of TMDs transits from the smaller indirect bandgap one to a larger direct bandgap one due to quantum confinement effects.<sup>65,66</sup> The lattice structure and band structure of monolayer MoS<sub>2</sub> are shown in Figs. 5(a) and 5(b), respectively. Due to the heavy transition metal atoms and the direct-gap band edges associated with *d*-orbital electrons, TMDs have strong spin-orbit coupling (SOC), which greatly differs from graphene.<sup>67,68</sup> The spin degeneracy at the *K* point in the valence band of monolayer TMD is removed by SOC, while the degeneracy at the conduction band is conserved [Fig. 5(b)].<sup>69</sup> The energy splitting of the valence band in monolayer MoS<sub>2</sub> and MoSe<sub>2</sub> is predicted to be 160 and 180 meV, respectively.<sup>67,70</sup> Energy valley is another degree of freedom in 2D TMDs beyond the spin. Two distinguished valleys *K* and *K'* points are presented at alternative corners of the hexagonal Brillouin zone. The inverse symmetry breaking leads to different orbital magnetic moments at *K* and *K'* points, making it possible to achieve valleytronic devices [Fig. 5(c)]. Valley polarization in monolayer MoS<sub>2</sub> can be approached by optical pumping with circularly polarized light, and the consequent valley-based devices can be fabricated.<sup>68,71</sup> The valley degree of freedom can generate an ultrahigh pseudo-magnetic field in monolayer TMDs and lead to the valley quantum Hall effect.<sup>72,73</sup>

BP exhibits narrow bandgaps ranging from 0.3 eV (for bulk) to 1.5 eV (for monolayer) depending on its thickness, which bridges the spectral gap between zero-gap graphene and relatively wide gap TMDs. Moreover, regardless of the number of layers, BP shows an intrinsic direct-gap feature, giving rise to potential applications in light detection and emission in the infrared range.<sup>74</sup> BP shows very strong in-plane anisotropy with two nonequivalent lattice directions: the zigzag one which is parallel to the phosphorus atomic ridge and the armchair one which is perpendicular to the ridge [Fig. 5(a)].<sup>75,76</sup> This unusual anisotropy makes the effective carrier mass of BP highly sensitive to the concerned direction in the momentum space, as shown in Fig. 5(d).<sup>17</sup> The consequent anisotropy electronic properties of BP are investigated with the angular dependence of the conductance.<sup>75</sup> Some other 2D semiconductors, such as ReS<sub>2</sub>, are also reported to have similar anisotropy characteristics.<sup>77,78</sup>

A summary of band alignments of 2D semiconductors is provided in Fig. 5(e).<sup>79</sup> By choosing proper band alignment

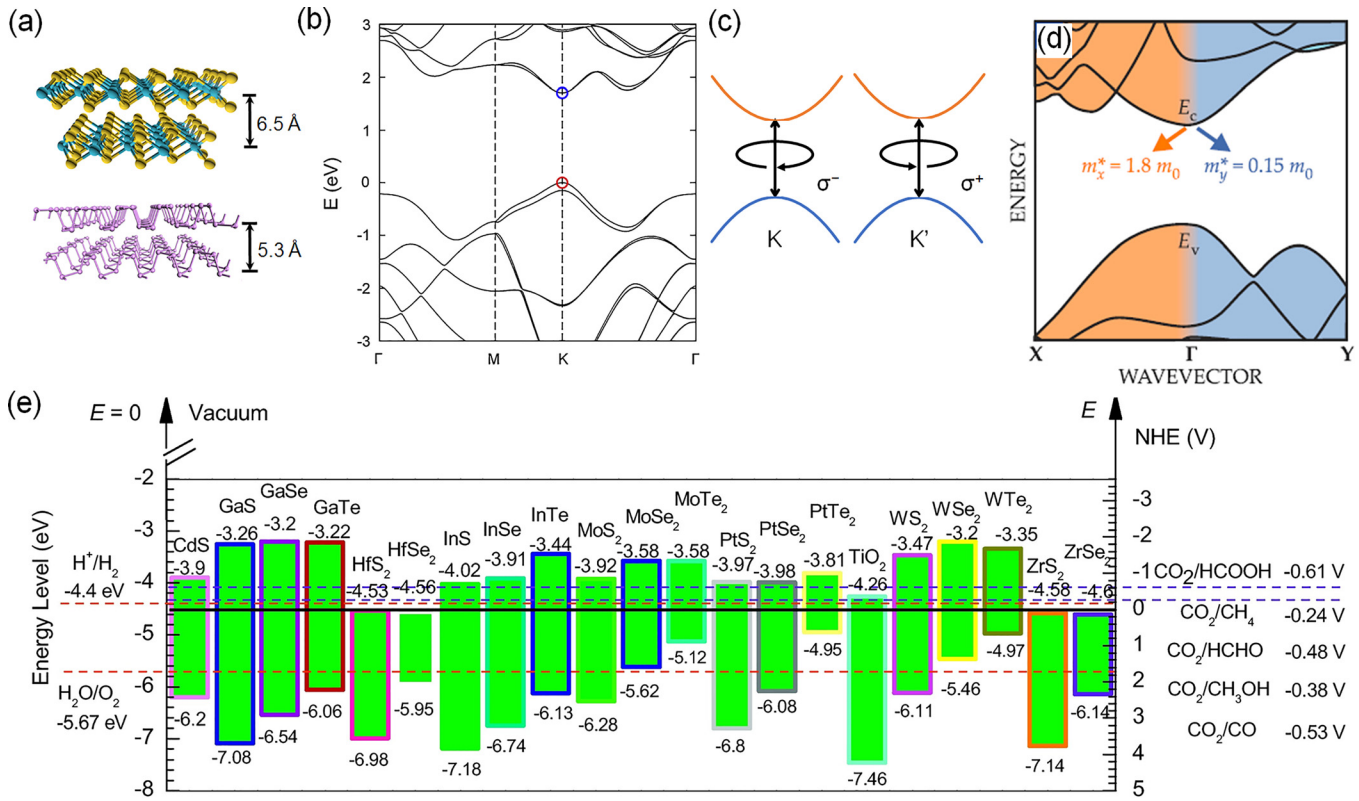


FIG. 5. (a) Lattice structure of MoS<sub>2</sub> and BP. (b) The band structure of monolayer MoS<sub>2</sub> and the valence band edge and conduction band edge are indicated by red and blue circles.<sup>69</sup> Reprinted with permission from Yazyev *et al.*, Mater. Today **18**, 20 (2015). Copyright 2015 Elsevier Ltd. (c) Different orbital magnetic moments at  $K$  and  $K'$  points in MoS<sub>2</sub>, which correspond to the excitation/emission of left and right polarized light, respectively. (d) The anisotropic band structure of BP, the red and blue arrows present the effective mass for the different directions in the momentum space.<sup>17</sup> Reprinted with permission from Phys. Today **69**(9), 38 (2016). Copyright 2016 AIP Publishing LLC. (e) Band alignments of 2D semiconductors relative to the vacuum level. The dotted lines indicate the H<sup>+</sup>/H<sub>2</sub>, H<sub>2</sub>O/O<sub>2</sub>, and CO<sub>2</sub> reduction potentials.<sup>79</sup> Reprinted with permission from Peng *et al.*, Nano Today **10**, 128 (2015). Copyright 2015 Elsevier Ltd.

(i.e., types I, II, and III) between 2D semiconductors, desired applications could be achieved.

## 2. Optical properties

When illuminating a 2D semiconductor with photon energy larger than its bandgap, the optical absorption occurs exciting the electrons in the valence band into the conduction band. The reverse process leads the electron and hole pairs to relax to the band edges and then recombine as emitting photons with energy equal to the bandgap of the semiconductor, resulting in photoluminescence (PL). As shown in Fig. 6(a), the electron and hole pair formed by a strong electrostatic Coulomb force is regarded as an elementary excitation called an exciton. The exciton is electrically neutral and has an energy level within the bandgap of the semiconductor. The binding energy of an exciton originating from the Coulomb interaction would reduce the optical transition energy but is negligible in bulk TMDs. However, the Coulomb interaction is strongly increased when the TMD is thinned down to the 2D system due to quantum confinement effects.<sup>80</sup> That is why in 2D TMD, the optical bandgap measured by optical methods is much smaller than the electronic bandgap measured by electronic methods. For monolayer MoS<sub>2</sub>, the exciton binding energy is in the range of 0.48 eV to 0.89 eV,<sup>81,82</sup> leading to the large difference between the optical and electronic bandgaps. Therefore, it is a significant

issue about which kind of bandgap should be considered in 2D TMD devices.

For monolayer TMD semiconductors, two feature peaks can be detected in PL and optical absorption (reflectance) spectra, corresponding to A and B excitonic transitions associated with the SOC-induced splitting of valence band edge [Fig. 6(b)].<sup>83</sup> The peak positions of A and B excitons of monolayer MoS<sub>2</sub> are 1.8 and 2.0 eV, respectively.<sup>84</sup> When increasing the MoS<sub>2</sub> film thickness, a slight red shift in both A and B exciton peaks (~20 meV) is detected originating from the fact that the direct bandgap of MoS<sub>2</sub> is weakly dependent on the thickness.<sup>84</sup> For monolayer TMDs such as MoS<sub>2</sub> and WS<sub>2</sub>, an absorption rate for sunlight up to 5%–10% was reported, which showed one order of magnitude higher than those in traditional semiconductors such as Si and GaAs.<sup>85</sup> Furthermore, electron-bound exciton, which is a negatively charged quasiparticle consisting of two electrons and a hole, is usually called a trion [Fig. 6(c)] and can be detected in PL and absorption spectra of TMD semiconductors [Fig. 6(d)].<sup>86</sup> Compared to the bulk semiconductor, the binding energies of trions in monolayer TMDs are much larger (~18 meV for monolayer MoS<sub>2</sub>), making the trion transition (A<sup>-</sup>) clearly observable.<sup>86</sup> By chemical doping and/or electrical gating on monolayer TMDs, switching between exciton and trion peaks can be detected in PL spectra.<sup>86,87</sup> The exciton PL intensity of monolayer MoS<sub>2</sub> can vary by two orders at different gating voltages, while the

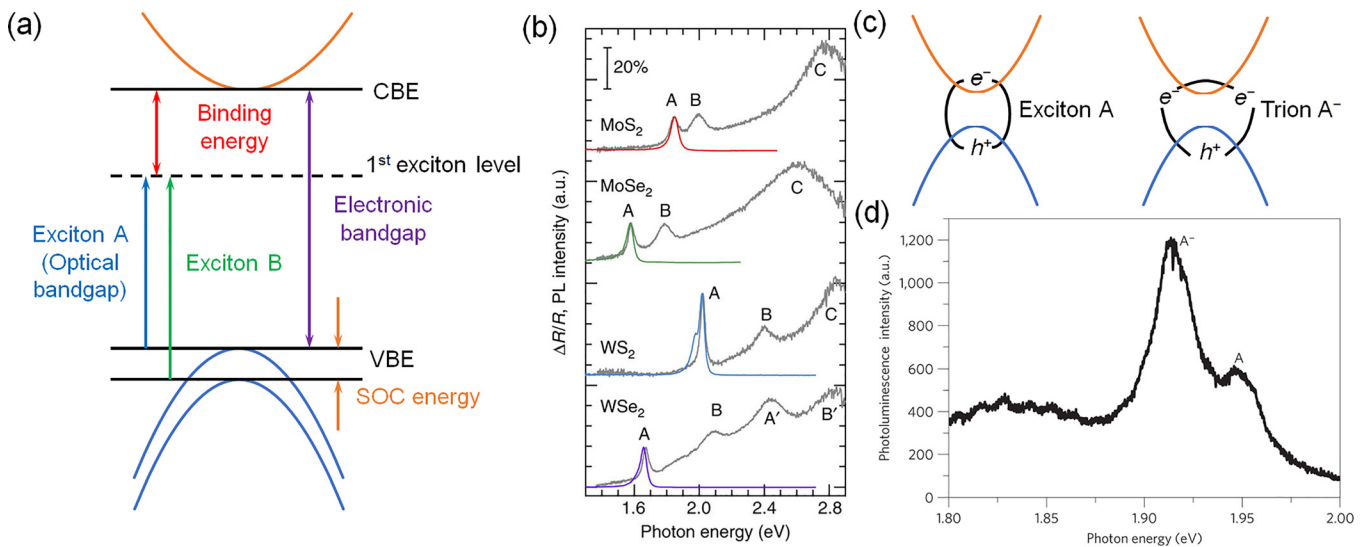


FIG. 6. (a) Optical transition processes in monolayer MoS<sub>2</sub>. (b) Reflectance and PL spectra of 2D TMDs on quartz substrates. The scale bar indicates the 20% absorption based on the reflectance spectra.<sup>83</sup> Reprinted with permission from Kozawa *et al.*, Nat. Commun. **5**, 4543 (2014). Copyright 2014 Macmillan Publishers Limited. (c) The dissociation of a trion into an exciton, along with an additional electron at the Fermi level in monolayer TMDs. (d) PL spectra of a monolayer MoS<sub>2</sub> on an *h*-BN substrate at 10 K with exciton (A) and trion (A<sup>-</sup>) emission.<sup>86</sup> Reprinted with permission from Mak *et al.*, Nat. Mater. **12**, 207 (2013). Copyright 2013 Macmillan Publishers Limited.

trion PL intensity almost remains the same.<sup>86</sup> The chemical doping induced PL intensity modification will be discussed in Sec. IV B.

As discussed above, intriguing optical properties can emerge in anisotropic 2D semiconductors. For instance, monolayer BP presents a strong angular polarization dependence of relative optical extinction and PL quantum yield.<sup>88</sup> Like graphene, nano-patterned BP can support localized plasmonic resonance at the wavelength of around 30 μm, because of the relatively high mobility.<sup>89</sup> A unique point is that the localized plasmonic effect presents a strong polarization dependence due to the anisotropy of BP.

Figure 4 presents a summary of bandgaps of 2D semiconductors. The diversity of 2D semiconductor family gives an appealing spectral coverage of the bandgaps ranging from the ultraviolet to the infrared. Through material selecting and structure designing of 2D semiconductors, various optoelectronic applications can be achieved in a certain spectral range.

### E. *h*-BN

Monolayer *h*-BN contains alternating boron and nitrogen atoms in arrangements of a hexagonal lattice with strong sp<sup>2</sup> bonds between them, which is similar to the lattice structure of graphene. *h*-BN, with a large bandgap of ∼5.97 eV, performs an intrinsically insulating behavior.<sup>90</sup> The band structure of 2D *h*-BN is not sensitive to the number of layers and is very close to that of the bulk crystal. Particularly, an ultra-smooth surface with the root mean square roughness of ∼50 pm can be found on *h*-BN, a much lower value than that of thermally grown SiO<sub>2</sub> (∼250 pm).<sup>91</sup> Due to the strong B-N covalent bonds in the plane and the absence of dangling bonds at the surface, *h*-BN has excellent chemical and thermal stability with high resistance to oxidation and to damage of high temperature up to ∼1500 °C in air. Moreover, *h*-BN

has a high dielectric breakdown field of 7.94 MV/cm, which is comparable with conventionally used dielectrics such as SiO<sub>2</sub>.<sup>92</sup> With the unique structural and physical advantages, *h*-BN is regarded as a promising assistant material to enhance the electronic and optoelectronic performance of other 2D materials.<sup>93</sup> What is more interesting on fundamental physics is that graphene/*h*-BN heterostructure provides a platform for studying many-body correlation effects of Dirac fermions in graphene, such as the fractional quantum Hall effect in the high magnetic field.<sup>94–96</sup> *h*-BN is also found to have other applications such as carrier tunneling layer<sup>92,97,98</sup> and deep ultraviolet optoelectronics.<sup>90</sup>

## III. SYNTHESIS AND PROCESSING

The electronic and optoelectronic properties of 2D materials affected by the structural characteristics are often induced by the synthesis and assembly process. Top-down and bottom-up are the two common approaches for the synthesis of 2D materials, including mechanical or liquid-phase exfoliation and chemical vapor deposition (CVD) or epitaxial growth, which provide a wide variety of options to determine the quality and cost of 2D materials for various potential applications. No matter what the method is to get the 2D material, integration with other materials by design is an important strategy to achieve specific functions and applications. Thus, the transfer and assembly process for 2D materials should be optimized to minimize the damage of the surface and interface of 2D materials and their heterostructures.

### A. Top-down

Mechanical or liquid-phase exfoliation is a typical top-down method for making 2D materials, in which the driving forces can break the weak vdW interaction between the layers in bulk layered materials. Since the first demonstration in one-atom-thick graphene exfoliated by scotch tape

[Fig. 7(a)], this easy yet approachable exfoliation has been serving as a promising processing method for proof-of-concept demonstrations.<sup>1</sup> The obtained 2D materials show high-quality with few defects, which present remarkable fundamental electronic and optoelectronic properties. However, this method is seriously restricted to wide applications due to the low-throughput and difficulty of control. Liquid-phase exfoliation is another top-down method which exfoliates the layered crystals in solvents. In this process, matched solvents (such as N-methyl-pyrrolidone and dimethylformamide) or intercalators (such as butyllithium and metal naphthalenide) are the key factors which could break the weak vdW interaction between the layers via sonication [Fig. 7(b)].<sup>99–104</sup> Particularly, the Hummers method has been used for synthesis of large-scale graphene oxide (GO).<sup>105–108</sup> The bulk graphite is first oxidized to form graphite oxide, and then the graphite oxide can be exfoliated into GO under sonication and centrifugation. The reduced graphene oxide (rGO) could be obtained by removal of oxygen-containing functional groups. All these liquid-phase exfoliation methods for preparing 2D materials are of low cost and provide high yield. However, the crystal quality of 2D materials is often degraded and many functional groups or residual solvent and ions would affect the electrical properties of 2D materials.

## B. Bottom-up

Due to the limitation of the top-down methods, bottom-up approaches for the synthesis of 2D materials are especially important and urgent. Early research primarily focused on the surface segregation of from the surface of transition metals<sup>6</sup> or epitaxial growth from the surface of silicon carbide.<sup>7</sup> After that, CVD is a widely used method to synthesize large-area and high-quality uniform 2D materials [Fig. 7(c)].

For the synthesis of graphene films, many metals, such as Cu,<sup>109,110</sup> Ni,<sup>111,112</sup> Ge,<sup>113</sup> and Pt<sup>114</sup> have been used as the growth substrates, where surface segregation/precipitation or surface adsorption process of carbon was considered to be the mechanism for graphene growth.<sup>115</sup> Here, gas, liquid, and solid carbon sources can be used for the synthesis of graphene.<sup>116–119</sup> In the case of hydrocarbon gas as a source, the growth of graphene can be divided into the following steps: (i) pyrolysis of hydrocarbon; (ii) adsorption, dehydrogenation, and diffusion of carbon species on or into metal; and (iii) nucleation and crystal growth. Thanks to the low carbon solubility and easy processing technology, Cu is considered to be a suitable choice for the growth of monolayer graphene films.<sup>109</sup> In this case, minimized carbon supply, high temperature, and smooth Cu surface with minimal active sites will result in a low nucleation density of graphene.<sup>120–122</sup> Due to the energetic favor of hydrogen-terminated graphene edges, high H<sub>2</sub> partial pressure can decrease the growth rate, while oxygen, which is conducive to the dissociation of hydrocarbons, is found to increase the growth rate of graphene domain.<sup>123–126</sup> All these parameters will lead to the fast growth of large single-crystal graphene.

Other 2D materials, such as *h*-BN,<sup>127–130</sup> MoS<sub>2</sub>,<sup>131–135</sup> WS<sub>2</sub>,<sup>136</sup> MoSe<sub>2</sub>,<sup>137</sup> WSe<sub>2</sub>,<sup>138</sup> MoTe<sub>2</sub>,<sup>139</sup> and ReS<sub>2</sub><sup>140,141</sup> are also synthesized *via* bottom-up methods. Predeposition of a metal layer on a substrate with a consequent chalcogenization process can produce scalable 2D TMDs.<sup>142</sup> Decomposition of thiomolybdate is an alternative approach to obtain sizable 2D TMDs.<sup>143</sup> However, the above methods are likely to obtain TMDs with nanoscale grain sizes. The most popular processes for synthesizing high-quality and scalable 2D TMDs are adopting metal oxide powders and chalcogen powders as the precursors in CVD systems.<sup>131–134</sup> It is found that the growth of atomically thin TMDs can be promoted by adding

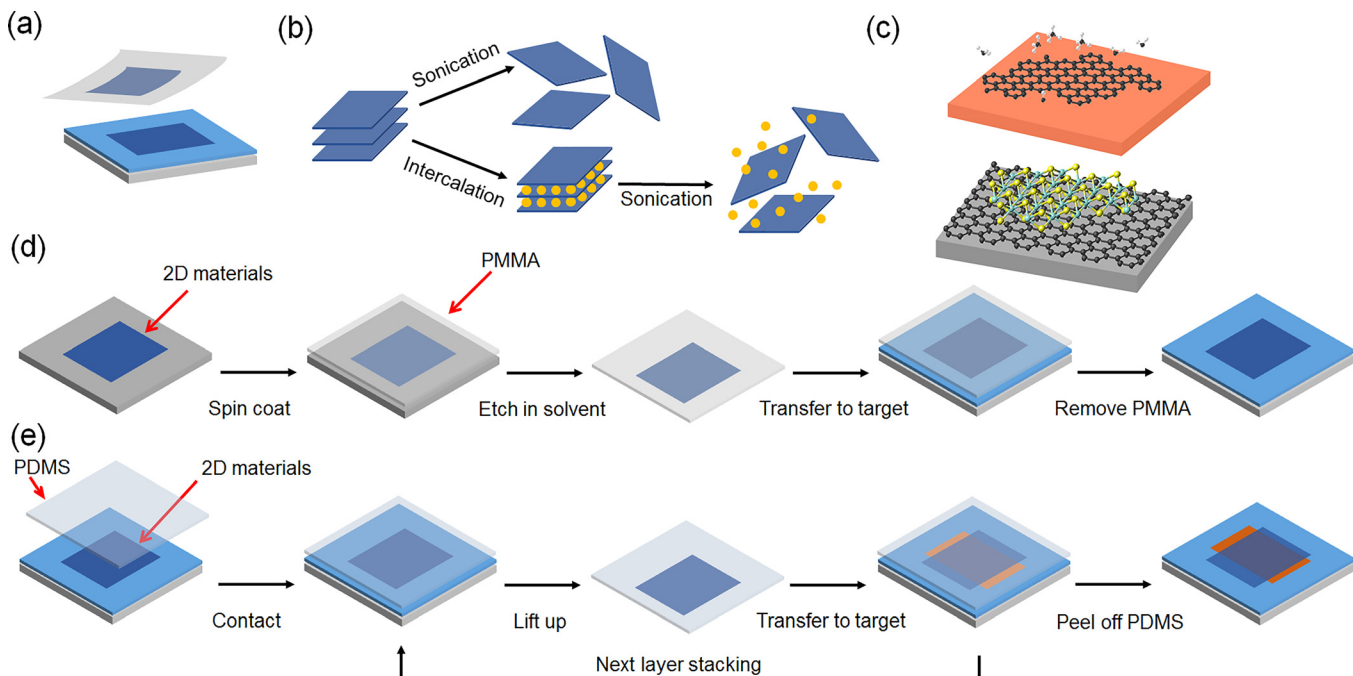


FIG. 7. (a) Mechanical exfoliation, (b) liquid-phase exfoliation, and (c) CVD approaches for the synthesis of 2D materials. (d) Wet transfer and (e) dry transfer techniques for assembly of 2D materials.

seed molecules or creating step-edge structures on the substrate due to the decreased nucleation energy barrier.<sup>133,144</sup> The morphologies of 2D TMDs obtained by CVD methods are highly dependent on the reaction temperature, the amounts of precursors, and the precursor-substrate distance.<sup>145</sup> Moreover, wafer-scale monolayer TMDs with high spatial homogeneity are synthesized by the metal-organic CVD technique.<sup>146</sup>

Furthermore, direct synthesis of vdWHs is of crucial importance for electronic and optoelectronic applications. Various kinds of vertical 2D heterostructures (e.g., graphene/*h*-BN,<sup>147</sup> MoS<sub>2</sub>-graphene<sup>148,149</sup> and WSe<sub>2</sub>-MoS<sub>2</sub><sup>150</sup>) are achieved by sequential CVD growth and vdW epitaxy method. Epitaxial 2D TMDs with controlled lattice orientation are obtained on nearly lattice matching substrates. On the other side, lateral 2D heterostructures are also achieved through strict control. Growing another 2D material on patterned graphene can produce lateral junctions such as graphene/*h*-BN<sup>151,152</sup> and MoS<sub>2</sub>-graphene.<sup>153,154</sup> Besides, 2D TMD lateral heterostructures (e.g., WSe<sub>2</sub>-MoS<sub>2</sub>)<sup>155–159</sup> can be grown by a two-step epitaxy growth strategy, in which the formation of TMD alloys is suppressed due to different growth temperatures and rates of each one.

### C. Transfer and assembly

Device fabrication and heterostructure assembly based on 2D materials require efficient and non-destructive transfer methods. The polymer-protected wet transfer method has been widely used for mechanical exfoliated or CVD-growth 2D materials.<sup>109,143,160</sup> First, polymer such as poly(methyl-methacrylate) (PMMA) is spin-coated onto the 2D material. Second, the sample with the polymer coating layer is detached from the substrate (e.g., etching Cu in a liquid etchant or SiO<sub>2</sub> in a NaOH/HF solution). At last, the polymer protected sample can be transferred to the target substrate and the polymer is dissolved in an organic solvent [Fig. 7(d)].

Although the wet transfer method is easy in the process, polymer residues can still be observed after dissolving and they affect the electrical properties of 2D materials.<sup>37,161</sup> Irregular wrinkles and cracks on the wet transferred 2D materials are also hard to avoid, which have a negative effect on electrical and optoelectronic performances of 2D materials. Dry transfer methods have been developed to resolve the above drawbacks of wet transfer processes.<sup>162–164</sup> For example, the poly(dimethylsiloxane) (PDMS) stamp first peels off one 2D material from the substrate. When the PDMS stamp with the 2D material is getting contact with another one, both 2D layers are lifted up on the PDMS. By repeating this procedure, more 2D layers can be added to achieve the 2D material stacking with clean interfaces [Fig. 7(e)].

## IV. STRUCTURAL MODIFICATIONS

This part will summarize the structural modifications of 2D materials, which could significantly adjust the physical properties of these layered materials and affect the performance of their electronic and optoelectronic devices. The unique structural properties of 2D materials, such as defects, dopants, component, phase, the number of layers, strain, and

corrugation at the nanoscale, which play a key role in properties, are emphatically surveyed.

### A. Defects

Having defects in crystals is one of the most important structural properties of semiconductors since it can alter their electronic and optoelectronic properties. For instance, defects can affect the local electronic structure, the carrier density, the thermal conductivity, and the mechanical strength of 2D materials. Point defects and line defects are the most important lattice imperfections for 2D materials, which are mainly generated at the synthesis process or/and chemical/physical post-treatment.<sup>165,166</sup> Moreover, the defects in 2D materials could be observed or characterized by High-resolution transmission electron microscopy (HRTEM), scanning tunneling microscopy (STM), and Raman spectroscopy, and theoretical calculations also provide the formation behavior of such structure.

#### 1. Point defects

*a. Stone-Wales defect.* Stone-Wales defect of graphene is a unique defect containing two pentagons and two heptagons (55–77) from rotating two  $\pi$ -bonded carbon atoms by 90° [Fig. 8(a)].<sup>167</sup> This reconstruction retains the pristine number of atoms and does not involve any dangling bonds. Although the formation energy of this Stone-Wales defect in graphene is approximately 5 eV via calculation, the substantial energy barrier is nearly 10 eV due to the rearrangements of carbon atoms.<sup>167</sup> This high energy means that the reconstruction is stable at room temperature as long as the Stone-Wales defect is formed.

*b. Vacancy defects.* Vacancy defects are the lattice sites where one or more atoms are missing. When an odd number of carbon atoms are missing in graphene, dangling bonds will remain due to geometrical reasons which make the structure chemically active and many functional groups, such as hydroxyl and carboxyl can be easily attached to the vacancy defects. For instance, single vacancy in graphene results in the formation of a (5–9) defect [Fig. 8(b)].<sup>168</sup> In particular, the formation energy for the single vacancy is as high as 7.4 eV in graphene, while its migration energy is about 1.7 eV by calculation.<sup>169</sup> On the other hand, when an even number of carbon atoms are missing, the dangling bonds can be healed for the connectivity of carbon atoms. For a double vacancy in graphene, no dangling bond is present and a reconstructed (5–8–5) defect is thermodynamically favored [Fig. 8(c)].<sup>170</sup> Meanwhile, the migration for the double vacancy is about 7 eV, higher than the energy for the single vacancy, making this double vacancy immobile.<sup>169</sup>

In contrast to the one-atom-thick graphene, the vacancy defects in 2D TMDs are far more complex because of the three-atom-thick binary element structures of monolayer TMDs. In monolayer MoS<sub>2</sub>, different types of defects are involved, including mono- and disulfur vacancies, vacancy complex of Mo and nearby three sulfur, and vacancy complex of Mo and nearby three di-sulfur pairs. Density functional theory (DFT) calculations show that the mono-sulfur

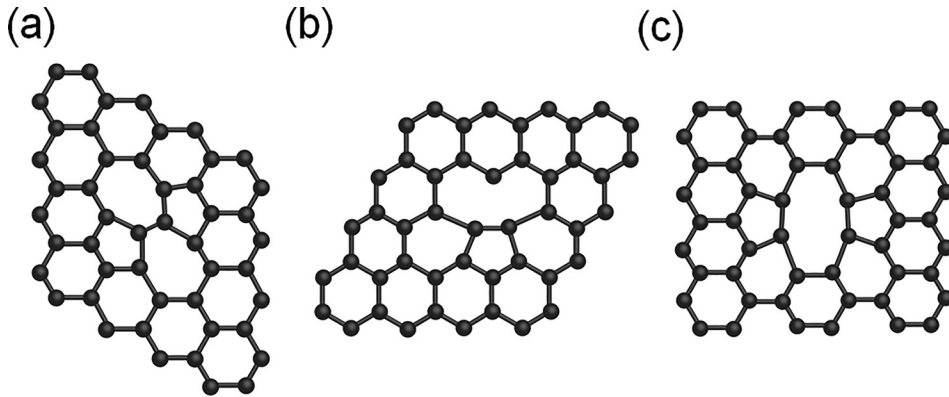


FIG. 8. (a) Stone–Wales defect (55–77) in graphene. (b) Single vacancy defect (5–9) in graphene. (c) Double vacancy defect (5–8–5) in graphene.

vacancy has the lowest formation energy across the whole range of S chemical potential.<sup>171</sup>

*c. Adatoms.* Unlike bulk crystals, interstitial defects are not thermodynamically favorable in 2D materials owing to the prohibitively high energy in the single atomic plane structure. Instead, additional atoms tend towards the third dimension to form defects in 2D materials. When the adatoms interact with a perfect carbon hexagon in graphene, physisorption with weak bonding or chemisorption with strong covalent bonding will occur. Yet, the adatoms can also be pinned or trapped by other defects which serve as reactive sites. In specific conditions, if additional carbon atoms interact with carbon atoms in graphene,  $sp^3$ -hybridization will possibly appear locally. However, the migration barrier for this additional carbon atom is about 0.4 eV by calculation, which means that the carbon atom on the graphene surface can migrate rapidly at room temperature.<sup>172</sup>

On the other hand, the interaction between additional foreign species (non-carbon atom) and carbon hexagon would affect the electrical properties of graphene. For example, gas molecules adsorbed on the surface of graphene can change the local carrier concentration.<sup>173</sup> Hydrogen or fluorine can also form hydrogenated or fluorinated graphene when C-H or C-F is added covalently upon chemical modification.<sup>174–176</sup> Since perfect graphene is relatively inert, the molecules from physisorption and chemisorption on graphene can desorb under high annealing temperature or other conditions and the initial state of graphene can be recovered.<sup>177</sup>

*d. Substitutions.* Foreign atoms can also be substituted to replace intrinsic atoms in 2D materials, leading to substitutional defects. In view of the different bond lengths between non-carbon and carbon atoms, the non-carbon atoms may be placed out of the plane.<sup>178</sup> What is more important is that the formed covalent bond is so strong that the substitutional impurities are very stable. The effect of substitutional defects on the properties will be discussed in Sec. IV B.

## 2. Line defects

*a. Grain boundary.* Line defects in polycrystalline 2D materials mainly include grain boundary and edge defects, both of which are also symmetry-breaking. For the synthesis of 2D materials by CVD or epitaxial growth, polycrystals

can be easily generated when the nucleation occurs simultaneously at different points and these domains coalesce with different lattice orientations on the substrate.<sup>179</sup> The grain boundaries, separating the rotationally disordered domains, are of great importance related to the grain size and the corresponding electrical properties of 2D materials.<sup>180–183</sup>

Normally, grain boundaries in graphene are described by a class of topological defects. The dislocation in graphene, for instance, can be considered as a semi-infinite strip of the structure with a pentagon-heptagon pair without dangling bonds. Here, Burgers vector ( $b$ ), which is a vector of the crystal lattice, can be introduced to describe this dislocation defect.  $b = (1,0)$  and  $b = (1,1)$  are shown in Fig. 9(a), reflecting the atomic structures of dislocation. Large dislocation density corresponds to large misorientation angles  $\theta$  ( $\theta = \theta_L + \theta_R$  ( $0^\circ < \theta < 60^\circ$ )), and two large-angle grain boundaries ( $\theta = 21.8^\circ$  and  $\theta = 32.2^\circ$ ) are represented in Fig. 9(b).<sup>184</sup> In normal conditions, grain boundaries can impede the electronic transport of graphene. For example, a significantly reduced conductance of crossed grain boundaries in graphene is found compared with each single-crystalline graphene [Fig. 9(c)].<sup>181</sup> However, when two domains have overlapped at their grain boundaries in graphene, the conductance would be enhanced because the scattering properties in the overlap region are improved [Fig. 9(d)].<sup>182</sup>

For monolayer MoS<sub>2</sub>, (5–7) and (8–4–4) defects are often observed at grain boundaries [Fig. 9(e)]. For example, the atomic structure of (1,0) dislocation can be found, following the same as  $b$  in graphene. Due to these three-atom-thick binary element structures of MoS<sub>2</sub>, two-layer of (5–7) rings are joined at the middle layer of Mo, accompanied by a Mo–Mo bond [Fig. 9(f)].<sup>133</sup> Particularly, in sulfur-rich conditions of the CVD process, two Mo–S bonds substituting the middle-layer Mo–Mo bond are more energetically favorable compared with other S<sub>2</sub> substitutions [Fig. 9(g)].<sup>133</sup> It is known that two main grain boundary types, tilt, and twin, exist in polycrystalline MoS<sub>2</sub> and it is found that tilt grain boundaries in MoS<sub>2</sub> can cause significant degrading of electrical properties [Fig. 9(h)].<sup>183</sup> Moreover, grain boundaries in monolayer TMDs can cause PL intensity decrease, providing a facile way to observe grain boundaries.<sup>131,134</sup>

*b. Edge defects.* 2D materials are always ended either with dangling bonds or with the saturation of the functional group. The typical edge structures in graphene are zigzag

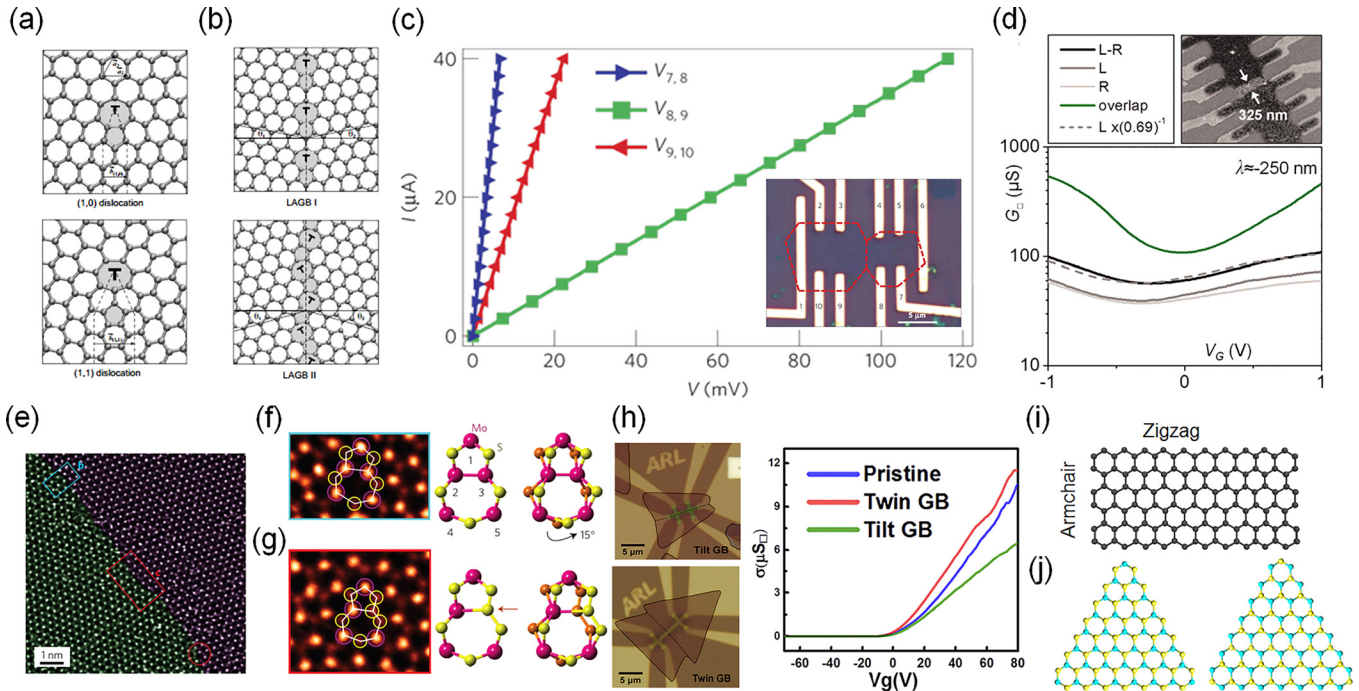


FIG. 9. (a) Dislocations with Burgers vector (1,0) and (1,1) in graphene. (b) Atomic structures of large-angle grain boundaries.<sup>184</sup> (a) and (b) Reprinted with permission from Yazyev *et al.*, Phys. Rev. B **81**, 195420 (2010). Copyright 2010 American Physical Society. (c) Current–voltage curves measured across the grain boundary of graphene (green) and within the each graphene grain (red and blue). The inset is the image of this device.<sup>181</sup> Reprinted with permission from Yu *et al.*, Nat. Mater. **10**, 443 (2011). Copyright 2011 Macmillan Publishers Limited. (d) Gate-voltage dependent conductance measured across an overlapped grain boundary of graphene (L–R) and within the each graphene grain (L and R). The inset is the image of this device with the 325 nm width of the overlap region.<sup>182</sup> Reprinted with permission from Tsen *et al.*, Science **336**, 1143 (2012). Copyright 2012 AAAS. (e) Scanning transmission electron microscopy (annular dark field) images of a MoS<sub>2</sub> grain boundary and schematics of the Mo-oriented (5–7) dislocation (f) and its S<sub>2</sub> substitutions (g). The purple sphere is Mo, and the yellow and orange ones represent top and bottom S, respectively.<sup>133</sup> Reprinted with permission from Najmaei *et al.*, Nat. Mater. **12**, 754 (2013). Copyright 2013 Macmillan Publishers Limited. (h) Electrical transport transfer curves for the pristine MoS<sub>2</sub> device and two devices with two types of grain boundaries (twin and tilt boundaries).<sup>183</sup> Reprinted with permission from Najmaei *et al.*, ACS Nano **8**, 7930 (2014). Copyright 2014 American Chemical Society. (i) The zigzag and the armchair edges in graphene. (j) The single-crystal triangles with well-defined edges orient either along Mo-zigzag or along S-zigzag directions in MoS<sub>2</sub>.

and armchair edges [Fig. 9(i)], which exhibit the minimized number of dangling bonds. Significantly, the bandgap of graphene nanoribbon with narrow widths ( $<10$  nm) and well-defined edge structures can be tuned, which makes it possible to be used in high-performance electronic devices. In the structure of CVD-grown monolayer MoS<sub>2</sub>, single-crystal triangles with well-defined edges orient either along Mo-zigzag or along S-zigzag directions [Fig. 9(j)]. For the case of narrow ribbons, particularly, edges can serve as the scattering centers for electrons and phonons.

## B. Dopants

Dopants are desirable because these foreign species can adjust the Fermi level, modify the electronic structure, or inject charge into the electron system of 2D materials. Spatially controlled doping by ion implantation has been widely used in bulk semiconductors. However, alternative methods for doping 2D materials have to be investigated, since the ion implantation technique is difficult to be adopted in the 2D system. Substitutions and adatoms in 2D materials are the important categories besides electrostatic doping.

### 1. Substitutional doping

Substitutional doping of foreign atoms offers a controllable and stable doping method for 2D materials. Typically,

boron (B, called an acceptor), the substitutional impurity atom replacing a carbon atom, can dope graphene as p-type (hole is created in the valence band). Similarly, nitrogen (N) atoms (called a donor) can dope graphene to n-type (the electron is donated to the lattice in the conduction band). These substitutional dopants may lead to strong scattering by which the electrical conduction of graphene is greatly affected. For example, n-type graphene can be achieved by introducing N-contained precursors, such as NH<sub>3</sub>, CH<sub>3</sub>CN, and C<sub>5</sub>H<sub>5</sub>N, accompanied by the carbon source in the CVD growth process [Fig. 10(a)].<sup>185–188</sup> Besides, post-growth treatments, such as plasma treatment in N-contained gas, are also implemented to dope graphene.<sup>189,190</sup> It is found that the N-doped graphene exhibits a lower carrier mobility but larger on/off ratio than that of intrinsic graphene.<sup>186</sup> Although the carrier-defect scattering can affect the carrier mobility, the substitutional N atoms can alter the electronic structure of graphene and make it meaningful in electronic and optoelectronic devices. In addition to B and N,<sup>191</sup> other substitutional atoms, such as phosphorus (P),<sup>192</sup> silicon (Si),<sup>193</sup> and sulfur (S),<sup>194</sup> can also dope graphene. Besides, some substitutional doping methods both during synthesis and post treatment are adopted in 2D semiconductors.<sup>195–198</sup> For instance, manganese (Mn) doped MoS<sub>2</sub> via *in situ* vapor phase deposition on graphene would modify its band structure, and the substrate surface chemistry is the dominant factor in this doping

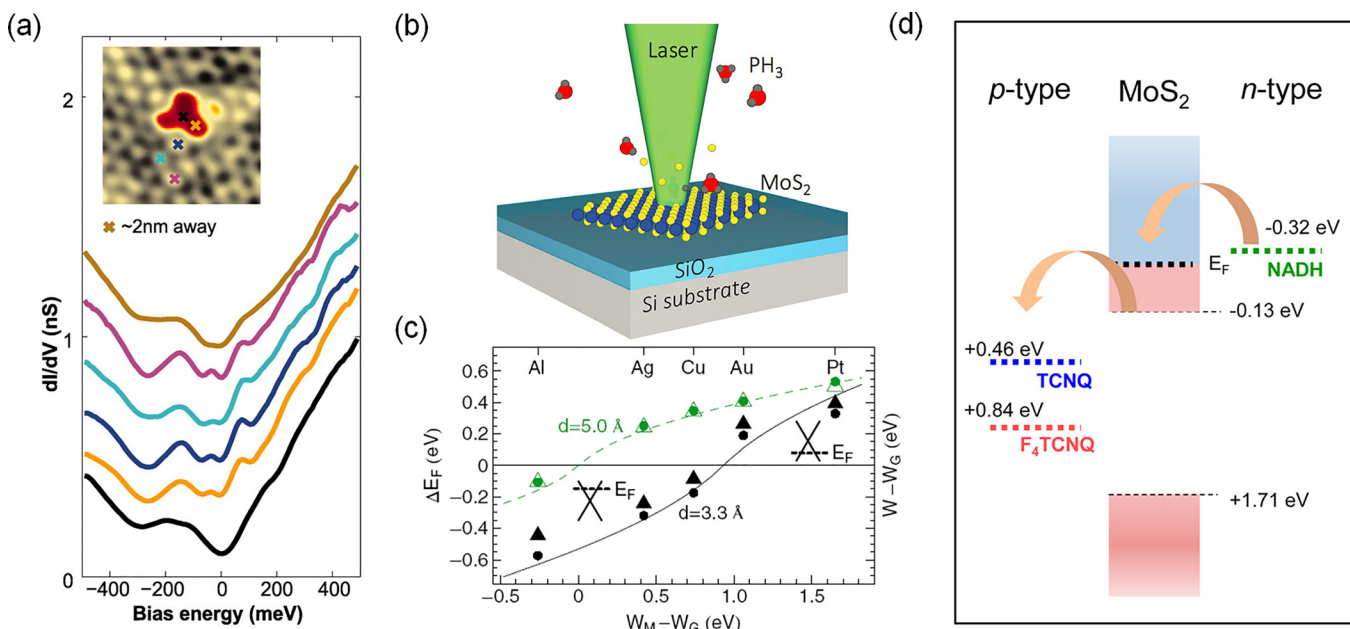


FIG. 10. (a)  $dI/dV$  curves measured on an N atom and near the N atom on N-doped graphene. As a contrast, the top curve is taken 2 nm away from the dopant graphene.<sup>185</sup> Reprinted with permission from Zhao *et al.*, Science **333**, 999 (2011). Copyright 2011 AAAS. (b) Schematic of the laser-assisted P substitutional doping in MoS<sub>2</sub>.<sup>198</sup> Reprinted with permission from Kim *et al.*, Adv. Mater. **28**, 341 (2016). Copyright 2016 Wiley-VCH Verlag GmbH & Co. (c) Doping graphene with metal contacts driven by the work function difference.  $W_M$  and  $W_G$  are the work functions of metal and graphene, respectively.<sup>206</sup> Reprinted with permission from Giovannetti *et al.*, Phys. Rev. Lett. **101**, 026803 (2008). Copyright 2008 American Physical Society. (d) Schematic of redox potentials of the dopants with respect to the Fermi level of monolayer MoS<sub>2</sub>, showing the charge transfer between dopants and MoS<sub>2</sub>.<sup>87</sup> Reprinted with permission from Moura *et al.*, Nano Lett. **13**, 5944 (2013). Copyright 2013 American Chemical Society.

process.<sup>198</sup> Laser-assisted spatial controlled P doping in MoS<sub>2</sub> also can be achieved [Fig. 10(b)].<sup>198</sup> The laser gives rise to creating S vacancies and dissociating the dopant molecules (PH<sub>3</sub>) and enables the substitution of S atoms with P.

## 2. Surface doping

Another method for doping 2D materials has been achieved by adsorbing inorganic or organic molecules on its surface. In general, adatoms, unlike substitution, do not disrupt strongly the electronic structure of graphene and the doping effect will weaken or disappear if these molecules desorb from graphene. Similarly, molecules with electron donating groups lead to n-type graphene and molecules with electron accepting groups lead to p-type graphene. For example, H<sub>2</sub>O<sub>2</sub>, NO<sub>2</sub>, Br<sub>2</sub>, I<sub>2</sub>, and tetrafluoro-tetracyanoquinodimethane (F<sub>4</sub>-TCNQ) are the strong electron acceptors and graphene can be p-type doped when interacting with these additional atoms.<sup>173,199,200</sup>

NH<sub>3</sub>, ethanol, and poly(ethylene imine) (PEI) can dope graphene with electrons, resulting in n-type doping.<sup>173,201</sup> Moreover, graphene can be chemical modified or doped via hydrogenation, fluorination or chlorination with covalent C-H, C-F or C-Cl bonds through plasma reaction or photochemical process.<sup>202,203</sup> On the other hand, graphene can also be doped by the substrate or metal electrode.<sup>204–206</sup> That means the electrical properties of graphene could be adjusted when it contacts with other materials in devices. For example, Au and Pt deposited on graphene can cause p-type doping, while Al, Ag, and Cu deposited on graphene induce n-type doping to graphene driven by the work function difference Fig. 10(c).<sup>206</sup>

Chemical doping in 2D semiconductors has also attracted considerable attention. The redox potentials of the dopants

with respect to the surface potentials of 2D semiconductors determine the doping type. Taking the monolayer MoS<sub>2</sub> as an example, nicotinamide adenine dinucleotide (NADH) molecules have an electron surface potential higher than that of MoS<sub>2</sub>, so electrons transferring from NADH to MoS<sub>2</sub> film will take place when the dopants are absorbed by MoS<sub>2</sub>, thus causing n-type doping [Fig. 10(d)].<sup>87</sup> On the contrary, for dopant molecules with surface potentials lower than that of MoS<sub>2</sub>, such as F<sub>4</sub>TCNQ and 7,7,8,8-tetracyanoquinodimethane (TCNQ), electrons will transfer from MoS<sub>2</sub> to the dopants, leading to p-type doping. Besides, various kinds of molecules, such as potassium (K),<sup>207</sup> benzyl viologen (BV),<sup>208</sup> and bis(trifluoromethyl) sulfonamide (TFSI)<sup>209</sup> as n-type dopants and O<sub>2</sub>,<sup>210</sup> H<sub>2</sub>O<sup>211</sup> and NO<sub>2</sub><sup>212</sup> as p-type dopants are used for 2D TMDs. For BP, Cs<sub>2</sub>CO<sub>3</sub>, and Cu adatoms have been adopted as the electron dopant and hole dopant, respectively.<sup>213,214</sup> Particularly, chemical dopants can induce great modifications to the PL properties of 2D TMDs. The PL intensity of monolayer MoS<sub>2</sub> is significantly enhanced when p-type dopants are adopted, while it decreases by n-type doping.<sup>87</sup> The switching between PL spectra with exciton and trion is responsible for the doping induced PL intensity evolution.

## C. Alloying

Alloying in 2D materials can bring continuously tunable bandgap by changing the composition percentages, which is similar to bulk semiconductors. For example, graphene can be hybridized with separated-domain *h*-BN and this BNC alloy has the tunable properties.<sup>215</sup> Moreover, the similar crystal structures and lattice constants between two different TMDs make the consequent 2D alloy materials chemically

stable. Figure 11(a) shows a schematic diagram of the 2D  $\text{MoS}_{2(1-x)}\text{Se}_{2x}$  and the corresponding bandgaps as a function of concentration index  $x$ .<sup>216</sup> The bandgap of the alloy retains direct, ranging from  $\sim 1.9$  to  $\sim 1.6$  eV as the index  $x$  increases from zero to unity. Optical properties (such as PL and Raman spectra) of the TMD alloy can reveal the complete tunability of bandgap.<sup>195,217</sup> For example, the PL peak position gradually shifts from 668 nm ( $\text{MoS}_2$ ) to 795 nm ( $\text{MoSe}_2$ ) as the  $x$  index increases for monolayer  $\text{MoS}_{2(1-x)}\text{Se}_{2x}$  [Fig. 11(b)].<sup>217</sup> Other ternary 2D TMD semiconductors, such as  $\text{WS}_{2(1-x)}\text{Se}_{2x}$  and  $\text{Mo}_{1-x}\text{W}_x\text{S}_2$ , are also experimentally achievable and their bandgap tuning can be observed.<sup>218,219</sup> It is worth noting that unlike semiconducting alloys, the monolayer  $\text{W}_x\text{Mo}_{1-x}\text{Te}_2$  alloy can lead to a metal-insulator transition as the composition index  $x$  changes because both H and T' phases are stable in this alloying system.<sup>220</sup>

#### D. Phase transition

Phase transition in bulk TMD semiconductors has been well studied for decades. The 2H semiconducting phase has

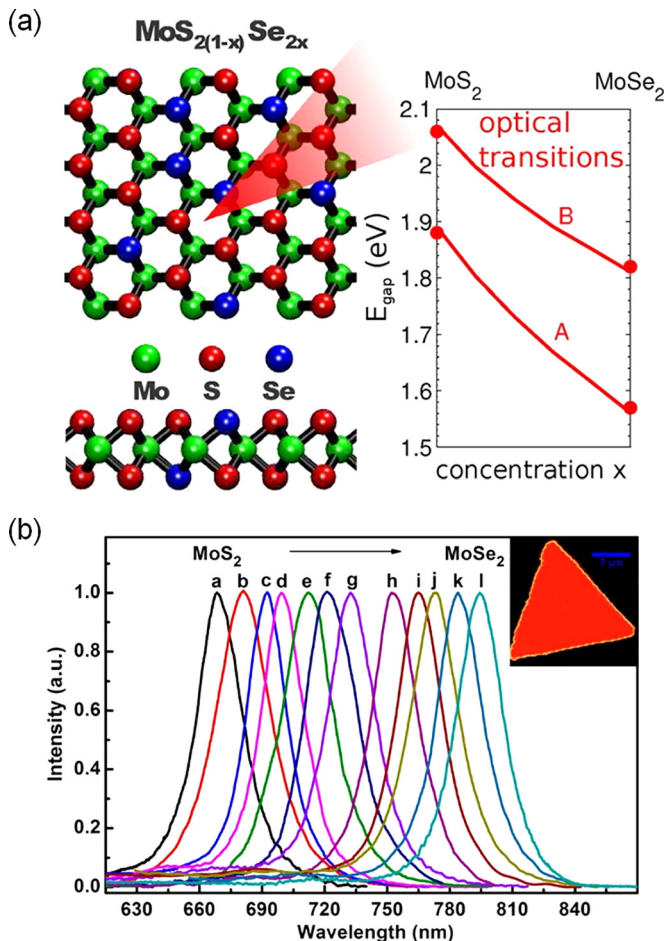


FIG. 11. (a) Schematic diagrams of top views and side views of ternary 2D  $\text{MoS}_{2(1-x)}\text{Se}_{2x}$  alloy and the corresponding bandgaps as a function of concentration index  $x$ . A and B indicate the two optical transitions.<sup>216</sup> Reprinted with permission from Komsa *et al.*, J. Phys. Chem. Lett., 3, 3652 (2012). Copyright 2012 American Chemical Society. (b) PL spectra of 2D  $\text{MoS}_{2(1-x)}\text{Se}_{2x}$  alloy with complete tunability of composition index  $x$  ( $0 \leq x \leq 1$ ). The inset is a typical PL mapping of a monolayer grain of the alloy (scale bar: 7  $\mu\text{m}$ ).<sup>217</sup> Reprinted with permission from Li *et al.*, J. Am. Chem. Soc., 136, 3756 (2014). Copyright 2014 American Chemical Society.

a trigonal prismatic arrangement of atomic layers (ABA stacking) which belongs to the group symmetry of  $D_{3h}$  [Fig. 12(a)], while the 1T phase has an octahedral arrangement (ABC stacking) with the symmetry  $D_{3d}$  [Fig. 12(b)]. For most layered TMD materials, the 1T phase is not stable thermodynamically even at room temperature.<sup>221</sup> Distorted 1T (1T') phase which is similar to the 1T phase but with lower symmetry [Fig. 12(c)] is energetically favorable in some layered TMDs like  $\text{MoTe}_2$ . Tuning the phases of TMDs can achieve transitions between semiconducting and metallic states [Fig. 12(d)], providing an effective approach to reducing the contact resistance in TMD-based FETs.<sup>222–224</sup> In contrast to the high resistance (0.7–10 k $\Omega$   $\mu\text{m}$ ) at metal contact in  $\text{MoS}_2$  FETs, a much lower resistance of 200–300  $\Omega$   $\mu\text{m}$  is realized at the 2H-1T interface of patterned  $\text{MoS}_2$  [Fig. 12(e)].<sup>223</sup>

Charge transfer to the TMD lattices (e.g.,  $\text{MoS}_2$ ,  $\text{WS}_2$ ,  $\text{MoSe}_2$ , and  $\text{WSe}_2$ ) can enhance the  $d$ -orbital electron density of the transition metal atom, leading to the 2H-1T phase transition.<sup>223–225</sup> Here, various methods for effective phase engineering of 2D TMDs are proposed: (1) Chemical treatment. For instance, 2H monolayer TMDs can be converted to the 1T phase via lithiation using butyllithium.<sup>225</sup> A consequent annealing process drives the 1T phase TMDs back to the stable 2H phase. In addition, long-term stability of the 1T' phase TMDs can be achieved by hydrogenating the intercalated Li to form lithium hydride (LiH).<sup>226</sup> (2) Plasmonic hot electron transfer. Monolayer  $\text{MoS}_2$  with gold nanoparticles deposited can generate a transient reversible 2H-1T phase transition when applying illumination, which is induced by plasmonic assisted hot electron transfer from gold nanoparticles to  $\text{MoS}_2$ .<sup>227</sup> (3) Electron beam irradiation (EBI). Electron beam irradiation (EBI) is known to cause the transition from the crystalline phase to the nanocrystalline phase in carbon materials including graphene.<sup>228,229</sup> For 2D TMDs, EBI can provide a top-down patterned fabrication of 1T phase and the consequent in-plane 2H-1T Schottky junction.<sup>230</sup> (4) Strain. The room-temperature 2H-1T' phase transition can be induced by applying tensile strain in the  $\text{MoTe}_2$  thin film.<sup>231</sup> Noting that both the semiconducting 2H phase and the metallic 1T' phase are stable in  $\text{MoTe}_2$ , so this repeatable and revisable phase transition under ambient conditions is more promising for device applications.

#### E. Number of layers

The band structures of 2D materials strongly depend on the number of layers because the vdW interaction plays an important role in the 2D system. For instance, in monolayer graphene, the energy dispersion near the Dirac point is linear, leading to its semimetal and massless Dirac fermion features. However, the energy dispersion relation in the low-energy regime is parabolic due to interlayer coupling in bilayer graphene.<sup>27</sup> By applying an external electric field across the vertical direction of the bilayer graphene, a finite bandgap can be opened [Fig. 13(a)].<sup>27</sup> Besides, the quantum dynamics in bilayer graphene is affected by a  $2\pi$  Berry's phase; as a result, an integer quantum Hall effect without the

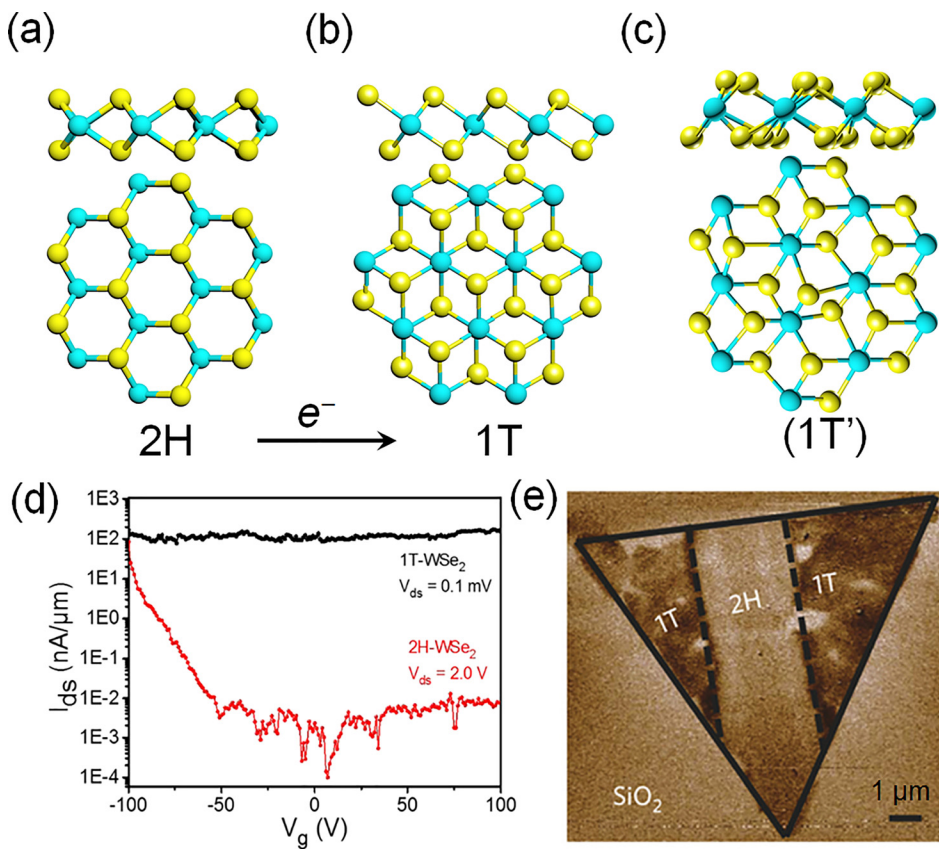


FIG. 12. Crystal structures with top view and side view of 2H (a), 1T (b), and 1T' (c) phases of TMDs. (d) FET device performance comparison between 1T and 2H WSe<sub>2</sub>.<sup>224</sup> Reprinted with permission from Ma *et al.*, ACS Nano **9**, 7383 (2015). Copyright 2015 American Chemical Society. (e). Electrostatic force microscopy phase image of patterned (2H-1T) 2D MoS<sub>2</sub>.<sup>225</sup> Reprinted with permission from Kappera *et al.*, Nat. Mater. **13**, 1128 (2014). Copyright 2014 Macmillan Publishers Limited.

zero-level plateau can be detected, which is very different from the case in monolayer graphene.<sup>232,233</sup>

The band structures of TMD semiconductors are also highly dependent on the number of layers. Figure 13(b) shows the calculated band structures of representative MoS<sub>2</sub> with a number of layers from the bulk to the monolayer.<sup>234</sup> The direct bandgap at the  $K$  point is associated with the  $d$  orbitals of electrons at the Mo atoms, which minimize the interlayer coupling effects.<sup>235</sup> As a result, the direct bandgap is not affected by the decrease of material thickness. On the other hand, the indirect bandgap from the valence band maximum at the  $\Gamma$  point is associated with both  $d$  orbitals at M atoms and  $p_z$  orbitals at X atoms. As the MoS<sub>2</sub> semiconductor is thinned, the indirect bandgap decreases due to the interlayer coupling, or in other words, the quantum confinement effects.<sup>66</sup> When the number of layers decreases to one, the indirect bandgap becomes larger than the direct one, leading to the transition of the material from the indirect bandgap to the direct bandgap.<sup>65,66,235</sup> For instance, bulk MoS<sub>2</sub> has an indirect bandgap of  $\sim 1.2$  eV while the monolayer exhibits a direct optical bandgap of  $\sim 1.9$  eV.<sup>235</sup> Exceptionally, the band structures of some other TMDs (Like NbS<sub>2</sub>, ReS<sub>2</sub>) with weak interlayer coupling do not change much with the thickness modification.<sup>66</sup> Figure 13(c) shows the bandgap change as a function of film thickness in some TMDs, BP, and ultra-thin Si. It is clear that the large bandgap broadening effect is estimated in Si with a thickness smaller than 3 nm. In this regard, 2D semiconductors with relatively small bandgaps are competitive candidates in ultra-thin and low-power devices in the post-silicon era.

PL investigations provide experimental evidence for this indirect-to-direct bandgap transition. The luminescence

efficiency of monolayer MoS<sub>2</sub> can reach a near-unity value of  $\sim 95\%$ ,<sup>209</sup> while a three-order decrease of PL quantum yield is detected in few-layer (2–6 layers) MoS<sub>2</sub> [Fig. 13(d)].<sup>235</sup> Besides, applying an external vertical electric field to bilayer TMD semiconductors, the bandgap decreases as the perpendicular electric field increases.<sup>236</sup> In particular, continuous bandgap tuning down to zero for the MoS<sub>2</sub> bilayer can be achieved by dual gating.<sup>237</sup> Besides, the low-frequency Raman breathing mode can be used as a good indicator for interlayer interactions.<sup>238</sup>

## F. Strain

Strain engineering is an effective way to tune the electronic properties of semiconductors because energy band characteristics around the Fermi level are very sensitive to orbital coupling neighboring atoms. However, bulk materials cannot endure a high enough elastic strain to have sufficient changes in their physical properties. In contrast, 2D materials have excellent elasticity and high Young's modulus for strain engineering.<sup>242,243</sup> Several ways have been demonstrated to introduce strain into 2D materials: (1) Using the piezoelectric substrate to generate controllable biaxial strain by applying voltage between the sides of the substrate, which can be efficiently transferred to the 2D materials.<sup>244,245</sup> (2) Inducing controllable biaxial strain on a certain point of the 2D materials by tuning the atomic force microscope tip.<sup>243,246</sup> (3) Applying strain to 2D materials via the patterned substrate.<sup>247</sup>

One of the indications induced by strain is the shifts in Raman spectra of 2D materials.<sup>248,249</sup> Typically, a tensile

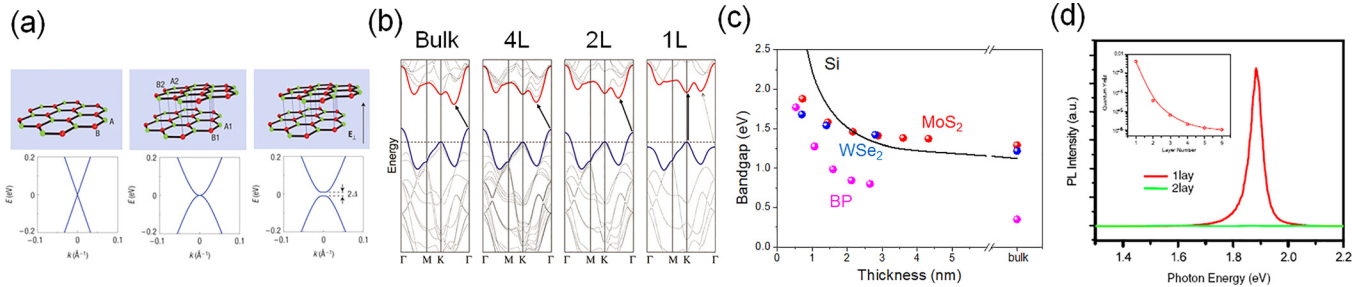


FIG. 13. (a) Schematic diagrams of lattice structures and the corresponding band structures of monolayer graphene, bilayer graphene, and bilayer graphene under the vertical electrical field. The opened bandgap  $2\Delta$  can be tuned by the magnitude of the field.<sup>27</sup> Reprinted with permission from Oostinga *et al.*, Nat. Mater. **7**, 151 (2008). Copyright 2008 Macmillan Publishers Limited. (b) Band structures of MoS<sub>2</sub> from the bulk to the monolayer (1L). The arrows show the transitions from valence band edge to the conduction band edge with the lowest energy.<sup>234</sup> Reprinted with permission from Splendiani *et al.*, Nano Lett. **10**, 1271 (2010). Copyright 2010 American Chemical Society. (c) Bandgap as a function of film thickness in TMDs, BP, and ultra-thin Si.<sup>235,239–241</sup> (d) PL spectra of monolayer and bilayer MoS<sub>2</sub>, while the inset shows PL quantum yield of MoS<sub>2</sub> (1L–6L).<sup>235</sup> Reprinted with permission from Mak *et al.*, Phys. Rev. Lett. **105**, 136805 (2010). Copyright 2010 American Physical Society.

strain induces redshifts while the compressive strain induces blue shifts in Raman in-plane vibrational modes. It has shown that under uniaxial tensile strain, the Raman G peak of graphene gives a redshift at a rate of  $\partial\omega_G/\partial\varepsilon_h = -14.2 \text{ cm}^{-1}/\%$ , where  $\omega_G$  is the frequency of the G mode and  $\varepsilon_h$  is the hydrostatic component of strain,<sup>29</sup> and that under biaxial compressive strain, the Raman G peak gives a blue shift at a rate of  $\partial\omega_G/\partial\varepsilon_{ll} = -57.3 \text{ cm}^{-1}/\%$ , where  $\varepsilon_{ll}$  indicates the parallel strain tensor component.<sup>244</sup> Unlike the biaxial strain, the uniaxial strain is anisotropic, thus breaking the hexagonal symmetry in 2D materials. As a result, some Raman modes associated with high symmetry of 2D materials will be split under large uniaxial strain [Fig. 14(a)].<sup>249</sup> In contrast, when biaxial strain is applied in monolayer MoS<sub>2</sub>, the E<sub>2g</sub> mode remains symmetrical.<sup>245</sup>

Strain engineering offers an efficient and controllable way to open graphene's bandgap. The first-principles calculation has predicted that 1% uniaxial strain could create a 300 meV bandgap opening in graphene [Fig. 14(b)].<sup>29</sup> Patterned substrate induced periodical strain in graphene could result in bandgap opening.<sup>247</sup> Strain-induced bandgap engineering of 2D semiconductors is another interesting topic. Theoretical works have shown that compressive strain makes the bandgap increase while tensile strain makes the bandgap decrease in 2D TMD semiconductors.<sup>250</sup> Furthermore, the direct to indirect bandgap transition in 2D TMDs would occur when strain is applied [Fig. 14(c)].<sup>65</sup> The biaxial compressive strain could make a 100 meV per % PL blueshift in monolayer MoS<sub>2</sub>,<sup>245</sup> while uniaxial tensile strain could induce PL red shifts in monolayer MoS<sub>2</sub> [Fig.

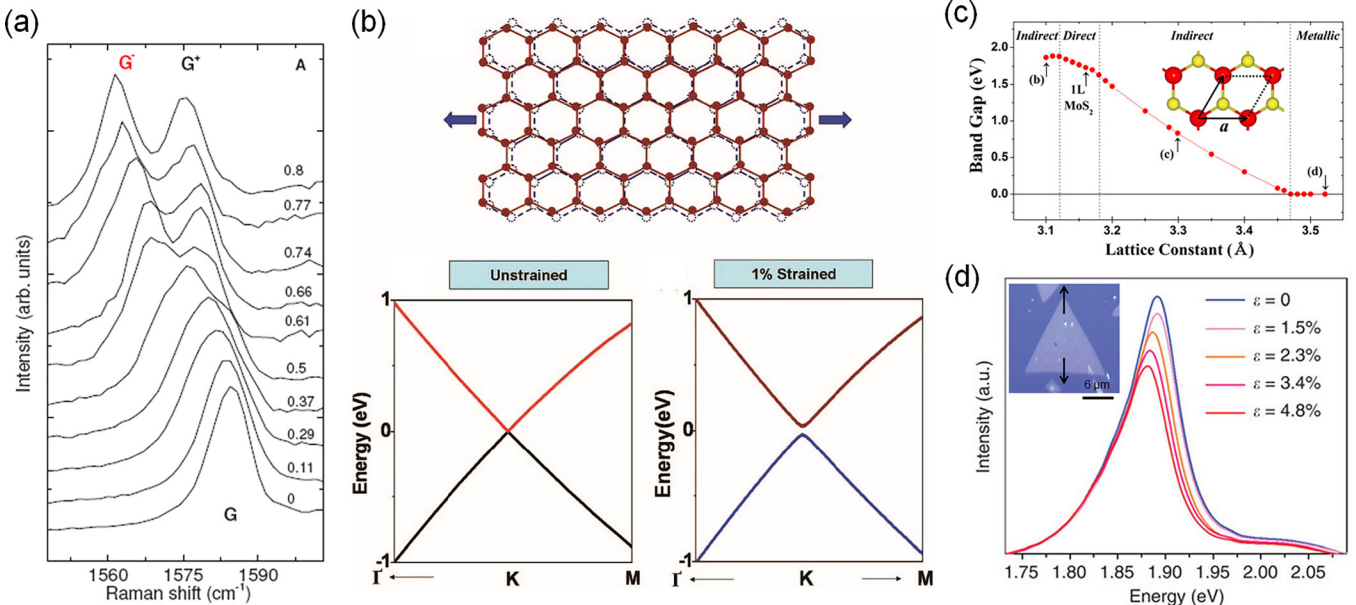


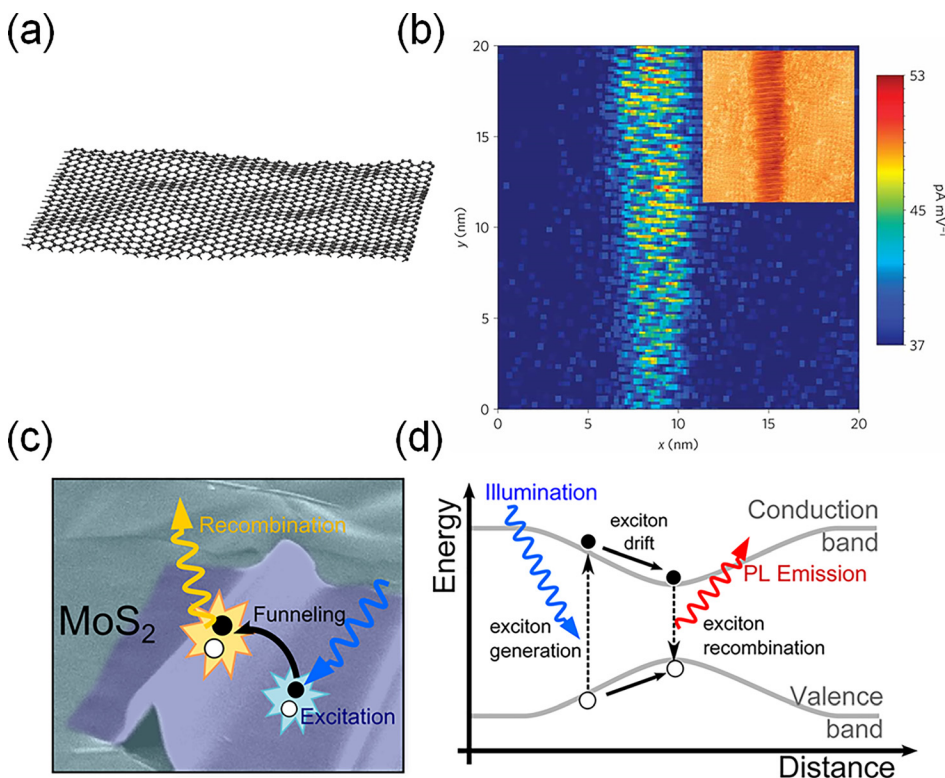
FIG. 14. (a) Raman G band of monolayer graphene as a function of applied uniaxial strain. G band splitting into G<sup>+</sup> and G<sup>-</sup> modes occurs at large strain, indicating the strain-induced symmetry breaking in graphene.<sup>249</sup> Reprinted with permission from Mohiuddin *et al.*, Phys. Rev. B **79**, 205433 (2009). Copyright 2009 American Physical Society. (b) Schematic of uniaxial tensile stress applied in graphene and the calculated band structure of 1% tensile strained graphene. An opened bandgap can be clearly observed.<sup>29</sup> Reprinted with permission from Ni *et al.*, ACS Nano **2**, 2301 (2008). Copyright 2008 American Chemical Society. (c) Bandgap of monolayer MoS<sub>2</sub> as a function of applied strain. The direct bandgap of pristine MoS<sub>2</sub> becomes indirect and even metallic when tensile strain is applied.<sup>65</sup> Reprinted with permission from Yun *et al.*, Phys. Rev. B **85**, 033305 (2012). Copyright 2012 American Physical Society. (d) PL spectra of monolayer MoS<sub>2</sub> (Inset, Scalar bar, 6 μm) under various magnitudes of tensile strain.<sup>251</sup> Reprinted with permission from Liu *et al.*, Nat. Commun. **5**, 5246 (2014). Copyright 2014 Macmillan Publishers Limited.

**14(d)].<sup>251</sup>** Non-uniform strain in monolayer MoS<sub>2</sub> applied by stretching flexible devices or by AFM tips makes the band bending occurs. The strain-induced charge polarization (also known as the piezoelectric effect) modifies the Schottky barrier at the contact interface and thus generates the electrical response to the strain.<sup>246</sup>

### G. Corrugations

Distinctive from bulk and other nanostructure materials, 2D materials would exhibit surface corrugations (such as ripples and wrinkles) due to the intrinsic thermal fluctuations or further processing when they are transferred to arbitrary substrates. In particular, these unique structural characteristics would influence their electrical properties.

Ripples in graphene can exist spontaneously by intrinsic thermal fluctuations. This surface corrugation makes this 2D crystal stable with finite out-of-plane deformation.<sup>252,253</sup> Unlike 3D crystals, there are no neighboring atoms above or below graphene, so the restoring forces perpendicular to graphene from the adjacent layers are much weaker than those of the bonds. Thus, the carbon atoms can be moved to out-of-plane by thermal motion [Fig. 15(a)]. Generally, the density of ripples mainly depends on the defects and edges of graphene.<sup>253,254</sup> The ripples could induce disorder in graphene which results in electron and hole puddles and thus the spatial charge inhomogeneity, leading to the modification of Dirac point with respect to the Fermi level of graphene. The differential tunneling conductivity mapping image of nanoscale structural ripples in graphene reveals the periodic modulation of the local density of states of graphene [Fig. 15(b)].<sup>255</sup> Although the ripples of this 2D crystal are an intrinsic property, they can also be suppressed through depositing graphene onto atomically smooth substrates.<sup>42,93</sup>



Typically, *h*-BN can suppress the ripples in graphene so that the CVD-grown graphene can yield a carrier mobility as high as  $\sim 24\,000\text{ cm}^2\text{ V}^{-1}\text{ s}^{-1}$ .<sup>130</sup>

Wrinkles nominally have a high aspect ratio in two dimensions, which are mainly formed during synthesis or processing of 2D materials.<sup>43,256–258</sup> In most conditions, this deformation is attributed to the uniaxial exterior force between 2D materials and the substrate. For graphene on substrates, the horizontal length of the graphene at the cooling step would be increased due to the negative thermal expansion coefficients while the substrates have an opposite polarity.<sup>257,258</sup> In addition, the wrinkles are also easily formed when 2D materials are transferred to other substrates with the wet transfer process. Water drain channels exist under the film so that these out-of-plane deformations can form along channels at the adhesion-to-substrate process.<sup>259</sup> To achieve wrinkle-free graphene, many approaches, such as less-deformation support polymers and low-surface-tension organic solvent, are introduced to improve the interaction between the film and substrates.<sup>260,261</sup> Wrinkles in 2D semiconductors, such as MoS<sub>2</sub>, can bring nonhomogeneous strain and consequently cause the local direct bandgap decreasing [Fig. 15(c)].<sup>262</sup> In this funnel-like bandstructure with spatially varied bandgaps [Fig. 15(d)], photoexcited excitons will drift to higher strain regions with lower bandgap and then recombine emitting photons with energy lower than the material's intrinsic bandgap.

### V. BUILDING BLOCKS

The integration of 2D materials into a device will always involve the interaction with other materials, which is critical to the real-life applications.<sup>13–18</sup> Generally, metal-semiconductor contacts, p-n junction, and their derivatives

FIG. 15. (a) Schematic diagram of rippled graphene. (b) Spatially resolved tunneling spectroscopy map of the local electronic density of states on the graphene nanoripples. The inset image is the corresponding position of graphene.<sup>255</sup> Reprinted with permission from Tapaszto *et al.*, Nat. Phys. **8**, 739 (2012). Copyright 2012 Macmillan Publishers Limited. (c) SEM image of wrinkled MoS<sub>2</sub>. (d) Schematic diagram of the wrinkle-induced local bandgap reducing in 2D MoS<sub>2</sub> and the exciton funneling effect.<sup>262</sup> Reprinted with permission from Castellanos-Gomez *et al.*, Nano Lett. **13**, 5361 (2013). Copyright 2013 American Chemical Society.

(e.g., metal-insulator-semiconductor structures and p-i-n junction) are the basic device building blocks for all major semiconductor devices. Besides, the 2D-dielectric interface is also an important aspect for high-performance devices, which is shown in Sec. VI A. As expected, 2D material-based building blocks for electronic and optoelectronic devices have been investigated in the last few years.

## A. Schottky junction

### 1. Graphene-semiconductor contacts

The conventional metal-semiconductor Schottky junction mode could be adopted to describe the transport at graphene-3D semiconductor interface. In general, the Fermi level difference between graphene and the semiconductor would induce charge transport and consequently band bending when they are interfacing with each other, forming a Schottky barrier. The band bending or the depletion layer mainly exists on the bulk semiconductor side because of its lower level of carrier density. Here, we show the proposed energy band diagrams of the Schottky junction enabling us to understand the formation and modification of this barrier height in Fig. 16(a).<sup>263</sup> Unlike conventional metal-semiconductor Schottky junctions where the Fermi level of the metal keeps constant because of its high density of electrons, the Fermi level of graphene could be sensitively tuned by the appropriate gate bias or doping.<sup>18</sup> Correspondingly, the barrier height can be modified for controlling the transport of carriers at the interface of the graphene-semiconductor Schottky junction. Doping graphene is inevitable during the etching transfer process or when exposed to the air, so the controllable doping method is of great importance. Also, the graphene-semiconductor Schottky junction can be fabricated as a triode device (a barristor) by adding a top gate on graphene which could control the Schottky barrier height and achieve a modulation of current.<sup>264</sup> By adopting 2D semiconductor like MoS<sub>2</sub> as the channel layer, graphene barristors with atomically thin vertical channels are achieved [Fig. 16(b)].<sup>265,266</sup> Thanks to the tunable Schottky barrier and the ultra short channel length, these 2D barristors

promise not only high current on/off ratio but also large on-current density, thus allowing their potentials in high-speed applications[Fig. 16(c)].<sup>265</sup> Besides, improving the quality of graphene-semiconductor interface, such as a minimum number of atomic defects, reduction of impurities, and prevention of charge trapping sites, contributes to the formation of ideal Schottky junction.<sup>267</sup>

### 2. Metal-2D semiconductor contacts

Metal contacts are frequently used in FETs and related optoelectronic devices based on 2D semiconductors. Generally, for metals with relatively low work functions (such as Sc and Ti), electron injection from metal to MoS<sub>2</sub> is expected to dominate the forward-bias current while for metals with relatively high work functions (such as Ni and Pt), hole injection is predominating. However, experimental results show that all the above four metals give electron injection to MoS<sub>2</sub>.<sup>268</sup> All the transfer curves exhibit *n*-type performance [Fig. 16(d)], indicating that the Fermi levels of all the adopted metals are close to the conduction band edge of MoS<sub>2</sub>.<sup>268</sup> These unexpected performances are attributed to the Fermi-level pinning effects in metal-2D semiconductor junctions, which originates from the chemical bond breaking and defect introduced in 2D semiconductors when depositing metal contacts. For some TMDs such as WSe<sub>2</sub>, the Fermi level of contact metal is pinned near the mid-gap level of WSe<sub>2</sub>, making it possible to tune the transport carrier type (electron, hole, or ambipolar) by adopting different contact metals.<sup>269,270</sup>

Fermi-level pinning effects make the Schottky barrier and the contact resistance of metal-2D semiconductor very large, which limits the application of 2D semiconductor FETs. A prevalent approach to eliminate the Fermi-level pinning is adopting graphene as alternative contact material.<sup>271</sup> An ultra clean and flat interface forms at the graphene-2D semiconductor junction with no chemical bond breaking, thus suppressing the Fermi-level pinning. Another way to reduce the contact resistance is to introduce an ultrathin tunneling barrier, which decouples the interface states of the

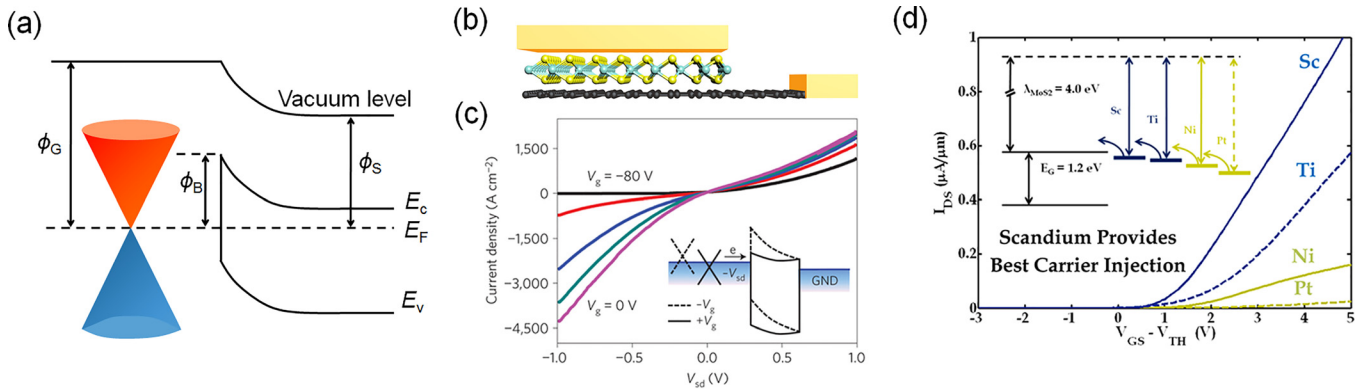


FIG. 16. (a) Energy band diagrams of the graphene-semiconductor Schottky junction. (b) Schematic of barristor made of graphene and 2D semiconductor with atomically thin vertical channel. (c) Current-voltage characteristics of graphene-MoS<sub>2</sub> barristor with vertical channel. The inset shows the band structure at the negative source bias at graphene-MoS<sub>2</sub> heterojunction is modulated by the gate electrode.<sup>265</sup> Reprinted with permission from Yu *et al.*, Nat. Mater. **12**, 246 (2013). Copyright 2013 Macmillan Publishers Limited. (d) Transfer curves of MoS<sub>2</sub> transistors with various metal contacts. The inset shows the actual line-up when contacts are formed, indicating the Fermi-level pinning effects.<sup>268</sup> Reprinted with permission from Das *et al.*, Nano Lett. **13**, 100 (2013). Copyright 2013 American Chemical Society.

2D semiconductor from the metal contacts.<sup>272,273</sup> Phase engineering, as the third method, is discussed in Sec. IV D.<sup>223</sup>

Two mechanisms of carrier transport occur in the metal-2D semiconductor Schottky junction depending on the band bending configurations: thermionic emission (TE) and thermally assisted tunneling (TAT). Carrier TE is dominating in the current-off state while TAT transport through the Schottky barrier dominates in the current-on state. The Schottky barrier height can be derived from the conventional TE theory when the TE process is dominating.<sup>268</sup>

## B. p-n junction

### 1. 2D-3D semiconductor heterostructures

A straightforward approach to combine the merits of both 2D semiconductors and conventional bulk semiconductors is to form a p-n junction. Various 2D-bulk p-n junctions, such as MoS<sub>2</sub>-Si, have been demonstrated to build promising devices, including broadband photodetectors and light-emitting diodes.<sup>274,275</sup> Based on the bilayer MoS<sub>2</sub>-Ge heterostructure, a novel tunnel-FET driven by the band-to-band tunneling mechanism is demonstrated, allowing the sub-threshold swing (down to 3.9 mV per decade) to overcome

the fundamental thermionic limitation of the conventional FET (60 mV per decade).<sup>276</sup> Charge transfer in the 2D-bulk p-n junction can greatly alter the properties of the 2D semiconductor. For instance, charge transfer in the MoS<sub>2</sub>-GaN heterojunction can cause a 20-fold PL enhancement of MoS<sub>2</sub>.<sup>277</sup>

### 2. 2D-2D semiconductor vertical heterostructures

vdWHs constructed by 2D materials offer novel platforms for building fundamental structures without requirements of lattice matching. Among these vdWHs, the 2D p-n junction as schematically illustrated in Fig. 17(a), which is the most basic building block for constructing various devices, exhibits a lot of intriguing properties including the unconventional depletion region, interlayer exciton coupling, gate tunable carrier transport, etc. Moreover, by exquisitely designing the configuration of the 2D p-n junction, some extraordinary performances in electrical and optoelectronic fields can be achieved.

As is well known, the carrier depletion region in the conventional p-n junction forms the built-in field, which accounts for the band bending within the depletion length (usually submicron level), resulting in the current rectifying

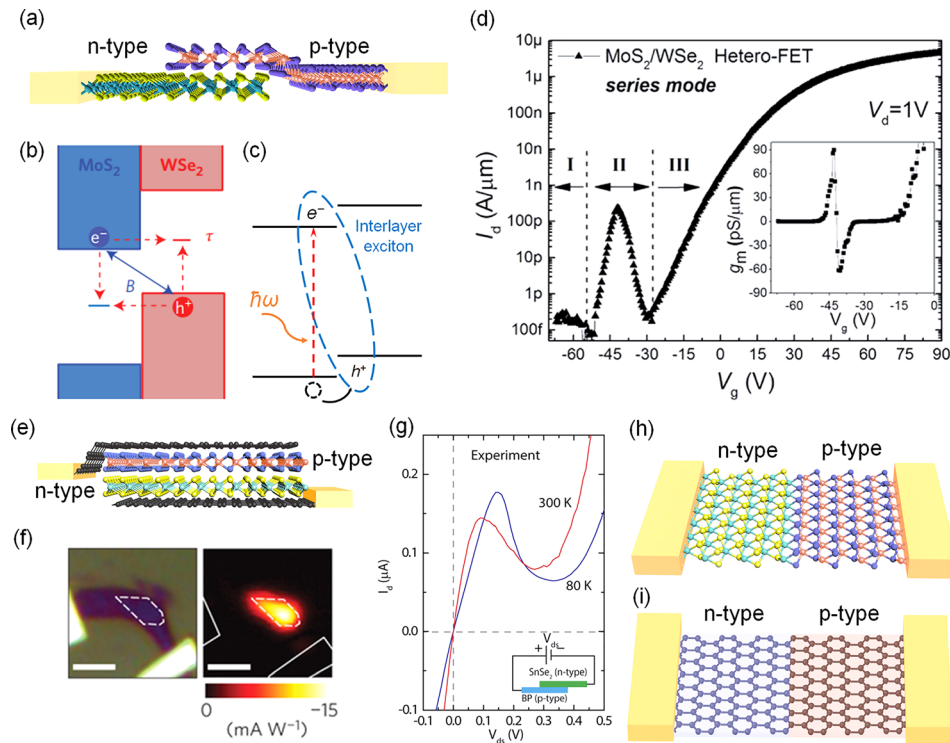


FIG. 17. (a) Schematic of vdW p-n junction. (b) Simulated band alignments in the vertical direction of the atomically thin WSe<sub>2</sub>-MoS<sub>2</sub> p-n junction under forward bias. Electrons in the conduction band edge of MoS<sub>2</sub> and holes in the valence band edge of WSe<sub>2</sub> undergo interlayer recombination. The red dashed arrows and blue arrows indicate the two possible recombination mechanisms: Shockley-Read-Hall and Langevin recombination, respectively.<sup>278</sup> Reprinted with permission from Lee *et al.*, Nat. Nanotechnol. **9**, 676 (2014). Copyright 2014 Macmillan Publishers Limited. (c) Schematic of the band alignment of the 2D type II heterojunction. Photoexcited electrons and holes are separated, forming an interlayer exciton (red dashed ellipse). (d) Transfer curve of the 2D WSe<sub>2</sub>-MoS<sub>2</sub> hetero-FET measured in the series mode (1 V drain voltage), which exhibits antibipolar behavior. The inset presents the transconductance near the peak in region II.<sup>287</sup> Reprinted with permission from Nourbakhsh *et al.*, Nano Lett. **16**, 1359 (2016). Copyright 2016 American Chemical Society. (e) Schematic of graphene electrodes sandwiched 2D vertical p-n junction. (f) Optical image and corresponding photocurrent map of the graphene sandwiched 2D vertical p-n junction. Scale bar: 3  $\mu$ m.<sup>278</sup> Reprinted with permission from Lee *et al.*, Nat. Nanotechnol. **9**, 676 (2014). Copyright 2014 Macmillan Publishers Limited. (g) Current-voltage characteristics of the 2D degenerated BP-SnSe<sub>2</sub> tunnel diode measured at 80 K and 300 K. The inset shows the schematic of the device.<sup>290</sup> Reprinted with permission from Yan *et al.*, Nano Lett. **15**, 5791 (2015). Copyright 2015 American Chemical Society. (h) Schematic of the lateral 2D p-n junction. (i) Schematic of the lateral graphene p-n homojunction.

behavior of the p-n junction. However, the 2D vdW p-n junction, in which both the vertical p- and n-channels are atomically thin, could have completely distinguished carrier transport mechanisms from those in the bulk p-n junction. Figure 17(b) illustrates the band diagrams of the WSe<sub>2</sub>-MoS<sub>2</sub> p-n junction under forward bias in the vertical direction. Within each semiconductor lateral transport channel, no appreciable potential barriers can be detected [Fig. 17(b)].<sup>278</sup> The lack of the depletion region in the 2D vdW p-n junction makes the forward bias current to be governed by interlayer carrier recombination instead of band bending modification. Two physical mechanisms may be attributed to the interlayer recombination between electrons in the conduction band of MoS<sub>2</sub> and holes in the valence band of WSe<sub>2</sub>: Shockley–Read–Hall recombination assisted by carrier tunneling into trap states and Langevin recombination associated with the interlayer exciton.<sup>278</sup> At a reverse bias, however, depletion of holes in WSe<sub>2</sub> and electrons in MoS<sub>2</sub> occurs in the junction area, causing the large band bending between overlapping (junction) and non-overlapping (homogeneous material) regions in the lateral direction.<sup>278</sup>

Theoretical calculations have predicted the type-II band alignment of various 2D vdWHs, such as WS<sub>2</sub>-MoS<sub>2</sub>, WS<sub>2</sub>-MoSe<sub>2</sub>, and WSe<sub>2</sub>-MoSe<sub>2</sub> vdWHs.<sup>279–281</sup> This facilitates the exciton dissociation in the 2D vdW p-n junction, which is essential in optoelectronic applications such as photodetection and light harvesting. Experimental results have shown ultrafast carrier transfer in the 2D p-n junction (hole transfer rate  $\sim$ 50 fs in the WS<sub>2</sub>-MoS<sub>2</sub> junction).<sup>282</sup> After the photo-excited electrons and holes relaxed to the conduction band edge of the n-type TMD and the valence band edge of the p-type TMD, interlayer excitons are formed by the Coulomb interaction (interlayer coupling), as shown in Fig. 17(c).<sup>283,284</sup> The novel interlayer exciton in the 2D p-n junction can be clearly detected by PL spectroscopy.<sup>284,285</sup> The lifetime of an interlayer exciton can be much longer than that of an intralayer exciton, resulting from the spatially indirect nature and the lowest energy configuration of the interlayer exciton. Moreover, electrical gating can modify the band alignment of the 2D p-n junction and thus tune the interlayer exciton resonance.<sup>284</sup> On the other hand, light absorption associated with the interlayer transition is observed in 2D vdW p-n junctions, while the photon energy is much lower than the intrinsic bandgap of each individual material.<sup>286</sup> These strong interlayer coupling effects in atomically thin p-n junction originate from the 2D nature and the lack of depletion region in vdWHs, which differs a lot from the case of the conventional bulk p-n junction.

The atomically thin nature of the 2D vdW p-n junction enables the electrostatically tunable carrier transport behavior. The gate-dependent transport of the 2D vdWHs results from the integrated effects of transfer characteristics of individual p- and n-channels. As is shown in Fig. 17(d), the transfer curve of the hetero-FET on the 2D WSe<sub>2</sub>-MoS<sub>2</sub> p-n junction has three distinct regions.<sup>287</sup> Large series resistance occurs at the junction when either of the 2D semiconductors is depleted, resulting in the low drain current even the other 2D semiconductor is carrier conducting. The intriguing anti-bipolar behavior of the p-n junction is exclusive to the 2D

system with tunable carrier concentration, providing a unique platform for circuit and optoelectronic applications, for instance, wavelength-selective light detection by electrical gating.<sup>288</sup>

Both the overlapping junction region and the non-overlapping individual 2D material region of the 2D vdW p-n junction contribute to its carrier transport. Taking 2D MoTe<sub>2</sub>-MoS<sub>2</sub> junction as an example, it is found that the device properties, such as drain current, are strongly dependent on the device configuration (short or long non-overlapping region).<sup>289</sup> In fact, the non-overlapping channel with high resistance causes the relatively low on-current density and low electrical/photonic response speed in the stacking 2D p-n diode, which limits its potential in practical applications. One solution is to apply transparent graphene as electrodes on the all-overlapping vertical stacking 2D p-n junction [Fig. 17(e)].<sup>278</sup> This device configuration enables an atomically thin semiconducting channel, giving rise to the large on-current density and efficient photoexcited carrier separation in the junction region [Fig. 17(f)].

The tunnel diode (Esaki diode) can be fabricated on 2D vdWHs using highly doped 2D materials or dual-gated configuration to achieve the broken-gap band alignment.<sup>290,291</sup> For example, prominent negative differential resistance (NDR) behavior was observed in the degenerate 2D BP-SnSe<sub>2</sub> p-n junction even at room temperature [Fig. 17(g)].<sup>290</sup> Carrier band-to-band tunneling dominates the forward-bias transport in the NDR region. 2D tunnel diodes pave the way for potential applications such as tunnel-FET for low-power electronics, oscillator circuit, and multi-valued logics.

### 3. 2D-2D semiconductor lateral heterostructures

Apart from the widely studied 2D vertical vdWHs, 2D lateral heterostructures [Fig. 17(h)] have gained increasing attention because of the atomically sharp interface with covalent bonds and the easier band offset tuning in the lateral junction.<sup>155–159,292</sup> The in-plane junction configuration results in carrier transporting through the lateral direction without interlayer transport. In this regard, the 2D lateral p-n heterojunction has band bending and finite depletion region, which is similar to the bulk p-n junction. Using scanning Kelvin probe force microscopy, researchers are able to determine the built-in field profile and the depletion length in the 2D lateral heterojunction.<sup>155,159</sup>

### 4. Homostructures

As the ion injection technique at present is not available for 2D materials, alternative methods, such as dual gating configuration, selective chemical doping, and layer engineering, are applied to fabricate the lateral p-n homostructure in 2D materials (such as MoS<sub>2</sub>, MoSe<sub>2</sub>, and WSe<sub>2</sub>) for optoelectronics.<sup>293–295</sup> On the other hand, the graphene p-n homojunction [Fig. 17(i)] shows some distinguished electronic properties due to its special carrier behaviors. The current rectifying effect cannot be observed because the electrons in graphene are ruled by the Klein tunneling effect.<sup>32</sup> However, open circuit voltage and photocurrent at the graphene p-n homojunction mainly come from the photo-thermoelectric

effect, which makes it promising for photodetectors.<sup>296,297</sup> Negative reflection and focus lens effects of electron in the graphene p-n homojunction can be observed.<sup>34,35,298</sup>

## VI. DEVICES AND APPLICATIONS

2D materials provide the opportunity for new device concepts due to the structural features and their device building blocks. With this announcement, interest in 2D material-based devices soared, and continuous progress has been very rapid. Here, we briefly summarize the electronic and optoelectronic device achievements when 2D materials ignited a revolution in condensed-matter physics and sparked the interest of device engineers.

### A. Field effect transistors

After the great breakthrough regarding the effects of electric fields in graphene in 2004, graphene FETs and integrated circuits have been successfully demonstrated.<sup>299–301</sup> Due to the zero bandgap as mentioned before, the on/off ratio is limited in graphene-based FETs.<sup>24</sup> On the other hand, graphene-based electronic devices have potential applications in radio frequency communications.<sup>302</sup>

Thanks to the opened bandgap, 2D semiconductors are attracting attention for FETs. More importantly, 2D semiconductors are competitive alternatives in post-silicon semiconductor devices, because of their 2D nature for overcoming the limit of short-channel effect and the higher mobility compared to ultra-thin silicon.<sup>241</sup> 2D semiconductors based short channel transistors that could potentially continue Moore's law in the deep sub-nanometer node.<sup>303</sup> As the first demonstrated 2D semiconductor transistor in 2011, the monolayer MoS<sub>2</sub> FET with high-*k* dielectric HfO<sub>2</sub> as the top gate material can have a highly tunable *n*-type behavior with a current on/off ratio up to 10<sup>8</sup>.<sup>304</sup> With proper choice of scandium to build low-resistance source/drain contacts, a high carrier mobility of ~184 cm<sup>2</sup> V<sup>-1</sup> s<sup>-1</sup> is presented in the MoS<sub>2</sub> FET.<sup>268</sup> In FETs made from tungsten dichalcogenides such as WS<sub>2</sub> and WSe<sub>2</sub>, electron and hole transports are both involved, originating from the metal Fermi level pinning close to the middle of the bandgap in semiconductors.<sup>270,305,306</sup> In the case of some molybdenum dichalcogenides including MoS<sub>2</sub> and MoSe<sub>2</sub>, the metal Fermi levels are pinned near the conduction band edges of the TMDs, making the electron transport dominating in corresponding FETs.<sup>307,308</sup> Besides, few-layer InSe FET encapsulated with *h*-BN exhibits higher room-temperature mobility and on/off ratio, which enables the detection of the quantum Hall effect.<sup>309</sup> When BP transistors come into the 2D FETs family, their higher mobilities than TMD FETs and higher on/off ratio than graphene FETs make them attractive in certain applications.<sup>76,310</sup> In addition to BP, more elemental 2D materials (such as borophene, silicene, germanene, and stanene) are expected to be in device platforms although these materials are not easily synthesized and extremely unstable.<sup>311</sup>

Adopting *h*-BN as protecting layers for 2D materials has been proposed to prevent device property degradations due to its ultra-smooth surface with the absence of dangling

bonds, which can eliminate the disturbance of the lattice of the channel materials and reduce the dielectric-related scattering. For example, the field effect mobility and current on/off ratio of graphene on the *h*-BN sheet are enhanced to ~3 times and ~2 times of those of graphene on a bare SiO<sub>2</sub>/Si substrate, respectively.<sup>312</sup> Using *h*-BN as a gate dielectric layer in 2D FETs is another attractive application, which gives rise to the high-current-density performance with good transparency and flexibility.<sup>313</sup>

Significantly, the lack of dangling bonds and the resulting more ideal interface of 2D heterostructures make 2D materials good candidates in tunnel-FETs for low-power applications,<sup>287,290,291,314</sup> and the carrier transport behavior is described in Sec. V B.

Figure 18 gives the comparison between FET properties (carrier mobility and on/off ratio) of various 2D materials. Generally, narrow bandgap brings high mobility but a low on/off ratio, while the wide bandgap results in a high on/off ratio and low mobility. High-mobility favors the high-frequency devices while high on/off ratio devices are available for low-power applications.

### B. Photodetectors

Photodetectors, which convert the absorbed optical signal into a measurable electrical signal, are one of the fundamental optoelectronic devices. Graphene and other 2D semiconductors are promising materials for photodetectors corresponding to the wavelength from visible light to far infrared. Generally, 2D material-based photodetectors can work in the photoconductor/phototransistor or photodiode mode.

The working principle of the photoconductor/phototransistor is based on the modification of carrier density and thus the conductivity of 2D materials under illumination [Fig. 19(a)]. Because of the ultrashort carrier lifetime and broadband light absorption, graphene is a promising material for photodetectors from visible light to far infrared [Fig. 19(b)].<sup>319,320</sup> However, the high dark current limits the detectivity of the graphene photoconductor. Photoconductor/

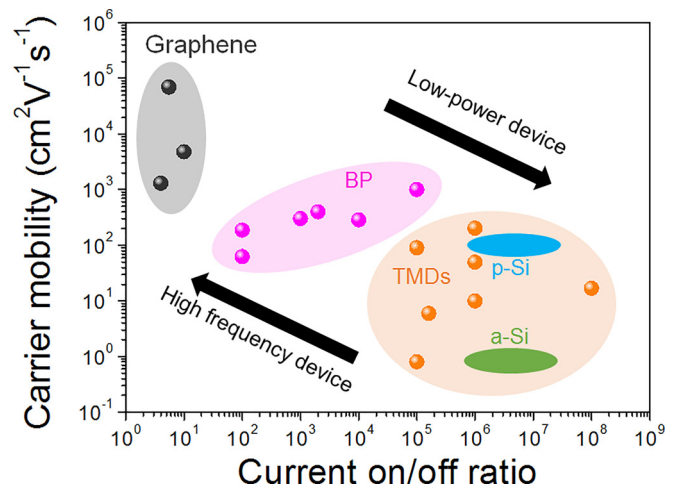


FIG. 18. Summary of carrier mobility and current on/off ratio of transistors made on various 2D materials and Si-based devices. Data are from Refs. 75, 76, 137, 138, 143, 269, 300, 301, 310, and 315–318.

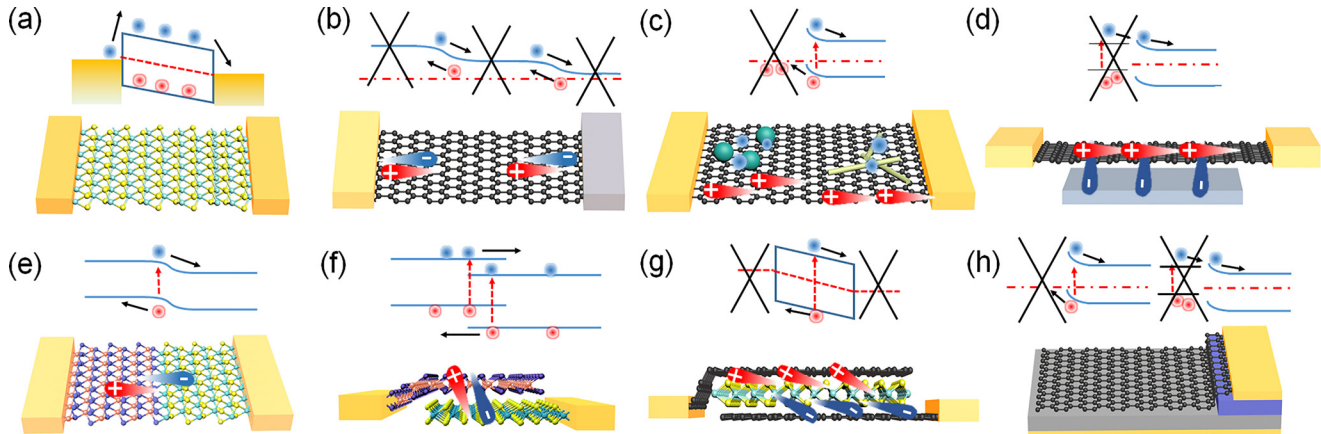


FIG. 19. Schematic of optoelectronic devices based on 2D materials, which are made of (a) 2D semiconductors; (b) graphene; (c) hybrid graphene/quantum dots or nanowires; (d) graphene-semiconductor junction, where graphene provides photo-induced carriers and the junction provides a vertical built-in field for separation of carriers; (e) lateral and (f) vertical 2D p-n junctions; (g) graphene-2D semiconductor-graphene junction; and (h) graphene-semiconductor Schottky junction for photodetection or photovoltaics.

phototransistors based on 2D TMDs exhibit low dark current and high responsivity, because of the large bandgap and relatively long carrier lifetime.<sup>321–325</sup> Through the gate effect, intrinsic carrier density and dark current of 2D TMDs can be further suppressed due to the easily tunable Fermi level. 2D semiconductors with narrow bandgaps are promising candidates for infrared photodetection. For example, BP phototransistors have an excellent external responsivity of 82 A/W in the mid-infrared range (3.39  $\mu\text{m}$ ).<sup>326</sup> There is another kind of novel hybrid photoconductor consisting of graphene and additional light absorption mediums (e.g., quantum dots, nanowires, and bulk semiconductors) [Fig. 19(c)].<sup>327,328</sup> In such a photoconductor, the built-in field formed by graphene and light absorption mediums can separate the photo-induced carriers generated at the absorption mediums and then inject holes/electrons into graphene. In fact, the photo-response beyond the light absorption region of semiconductors can also be detected contributing to the photo-induced carriers provided by graphene.<sup>329–331</sup> Unlike the pure graphene photoconductor/phototransistor, the built-in field at the interface can efficiently separate the photo-induced carriers and prolong their lifetime, resulting in the relatively high responsivity [Fig. 19(d)].<sup>331</sup> Besides, through introducing optical structures (e.g., plasmonic nanostructures,<sup>331–333</sup> photonic crystals,<sup>334</sup> optical cavities,<sup>335</sup> waveguides<sup>336–338</sup>) onto the device, the light-matter interaction in 2D materials can be improved and the performance of the 2D material-based photodetector can be enhanced.

Another working principle is the photodiode mode, which is based on the collection of the photoinduced carriers in the p-n junction or Schottky junction. Generally, the photodiode is working at the reverse bias in order to improve the built-in field and to accelerate the separation of carriers. For the lateral junction of 2D semiconductors, a built-in field forming in the depletion region can sweep out the photo-induced carriers, which is similar to that of the traditional photodiode. Normally, the dual gate is used to apply the lateral p-n homostructures [Fig. 17(i)]<sup>293,339</sup> or heterostructures [Fig. 19(e)],<sup>295</sup> and thus, the barrier height is tunable through the electrical gating. Therefore, it is possible to tune the

density of photo-induced carriers and get different photoresponses. In the vertical junction based on 2D semiconductors, the depletion region takes place at the whole interface of 2D materials, which differs from the lateral junction in which the depletion region only exists near the boundary line of two materials, allowing the higher external quantum efficiency [Fig. 19(f)].<sup>278,340,341</sup> Particularly, the interlayer transition between two materials can also be used for infrared photodetection, such as in the MoTe<sub>2</sub>-MoS<sub>2</sub> junction at 1.55  $\mu\text{m}$ .<sup>286</sup> In fact, graphene-2D semiconductor-graphene can form vertical heterostructures, in which a ultrafast response time and high quantum efficiency can be observed because of the atomic thick semiconductor layer [Fig. 19(g)].<sup>342–345</sup> Besides, the graphene-semiconductor Schottky junction is an important type of graphene-based photodetector [Fig. 19(h)], which can exhibit photoresponse from visible light to infrared light.<sup>346–353</sup> In particular, low-energy photons can be detected in graphene-based heterostructures through the photo-thermionic effect, in which the hot carriers are emitted over the barrier, thus creating photocurrent.<sup>354–356</sup>

### C. Photovoltaic devices

Photovoltaic devices are the devices (also known as solar cells) that convert solar energy into electrical energy through the photovoltaic effect based on the p-n junction or the Schottky junction. In recent decades, the dramatic appearance of single atomic layer materials provided a promising trend to the development of photovoltaic devices.

This photovoltaic concept of 2D material-based heterostructures is first demonstrated in the graphene-Si Schottky junction in 2010 [Fig. 19(h)].<sup>263</sup> In this simple structure, graphene served not only as a transparent electrode but also as the layer for hole transport. Moreover, graphene and other 2D semiconductors can form Schottky or p-n heterojunctions with other inorganic or organic semiconductors to form photovoltaic devices.<sup>357–359</sup> To obtain high-efficiency performance, more collection and less recombination of electron-hole pairs throughout the photovoltaic devices are necessary.<sup>360</sup> Some improved methods, such as interface

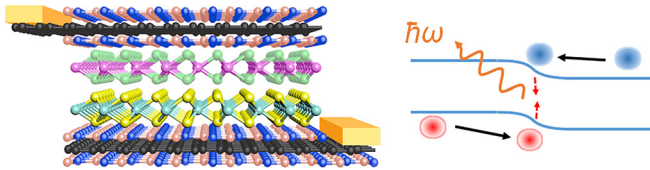


FIG. 20. Schematic of the LED made of the graphene sandwiched 2D p-n junction.

improvement,<sup>361</sup> material doping,<sup>362–366</sup> and optical structure design,<sup>361,367</sup> are applied to the much more efficient and stable photovoltaic devices, and the power conversion efficiency has exceeded 15%.<sup>361</sup> Furthermore, in the atomically sharp 2D vdW p-n junctions (such as MoS<sub>2</sub>-WSe<sub>2</sub>), efficient photoinduced carriers can be separated and high external quantum efficiencies can be achieved [Fig. 19(f)].<sup>85,368</sup> A unique feature of these vdW photovoltaic devices is the tunable majority carrier density by the gate voltage. In particular, the sandwich structure with 2D semiconductors for the light absorber between graphene (such as graphene-TMDs-graphene) can achieve efficient photoinduced carrier separation when the work function of graphene is modified by gate voltage or doping methods [Fig. 19(g)].<sup>342–344</sup> In the future, various other configured designs and optoelectronic effects of 2D material-based heterostructures, for instance, multiple junctions, localized surface plasmons, thermophotovoltaic effect, and hot carrier concept, are urgently needed for enhancing the power conversion efficiency.

#### D. Light emission devices

The unique band structures of monolayer TMD semiconductors with direct bandgaps of visible to NIR ranges make them promising candidates for light generation. Electroluminescence (EL) is realized in the monolayer MoS<sub>2</sub> FET, which arises from the same excited state (exciton A).<sup>369</sup> It is found that the EL emission is localized at the metal contacts, which can be attributed to the maximized exciton generation efficiency through impact excitation at carrier injection areas. Hence, the homogeneous 2D material device is not likely suitable for practical light emission application since the quantum efficiency is limited ( $\sim 10^{-5}$  for monolayer MoS<sub>2</sub>).<sup>370</sup> An effective solution is to build a p-n

junction (light emission diode, LED) for light generation (Fig. 20). The lateral p-n junction in monolayer TMDs by the dual-gating strategy is first achieved for light emission in 2014.<sup>293,370,371</sup> Apart from the lateral LED where the active region is still localized by the depletion region, vertical vdWHs are also raised up for efficient carrier injection in LED with its large active region at the whole overlapping area.<sup>278,340</sup> In order to reduce the leakage current in the vertical stacking structures, functional stacking structures for light emission are developed by inserting tunneling layers (e.g., *h*-BN and Al<sub>2</sub>O<sub>3</sub>) into the p-n junction and/or the electrode contacts, which enables the long lifetime of excitons in TMD quantum wells.<sup>372,373</sup> With this band-structure engineering strategy, the EL quantum efficiency of 10% could be achieved in monolayer TMDs, which is comparable to those of organic LEDs.<sup>372</sup>

Quantum emitters (made of quantum confined structures such as quantum dots and defects) can generate single photons, which is crucial for applications such as quantum information and high-resolution metrology. TMD quantum emitters with a very sharp photon emission spectrum are fabricated.<sup>374–376</sup> Furthermore, laser, which generates coherent light source, has been implemented in the 2D system. Monolayer WSe<sub>2</sub> as the gain medium coupling to an exquisitely designed photonic crystal cavity structure shows an ultralow optical pumping threshold (27 nW at 130 K).<sup>377</sup>

#### E. Electro-optic modulators

The optical modulator is used for tuning the properties (e.g., intensity and phase) of the incident EMW. Graphene is a promising material for the modulator device due to its tunable dielectric constant.

According to the discussion in Sec. II B, the transmission of graphene can be changed by electrostatic gating and the light absorption can be modified from 0.5% (out of interband transition) to 2.3% (constant absorption of interband transition). The modulation depth is limited due to the ultra-short interaction length (atomic thickness) between graphene and light. For increasing the interaction length, graphene can be integrated into the waveguide, which is first demonstrated in 2011 [Fig. 21(a)].<sup>378</sup> Another way is using the optical resonance structures, such as plasmonic structures<sup>379</sup> and

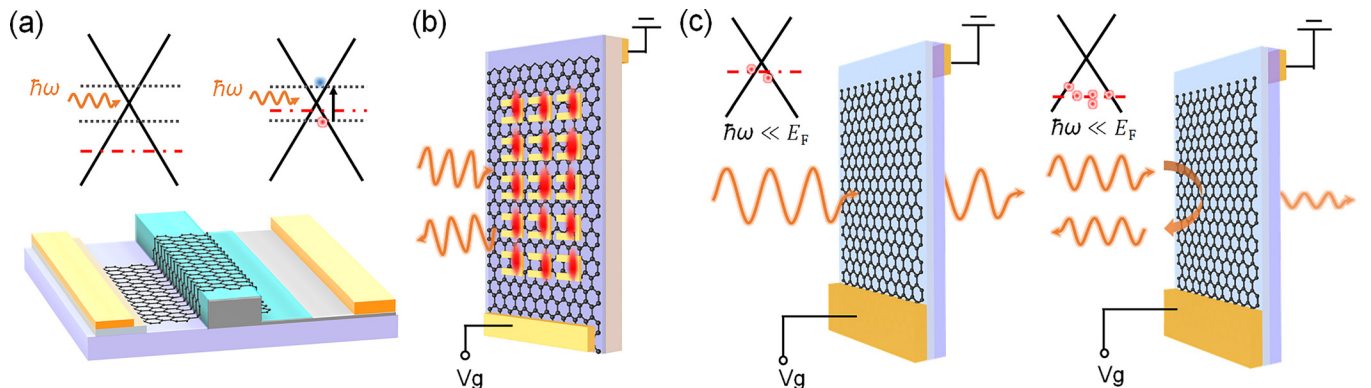


FIG. 21. Schematic of electro-optic modulators based on graphene. (a) Graphene-based waveguide-integrated optical modulator. (b) Mid-infrared modulator based on the hybridization of metal plasmonic and graphene. (c) Graphene-based THz modulator.

optical cavities,<sup>380</sup> in which light will be trapped and the interaction time with graphene will be improved. In theory, the special plasmonic structure can be designed to support polarization-independent/depend on resonance, even chiral resonance. Therefore, it is possible to design a graphene modulator with polarization or chiral properties.

In this mid/far infrared region, the photon energy is beyond the interband transition and the electrons in graphene behave similar to those in the novel metal. The dielectric constant of graphene is composed of the apparent negative real part and a small imaginary part, which can support the intrinsic plasmonic effect. One unique property in this region is the highly tunable dielectric constant of graphene, resulting in a tunable intrinsic plasmonic effect for modulator design.<sup>56,58</sup> In fact, the tunable Ohmic loss of graphene (imaginary part of the dielectric constant) can also be used for designing the modulator. This effect is found in the localized plasmonic effect of graphene nanopatterns, in which the absorption efficiency can be modulated from less than 3% to 30% in the infrared region.<sup>381</sup> On the other hand, a modulator can also be designed based on hybrid plasmonics, where graphene with a highly tunable dielectric constant is used as a media introduced into a metal plasmonic structure [Fig. 21(b)]. The graphene hybrid plasmonic device with a modulation depth up to 100% can be achieved on the metasurface (one kind of plasmonic structure).<sup>382–384</sup>

In the THz region, the optical property of graphene is dominated by the imaginary part of the dielectric constant, because the frequency of this region is near the damping frequency ( $\tau^{-1}$ ) of graphene. The damping will consume the incident light's energy, which depends on the carrier concentration of graphene, and thus, the graphene-based THz modulator can be designed [Fig. 21(c)]. In order to improve the interaction between graphene and THz wave, many optical structures are introduced, including internal total reflection,<sup>385</sup> Fabry-Pérot cavities,<sup>386</sup> metamaterials,<sup>387</sup> plasmonic structures<sup>388</sup> and so on.

## VII. OUTLOOK: LEARN FROM THE HISTORY

The new revolution in semiconductor technology is emerging. 2D materials provide the most exciting solutions for next generation nanoelectronics and optoelectronics. The breakthrough of science and technology in 2D materials has been extended for the past decade, bringing together the community of scientists and engineers.<sup>389,390</sup> Although the fundamental research of structure-property relationships of 2D materials for electronics and optoelectronics has made rapid progress, the killer applications and niche markets still seem to face great challenges ahead. Learn from the success of Si's story: Si-based technology has been dominant in the semiconductor industry since the end of the 1950s although Si is a mediocre material. The major reasons for the wide applications of Si in integrated circuits and devices are unique planar technology (such as growth, oxidation, lithography, etching, and doping) and its superb oxide directly grown on Si with superior mechanical and thermal stability, electrical insulation, and chemical passivation at the interface. Now from the scientific and technological viewpoints,

manipulation of the atomic-layer materials to precisely tailor the performance requirements of the device still faces major urgent challenges:

- Developing new techniques for the scalable and fast synthesis of defect-free 2D materials, particularly on multiple substrates with the transfer or transfer-free process compatible with existing technologies;
- Controlling the number of layers, domain size, and doping level of 2D materials;
- Utilizing the surface and interface-induced novel effects in 2D material-based mixed-dimensional heterostructures;
- Designing the novel functions and unique features of 2D material-based competitive devices (e.g., tunnel devices, flexible or wearable electronics, and sensors/detectors/modulators with performances beyond the state-of-the-art).

Science and technology are concomitantly advancing, and a new class of phenomena may contribute to the development of novel technological capabilities. Graphene, other 2D materials, and related heterostructures offer the promise for people to play at the bottom and evoke our expectations for future technological revolution, thus further challenging the existing models of physics and providing new phenomena for scientists to explore. It should be clearly reminded that active research and development of 2D materials is still in the early stages. When we look at the history books of science and technology, to a large extent, every story looks similar in that progress was always slow and difficult, and it took time for the commercial applications of most advanced materials.

## ACKNOWLEDGMENTS

This work was supported by the National Natural Science Foundation of China (51402060, 51372133, 61229401, and 61325020). X. R. Wang would like to thank the National Key Basic Research Program of China (2013CBA01604). J. B. Xu would like to thank the Research Grants Council of Hong Kong, particularly, via Grant Nos. AoE/P-03/08, AoE/P-02/12, 14207515, 14204616, and CUHK Group Research Scheme. We also thank Yuxuan Lin (Massachusetts Institute of Technology, USA) and Shijun Liang (Singapore University of Technology and Design) for proof reading and scientific discussions.

<sup>1</sup>K. S. Novoselov, A. K. Geim, S. V. Morozov, D. Jiang, Y. Zhang, S. V. Dubonos, I. V. Grigorieva, and A. A. Firsov, *Science* **306**, 666 (2004).

<sup>2</sup>H. Kroemer, *Rev. Mod. Phys.* **73**, 783 (2001).

<sup>3</sup>R. P. Feynman, *Eng. Sci.* **23**, 22 (1960), see <http://caltech.library.caltech.edu/1976/>.

<sup>4</sup>P. R. Wallace, *Phys. Rev.* **71**, 622 (1947).

<sup>5</sup>H. P. Boehm, A. Clauss, G. O. Fischer, and U. Hofmann, *Z. Naturforsch. B* **17**, 150 (1962), see [http://zfn.mpd1.mpg.de/data/Reihe\\_B/17/ZNB-1962-17b-0150.pdf](http://zfn.mpd1.mpg.de/data/Reihe_B/17/ZNB-1962-17b-0150.pdf).

<sup>6</sup>J. C. Shelton, H. R. Patil, and J. M. Blakely, *Surf. Sci.* **43**, 493 (1974).

<sup>7</sup>A. J. Van Bommel, J. E. Crombeen, and A. Van Tooren, *Surf. Sci.* **48**, 463 (1975).

<sup>8</sup>X. Lu, M. Yu, H. Huang, and R. S. Ruoff, *Nanotechnology* **10**, 269 (1999).

<sup>9</sup>E. Fitzer, K. H. Kochling, H. P. Boehm, and H. Marsh, *Pure Appl. Chem.* **67**, 473 (1995).

<sup>10</sup>P. Avouris, Z. Chen, and V. Perebeinos, *Nat. Nanotechnol.* **2**, 605 (2007).

- <sup>11</sup>D. Jariwala, V. K. Sangwan, L. J. Lauhon, T. J. Marks, and M. C. Hersam, *Chem. Soc. Rev.* **42**, 2824 (2013).
- <sup>12</sup>X. M. Li, Z. Lv, and H. W. Zhu, *Adv. Mater.* **27**, 6549 (2015).
- <sup>13</sup>A. K. Geim and I. V. Grigorieva, *Nature* **499**, 419 (2013).
- <sup>14</sup>Y. Liu, N. O. Weiss, X. Duan, H. Cheng, Y. Huang, and X. Duan, *Nat. Rev. Mater.* **1**, 16042 (2016).
- <sup>15</sup>D. Jariwala, T. J. Marks, and M. C. Hersam, *Nat. Mater.* **16**, 170 (2017).
- <sup>16</sup>K. S. Novoselov, A. Mishchenko, A. Carvalho, and A. H. Castro Neto, *Science* **353**, aac9439 (2016).
- <sup>17</sup>P. Ajayan, P. Kim, and K. Banerjee, *Phys. Today* **69**(9), 38 (2016).
- <sup>18</sup>X. Li and H. Zhu, *Phys. Today* **69**(9), 46 (2016).
- <sup>19</sup>A. H. Castro Neto, F. Guinea, N. M. R. Peres, K. S. Novoselov, and A. K. Geim, *Rev. Mod. Phys.* **81**, 109 (2009).
- <sup>20</sup>K. S. Novoselov, A. K. Geim, S. V. Morozov, D. Jiang, M. I. Katsnelson, I. V. Grigorieva, S. V. Dubonos, and A. A. Firsov, *Nature* **438**, 197 (2005).
- <sup>21</sup>S. Das Sarma, S. Adam, E. H. Hwang, and E. Rossi, *Rev. Mod. Phys.* **83**, 407 (2011).
- <sup>22</sup>Y. W. Tan, Y. Zhang, K. Bolotin, Y. Zhao, S. Adam, E. H. Hwang, S. Das Sarma, H. L. Stormer, and P. Kim, *Phys. Rev. Lett.* **99**, 246803 (2007).
- <sup>23</sup>J. H. Chen, C. Jang, S. Adam, M. S. Fuhrer, E. D. Williams, and M. Ishigami, *Nat. Phys.* **4**, 377 (2008).
- <sup>24</sup>F. Schwierz, *Nat. Nanotechnol.* **5**, 487 (2010).
- <sup>25</sup>Y. Son, M. L. Cohen, and S. G. Louie, *Phys. Rev. Lett.* **97**, 216803 (2006).
- <sup>26</sup>M. Y. Han, B. Özyilmaz, Y. Zhang, and P. Kim, *Phys. Rev. Lett.* **98**, 206805 (2007).
- <sup>27</sup>J. B. Oostinga, H. B. Heersche, X. Liu, A. F. Morpurgo, and L. M. K. Vandersypen, *Nat. Mater.* **7**, 151 (2008).
- <sup>28</sup>Y. Zhang, T. Tang, C. Girit, Z. Hao, M. C. Martin, A. Zettl, M. F. Crommie, Y. Ron Shen, and F. Wang, *Nature* **459**, 820 (2009).
- <sup>29</sup>Z. H. Ni, T. Yu, Y. H. Lu, Y. Y. Wang, Y. P. Feng, and Z. X. Shen, *ACS Nano* **2**, 2301 (2008).
- <sup>30</sup>P. E. Allain and J. N. Fuchs, *Eur. Phys. J. B* **83**, 301 (2011).
- <sup>31</sup>M. I. Katsnelson, K. S. Novoselov, and A. K. Geim, *Nat. Phys.* **2**, 620 (2006).
- <sup>32</sup>N. Stander, B. Huard, and D. Goldhaber-Gordon, *Phys. Rev. Lett.* **102**, 026807 (2009).
- <sup>33</sup>A. G. Moghaddam and M. Zareyan, *Phys. Rev. Lett.* **105**, 146803 (2010).
- <sup>34</sup>S. Chen, Z. Han, M. M. Elahi, K. M. Masum Habib, L. Wang, B. Wen, Y. Gao, T. Taniguchi, K. Watanabe, J. Hone, A. W. Ghosh, and C. R. Dean, *Science* **353**, 1522 (2016).
- <sup>35</sup>V. V. Cheianov, V. Fal'ko, and B. L. Altshuler, *Science* **315**, 1252 (2007).
- <sup>36</sup>K. I. Bolotin, K. J. Sikes, Z. Jiang, M. Klima, G. Fudenberg, J. Hone, P. Kim, and H. L. Stormer, *Solid State Commun.* **146**, 351 (2008).
- <sup>37</sup>J. Chen, C. Jang, S. Xiao, M. Ishigami, and M. S. Fuhrer, *Nat. Nanotechnol.* **3**, 206 (2008).
- <sup>38</sup>K. Chen, X. Wan, D. Liu, Z. Kang, W. Xie, J. Chen, Q. Miao, and J. Xu, *Nanoscale* **5**, 5784 (2013).
- <sup>39</sup>E. H. Hwang and S. Das Sarma, *Phys. Rev. B* **77**, 115449 (2008).
- <sup>40</sup>J. Chen, W. G. Cullen, C. Jang, M. S. Fuhrer, and E. D. Williams, *Phys. Rev. Lett.* **102**, 236805 (2009).
- <sup>41</sup>T. O. Wehling, S. Yuan, A. I. Lichtenstein, A. K. Geim, and M. I. Katsnelson, *Phys. Rev. Lett.* **105**, 056802 (2010).
- <sup>42</sup>C. H. Lui, L. Liu, K. F. Mak, G. W. Flynn, and T. F. Heinz, *Nature* **462**, 339 (2009).
- <sup>43</sup>W. Zhu, T. Low, V. Perebeinos, A. A. Bol, Y. Zhu, H. Yan, J. Tersoff, and P. Avouris, *Nano Lett.* **12**, 3431 (2012).
- <sup>44</sup>L. Levitov and G. Falkovich, *Nat. Phys.* **12**, 672 (2016).
- <sup>45</sup>J. Crossno, J. K. Shi, K. Wang, X. Liu, A. Harzheim, A. Lucas, S. Sachdev, P. Kim, T. Taniguchi, K. Watanabe, T. A. Ohki, and K. C. Fong, *Science* **351**, 1058 (2016).
- <sup>46</sup>D. A. Bandurin, I. Torre, R. K. Kumar, M. B. Shalom, A. Tomadin, A. Principi, G. H. Auton, E. Khestanova, K. S. Novoselov, I. V. Grigorieva, L. A. Ponomarenko, A. K. Geim, and M. Polini, *Science* **351**, 1055 (2016).
- <sup>47</sup>P. Avouris, *Nano Lett.* **10**, 4285 (2010).
- <sup>48</sup>Z. Q. Li, E. A. Henriksen, Z. Jiang, Z. Hao, M. C. Martin, P. Kim, H. L. Stormer, and D. N. Basov, *Nat. Phys.* **4**, 532 (2008).
- <sup>49</sup>K. F. Allison, D. Borka, I. Radović, L. Hadžievski, and Z. L. Mišković, *Phys. Rev. B* **80**, 195405 (2009).
- <sup>50</sup>M. Jablan, H. Buljan, and M. Soljačić, *Phys. Rev. B* **80**, 245435 (2009).
- <sup>51</sup>R. R. Nair, P. Blake, A. N. Grigorenko, K. S. Novoselov, T. J. Booth, T. Stauber, N. M. R. Peres, and A. K. Geim, *Science* **320**, 1308 (2008).
- <sup>52</sup>S. Winnerl, M. Orlita, P. Plochocka, P. Kossacki, M. Potemski, T. Winzer, E. Malic, A. Knorr, M. Sprinkle, C. Berger, W. A. de Heer, H. Schneider, and M. Helm, *Phys. Rev. Lett.* **107**, 237401 (2011).
- <sup>53</sup>F. H. L. Koppens, D. E. Chang, and F. Javier García de Abajo, *Nano Lett.* **11**, 3370 (2011).
- <sup>54</sup>E. H. Hwang and S. Das Sarma, *Phys. Rev. B* **75**, 205418 (2007).
- <sup>55</sup>Z. Fei, A. S. Rodin, G. O. Andreev, W. Bao, A. S. McLeod, M. Wagner, L. M. Zhang, Z. Zhao, M. Thiemens, G. Dominguez, M. M. Fogler, A. H. Castro Neto, C. N. Lau, F. Keilmann, and D. N. Basov, *Nature* **487**, 82 (2012).
- <sup>56</sup>J. Chen, M. Badioli, P. Alonso-Gonzalez, S. Thongrattanasiri, F. Huth, J. Osmond, M. Spasenovic, A. Centeno, A. Pesquera, P. Godignon, A. Z. Elorza, N. Camara, F. Javier Garcia de Abajo, R. Hillenbrand, and F. H. L. Koppens, *Nature* **487**, 77 (2012).
- <sup>57</sup>A. Woessner, M. B. Lundeberg, Y. Gao, A. Principi, P. Alonso-González, M. Carrega, K. Watanabe, T. Taniguchi, G. Vignale, M. Polini, J. Hone, R. Hillenbrand, and F. H. L. Koppens, *Nat. Mater.* **14**, 421 (2015).
- <sup>58</sup>G. X. Ni, L. Wang, M. D. Goldflam, M. Wagner, Z. Fei, A. S. McLeod, M. K. Liu, F. Keilmann, B. Özyilmaz, A. H. Castro Neto, J. Hone, M. M. Fogler, and D. N. Basov, *Nat. Photonics* **10**, 244 (2016).
- <sup>59</sup>D. Ansell, I. P. Radko, Z. Han, F. J. Rodriguez, S. I. Bozhevolnyi, and A. N. Grigorenko, *Nat. Commun.* **6**, 8846 (2015).
- <sup>60</sup>A. Y. Nikitin, P. Alonso González, S. Vélez, S. Mastel, A. Centeno, A. Pesquera, A. Zurutuza, F. Casanova, L. E. Hueso, F. H. L. Koppens, and R. Hillenbrand, *Nat. Photonics* **10**, 239 (2016).
- <sup>61</sup>H. Yan, T. Low, W. Zhu, Y. Wu, M. Freitag, X. Li, F. Guinea, P. Avouris, and F. Xia, *Nat. Photonics* **7**, 394 (2013).
- <sup>62</sup>H. Yan, X. Li, B. Chandra, G. Tulevski, Y. Wu, M. Freitag, W. Zhu, P. Avouris, and F. Xia, *Nat. Nanotechnol.* **7**, 330 (2012).
- <sup>63</sup>S. Thongrattanasiri, F. H. L. Koppens, and F. Javier García de Abajo, *Phys. Rev. Lett.* **108**, 047401 (2012).
- <sup>64</sup>S. J. Allen, H. L. Störmer, and J. C. M. Hwang, *Phys. Rev. B* **28**, 4875 (1983).
- <sup>65</sup>W. S. Yun, S. W. Han, S. C. Hong, I. G. Kim, and J. D. Lee, *Phys. Rev. B* **85**, 033305 (2012).
- <sup>66</sup>A. Kuc, N. Zibouche, and T. Heine, *Phys. Rev. B* **83**, 245213 (2011).
- <sup>67</sup>D. Xiao, G. Liu, W. Feng, X. Xu, and W. Yao, *Phys. Rev. Lett.* **108**, 196802 (2012).
- <sup>68</sup>H. Zeng, J. Dai, W. Yao, D. Xiao, and X. Cui, *Nat. Nanotechnol.* **7**, 490 (2012).
- <sup>69</sup>O. V. Yazyev and A. Kis, *Mater. Today* **18**, 20 (2015).
- <sup>70</sup>J. S. Ross, S. Wu, H. Yu, N. J. Ghimire, A. M. Jones, G. Aivazian, J. Yan, D. G. Mandrus, D. Xiao, and W. Yao, *Nat. Commun.* **4**, 1474 (2013).
- <sup>71</sup>K. F. Mak, K. He, J. Shan, and T. F. Heinz, *Nat. Nanotechnol.* **7**, 494 (2012).
- <sup>72</sup>J. Kim, X. Hong, C. Jin, S. Shi, C. S. Chang, M. H. Chiu, L. J. Li, and F. Wang, *Science* **346**, 1205 (2014).
- <sup>73</sup>K. F. Mak, K. L. McGill, J. Park, and P. L. McEuen, *Science* **344**, 1489 (2014).
- <sup>74</sup>A. N. Rudenko and M. I. Katsnelson, *Phys. Rev. B* **89**, 201408 (2014).
- <sup>75</sup>F. Xia, H. Wang, and Y. Jia, *Nat. Commun.* **5**, 4458 (2014).
- <sup>76</sup>L. Li, Y. Yu, G. J. Ye, Q. Ge, X. Ou, H. Wu, D. Feng, X. H. Chen, and Y. Zhang, *Nat. Nanotechnol.* **9**, 372 (2014).
- <sup>77</sup>D. A. Chenet, O. B. Aslan, P. Y. Huang, C. Fan, A. M. van der Zande, T. F. Heinz, and J. C. Hone, *Nano Lett.* **15**, 5667 (2015).
- <sup>78</sup>F. Liu, S. Zheng, X. He, A. Chaturvedi, J. He, W. L. Chow, T. R. Mion, X. Wang, J. Zhou, Q. Fu, H. J. Fan, B. K. Tay, L. Song, R. H. He, C. Kloc, P. M. Ajayan, and Z. Liu, *Adv. Funct. Mater.* **26**, 1169 (2016).
- <sup>79</sup>B. Peng, P. K. Ang, and K. P. Loh, *Nano Today* **10**, 128 (2015).
- <sup>80</sup>J. A. Schuller, S. Karaveli, T. Schiros, K. He, S. Yang, I. Kymissis, J. Shan, and R. Zia, *Nat. Nanotechnol.* **8**, 271 (2013).
- <sup>81</sup>Y. L. Huang, Y. Chen, W. Zhang, S. Y. Quek, C. H. Chen, L. J. Li, W. T. Hsu, W. H. Chang, Y. J. Zheng, W. Chen, and A. T. S. Wee, *Nat. Commun.* **6**, 6298 (2015).
- <sup>82</sup>T. Cheiwchanchamnangij and W. R. L. Lambrecht, *Phys. Rev. B* **85**, 205302 (2012).
- <sup>83</sup>D. Kozawa, R. Kumar, A. Carvalho, K. K. Amara, W. Zhao, S. Wang, M. Toh, R. M. Ribeiro, A. H. Castro Neto, K. Matsuda, and G. Eda, *Nat. Commun.* **5**, 4543 (2014).
- <sup>84</sup>G. Eda, H. Yamaguchi, D. Voiry, T. Fujita, M. Chen, and M. Chhowalla, *Nano Lett.* **11**, 5111 (2011).

- <sup>85</sup>M. Bernardi, M. Palummo, and J. C. Grossman, *Nano Lett.* **13**, 3664 (2013).
- <sup>86</sup>K. F. Mak, K. He, C. Lee, G. H. Lee, J. Hone, T. F. Heinz, and J. Shan, *Nat. Mater.* **12**, 207 (2013).
- <sup>87</sup>S. Mouris, Y. Miyauchi, and K. Matsuda, *Nano Lett.* **13**, 5944 (2013).
- <sup>88</sup>X. Wang, A. M. Jones, K. L. Seyler, V. Tran, Y. Jia, H. Zhao, H. Wang, L. Yang, X. Xu, and F. Xia, *Nat. Nanotechnol.* **10**, 517 (2015).
- <sup>89</sup>Z. Liu and K. Aydin, *Nano Lett.* **16**, 3457 (2016).
- <sup>90</sup>K. Watanabe, T. Taniguchi, and H. Kanda, *Nat. Mater.* **3**, 404 (2004).
- <sup>91</sup>H. Wang, T. Taychatanapat, A. Hsu, K. Watanabe, T. Taniguchi, P. Jarillo-Herrero, and T. Palacios, *IEEE Electron Devices Lett.* **32**, 1209 (2011).
- <sup>92</sup>G. H. Lee, Y. J. Yu, C. Lee, C. Dean, K. L. Shepard, P. Kim, and J. Hone, *Appl. Phys. Lett.* **99**, 243114 (2011).
- <sup>93</sup>C. R. Dean, A. F. Young, I. Meric, C. Lee, L. Wang, S. Sorgenfrei, W. Watanabe, T. Taniguchi, P. Kim, K. L. Shepard, and J. Hone, *Nat. Nanotechnol.* **5**, 722 (2010).
- <sup>94</sup>C. R. Dean, L. Wang, P. Maher, C. Forsythe, F. Ghahari, Y. Gao, J. Katoch, M. Ishigami, P. Moon, and M. Koshino, *Nature* **497**, 598 (2013).
- <sup>95</sup>L. A. Ponomarenko, R. V. Gorbachev, G. L. Yu, D. C. Elias, R. Jalil, A. A. Patel, A. Mishchenko, A. S. Mayorov, C. R. Woods, and J. R. Wallbank, *Nature* **497**, 594 (2013).
- <sup>96</sup>B. Hunt, J. D. Sanchez-Yamagishi, A. F. Young, M. Yankowitz, B. J. LeRoy, K. Watanabe, T. Taniguchi, P. Moon, M. Koshino, and P. Jarillo-Herrero, *Science* **340**, 1427 (2013).
- <sup>97</sup>L. Britnell, R. V. Gorbachev, R. Jalil, B. D. Belle, F. Schedin, A. Mishchenko, T. Georgiou, M. I. Katsnelson, L. Eaves, and S. V. Morozov, *Science* **335**, 947 (2012).
- <sup>98</sup>S. Kang, N. Prasad, H. C. P. Movva, A. Rai, K. Kim, X. Mou, T. Taniguchi, K. Watanabe, L. F. Register, E. Tutuc, and S. K. Banerjee, *Nano Lett.* **16**, 4975 (2016).
- <sup>99</sup>Y. Hernandez, V. Nicolosi, M. Lotya, F. M. Blighe, Z. Sun, S. De, I. T. McGovern, B. Holland, M. Byrne, Y. K. Gun'Ko, J. J. Boland, P. Niraj, G. Duesberg, S. Krishnamurthy, R. Goodhue, J. Hutchison, V. Scardaci, A. C. Ferrari, and J. N. Coleman, *Nat. Nanotechnol.* **3**, 563 (2008).
- <sup>100</sup>W. Gu, W. Zhang, X. Li, H. Zhu, J. Wei, Z. Li, Q. Shu, C. Wang, K. Wang, W. Shen, F. Kang, and D. Wu, *J. Mater. Chem.* **19**, 3367 (2009).
- <sup>101</sup>Z. Zeng, Z. Yin, X. Huang, H. Li, Q. He, G. Lu, F. Boey, and H. Zhang, *Angew. Chem., Int. Ed.* **50**, 11093 (2011).
- <sup>102</sup>J. N. Coleman, M. Lotya, A. O'Neill, S. D. Bergin, P. J. King, U. Khan, K. Young, A. Gaucher, S. De, R. J. Smith, I. V. Shvets, S. K. Arora, G. Stanton, H. Y. Kim, K. Lee, G. T. Kim, G. S. Duesberg, T. Hallam, J. J. Boland, J. J. Wang, J. F. Donegan, J. C. Grunlan, G. Moriarty, A. Shmeliov, R. J. Nicholls, J. M. Perkins, E. M. Grieveson, K. Theuwissen, D. W. McComb, P. D. Nellist, and V. Nicolosi, *Science* **331**, 568 (2011).
- <sup>103</sup>J. Zheng, H. Zhang, S. Dong, Y. Liu, C. T. Nai, H. S. Shin, H. Y. Jeong, B. Liu, and K. P. Loh, *Nat. Commun.* **5**, 2995 (2014).
- <sup>104</sup>X. Li, T. Yang, Y. Yang, J. Zhu, L. Li, F. E. Alam, X. Li, K. Wang, H. Cheng, C. Lin, Y. Fang, and H. Zhu, *Adv. Funct. Mater.* **26**, 1322 (2016).
- <sup>105</sup>V. C. Tung, M. J. Allen, Y. Yang, and R. B. Kaner, *Nat. Nanotechnol.* **4**, 25 (2009).
- <sup>106</sup>S. Park, J. An, I. Jung, R. D. Piner, S. J. An, X. Li, A. Velamakanni, and R. S. Ruoff, *Nano Lett.* **9**, 1593 (2009).
- <sup>107</sup>D. C. Marcano, D. V. Kosynkin, J. M. Berlin, A. Sinitskii, Z. Sun, A. Slesarev, L. B. Alemany, W. Lu, and J. M. Tour, *ACS Nano* **4**, 4806 (2010).
- <sup>108</sup>D. Voiry, J. Yang, J. Kupferberg, R. Fullon, C. Lee, H. Y. Jeong, H. S. Shin, and M. Chhowalla, *Science* **353**, 1413 (2016).
- <sup>109</sup>X. Li, W. Cai, J. An, S. Kim, J. Nah, D. Yang, R. Piner, A. Velamakanni, I. Jung, E. Tutuc, S. K. Banerjee, L. Colombo, and R. S. Ruoff, *Science* **324**, 1312 (2009).
- <sup>110</sup>S. Bae, H. Kim, Y. Lee, X. Xu, J. Park, Y. Zheng, J. Balakrishnan, T. Lei, H. R. Kim, Y. Il Song, Y. Kim, K. S. Kim, B. Ozylilmaz, J. Ahn, B. H. Hong, and S. Iijima, *Nat. Nanotechnol.* **5**, 574 (2010).
- <sup>111</sup>A. Reina, X. Jia, J. Ho, D. Nezich, H. Son, V. Bulovic, M. S. Dresselhaus, and J. Kong, *Nano Lett.* **9**, 30 (2009).
- <sup>112</sup>K. S. Kim, Y. Zhao, H. Jang, S. Y. Lee, J. M. Kim, K. S. Kim, J. H. Ahn, P. Kim, J. Choi, and B. H. Hong, *Nature* **457**, 706 (2009).
- <sup>113</sup>J. Lee, E. K. Lee, W. J. Joo, Y. Jang, B. S. Kim, J. Y. Lim, S. H. Choi, S. J. Ahn, J. R. Ahn, M. Park, C. Yang, B. L. Choi, S. Hwang, and D. Whang, *Science* **344**, 286 (2014).
- <sup>114</sup>L. Gao, W. Ren, H. Xu, L. Jin, Z. Wang, T. Ma, L. Ma, Z. Zhang, Q. Fu, L. Peng, X. Bao, and H. Cheng, *Nat. Commun.* **3**, 699 (2012).
- <sup>115</sup>X. Li, W. Cai, L. Colombo, and R. S. Ruoff, *Nano Lett.* **9**, 4268 (2009).
- <sup>116</sup>Z. Sun, Z. Yan, J. Yao, E. Beitler, Y. Zhu, and J. M. Tour, *Nature* **468**, 549 (2010).
- <sup>117</sup>Z. Li, P. Wu, C. Wang, X. Fan, W. Zhang, X. Zhai, C. Zeng, Z. Li, J. Yang, and J. Hou, *ACS Nano* **5**, 3385 (2011).
- <sup>118</sup>X. Wan, K. Chen, D. Liu, J. Chen, Q. Miao, and J. Xu, *Chem. Mater.* **24**, 3906 (2012).
- <sup>119</sup>L. Li, X. Li, M. Du, Y. Guo, Y. Li, H. Li, Y. Yang, F. E. Alam, C.-T. Lin, and Y. Fang, *Chem. Mater.* **28**, 3360 (2016).
- <sup>120</sup>X. Li, C. W. Magnuson, A. Venugopal, J. An, J. W. Suk, B. Han, M. Borysiak, W. Cai, A. Velamakanni, Y. Zhu, L. Fu, E. M. Vogel, E. Voelkl, L. Colombo, and R. S. Ruoff, *Nano Lett.* **10**, 4328 (2010).
- <sup>121</sup>Z. Yan, J. Lin, Z. Peng, Z. Sun, Y. Zhu, L. Li, C. Xiang, E. Loic Samuel, C. Kittrell, and J. M. Tour, *ACS Nano* **6**, 9110 (2012).
- <sup>122</sup>X. Li, C. W. Magnuson, A. Venugopal, R. M. Tromp, J. B. Hannon, E. M. Vogel, L. Colombo, and R. S. Ruoff, *J. Am. Chem. Soc.* **133**, 2816 (2011).
- <sup>123</sup>Y. Hao, M. S. Bharathi, L. Wang, Y. Liu, H. Chen, S. Nie, X. Wang, H. Chou, C. Tan, B. Fallahazad, H. Ramanarayanan, C. W. Magnuson, E. Tutuc, B. I. Yakobson, K. F. McCarty, Y. Zhang, P. Kim, J. Hone, L. Colombo, and R. S. Ruoff, *Science* **342**, 720 (2013).
- <sup>124</sup>I. Vlassiouk, M. Regmi, P. Fulvio, S. Dai, P. Datskos, G. Eres, and S. Smirnov, *ACS Nano* **5**, 6069 (2011).
- <sup>125</sup>Y. Hao, L. Wang, Y. Liu, H. Chen, X. Wang, C. Tan, S. Nie, J. W. Suk, T. Jiang, T. Liang, J. Xiao, W. Ye, C. R. Dean, B. I. Yakobson, K. F. McCarty, P. Kim, J. Hone, L. Colombo, and R. S. Ruoff, *Nat. Nanotechnol.* **11**, 426 (2016).
- <sup>126</sup>X. Xu, Z. Zhang, L. Qiu, J. Zhuang, L. Zhang, H. Wang, C. Liao, H. Song, R. Qiao, P. Gao, Z. Hu, L. Liao, Z. Liao, D. Yu, E. Wang, F. Ding, H. Peng, and K. Liu, *Nat. Nanotechnol.* **11**, 930 (2016).
- <sup>127</sup>L. Song, L. Ci, H. Lu, P. B. Sorokin, C. Jin, J. Ni, A. G. Kvashnin, D. G. Kvashnin, J. Lou, B. I. Yakobson, and P. M. Ajayan, *Nano Lett.* **10**, 3209 (2010).
- <sup>128</sup>K. K. Kim, A. Hsu, X. Jia, S. M. Kim, Y. Shi, M. Hofmann, D. Nezich, J. F. Rodriguez-Nieva, M. Dresselhaus, T. Palacios, and J. Kong, *Nano Lett.* **12**, 161 (2012).
- <sup>129</sup>N. Guo, J. Wei, Y. Jia, H. Sun, Y. Wang, K. Zhao, X. Shi, L. Zhang, X. Li, A. Cao, H. Zhu, K. Wang, and D. Wu, *Nano Res.* **6**, 602 (2013).
- <sup>130</sup>S. M. Kim, A. Hsu, M. H. Park, S. H. Chae, S. J. Yun, J. S. Lee, D. Cho, W. Fang, C. Lee, T. Palacios, M. Dresselhaus, K. K. Kim, Y. H. Lee, and J. Kong, *Nat. Commun.* **6**, 8662 (2015).
- <sup>131</sup>L. Tao, K. Chen, Z. Chen, W. Chen, X. Gui, H. Chen, X. Li, and J. Xu, *ACS Appl. Mater. Interfaces* **9**, 12073 (2017).
- <sup>132</sup>Y. H. Lee, X. Q. Zhang, W. Zhang, M. T. Chang, C. Lin, K. Chang, Y. Yu, J. T.-W. Wang, C. Chang, L. Li, and T. Lin, *Adv. Mater.* **24**, 2320 (2012).
- <sup>133</sup>S. Najmaei, Z. Liu, W. Zhou, X. Zou, G. Shi, S. Lei, B. I. Yakobson, J. Idrobo, P. M. Ajayan, and J. Lou, *Nat. Mater.* **12**, 754 (2013).
- <sup>134</sup>A. M. van der Zande, P. Y. Huang, D. A. Chenet, T. C. Berkelbach, Y. You, G. Lee, T. F. Heinz, D. R. Reichman, D. A. Muller, and J. C. Hone, *Nat. Mater.* **12**, 554 (2013).
- <sup>135</sup>X. Li, X. Li, X. Zang, M. Zhu, Y. He, K. Wang, D. Xie, and H. Zhu, *Nanoscale* **7**, 8398 (2015).
- <sup>136</sup>A. L. Elías, N. Perea-López, A. Castro-Beltrán, A. Berkdemir, R. Lv, S. Feng, A. D. Long, T. Hayashi, Y. A. Kim, M. Endo, H. R. Gutiérrez, N. R. Pradhan, L. Balicas, T. E. Mallouk, F. López-Urías, H. Terrones, and M. Terrones, *ACS Nano* **7**, 5235 (2013).
- <sup>137</sup>X. Wang, Y. Gong, G. Shi, W. L. Chow, K. Keyshar, G. Ye, R. Vajtai, J. Lou, Z. Liu, E. Ringe, B. K. Tay, and P. M. Ajayan, *ACS Nano* **8**, 5125 (2014).
- <sup>138</sup>J. Huang, J. Pu, C. Hsu, M. Chiu, Z. Juang, Y. Chang, W. Chang, Y. Iwasa, T. Takenobu, and L. Li, *ACS Nano* **8**, 923 (2014).
- <sup>139</sup>L. Zhou, K. Xu, A. Zubair, A. D. Liao, W. Fang, F. Ouyang, Y. Lee, K. Ueno, R. Saito, T. Palacios, J. Kong, and M. S. Dresselhaus, *J. Am. Chem. Soc.* **137**, 11892 (2015).
- <sup>140</sup>K. Keyshar, Y. Gong, G. Ye, G. Brunetto, W. Zhou, D. P. Cole, K. Hackenberg, Y. He, L. Machado, M. Kabbani, A. H. C. Hart, B. Li, D. S. Galvao, A. George, R. Vajtai, C. S. Tiwary, and P. M. Ajayan, *Adv. Mater.* **27**, 4640 (2015).
- <sup>141</sup>M. Hafeez, L. Gan, H. Li, Y. Ma, and T. Zhai, *Adv. Funct. Mater.* **26**, 4551 (2016).
- <sup>142</sup>Y. Zhan, Z. Liu, S. Najmaei, P. M. Ajayan, and J. Lou, *Small* **8**, 966 (2012).
- <sup>143</sup>K. Liu, W. Zhang, Y. Lee, Y. Lin, M. Chang, C. Su, C. Chang, H. Li, Y. Shi, H. Zhang, C. Lai, and L. Li, *Nano Lett.* **12**, 1538 (2012).

- <sup>144</sup>X. Ling, Y. H. Lee, Y. Lin, W. Fang, L. Yu, M. S. Dresselhaus, and J. Kong, *Nano Lett.* **14**, 464 (2014).
- <sup>145</sup>S. Wang, Y. Rong, Y. Fan, M. Pacios, H. Bhaskaran, K. He, and J. H. Warner, *Chem. Mater.* **26**, 6371 (2014).
- <sup>146</sup>K. Kang, S. Xie, L. Huang, Y. Han, P. Y. Huang, K. F. Mak, C. J. Kim, D. Muller, and J. Park, *Nature* **520**, 656 (2015).
- <sup>147</sup>W. Yang, G. Chen, Z. Shi, C. Liu, L. Zhang, G. Xie, M. Cheng, D. Wang, R. Yang, D. Shi, K. Watanabe, T. Taniguchi, Y. Yao, Y. Zhang, and G. Zhang, *Nat. Mater.* **12**, 792 (2013).
- <sup>148</sup>Y. Shi, W. Zhou, A. Lu, W. Fang, Y. Lee, A. L. Hsu, S. M. Kim, K. K. Kim, H. Y. Yang, L. Li, J. Idrobo, and J. Kong, *Nano Lett.* **12**, 2784 (2012).
- <sup>149</sup>Y. Lin, N. Lu, N. Perea-Lopez, J. Li, Z. Lin, X. Peng, C. H. Lee, C. Sun, L. Calderin, P. N. Browning, M. S. Breshehan, M. J. Kim, T. S. Mayer, M. Terrones, and J. A. Robinson, *ACS Nano* **8**, 3715 (2014).
- <sup>150</sup>Y. Lin, R. K. Ghosh, R. Addou, N. Lu, S. M. Eichfeld, H. Zhu, M.-Y. Li, X. Peng, M. J. Kim, L. Li, R. M. Wallace, S. Datta, and J. A. Robinson, *Nat. Commun.* **6**, 7311 (2015).
- <sup>151</sup>M. P. Levendorf, C. Kim, L. Brown, P. Y. Huang, R. W. Havener, D. A. Muller, and J. Park, *Nature* **488**, 627 (2012).
- <sup>152</sup>Z. Liu, L. Ma, G. Shi, W. Zhou, Y. Gong, S. Lei, X. Yang, J. Zhang, J. Yu, K. P. Hackenberg, A. Babakhani, J. Idrobo, R. Vajtai, J. Lou, and P. M. Ajayan, *Nat. Nanotechnol.* **8**, 119 (2013).
- <sup>153</sup>M. Zhao, Y. Ye, Y. Han, Y. Xia, H. Zhu, S. Wang, Y. Wang, D. A. Muller, and X. Zhang, *Nat. Nanotechnol.* **11**, 954 (2016).
- <sup>154</sup>X. Ling, Y. Lin, Q. Ma, Z. Wang, Y. Song, L. Yu, S. Huang, W. Fang, X. Zhang, A. L. Hsu, Y. Bie, Y. Lee, Y. Zhu, L. Wu, J. Li, P. Jarillo-Herrero, M. Dresselhaus, T. Palacios, and J. Kong, *Adv. Mater.* **28**, 2322 (2016).
- <sup>155</sup>M. Li, Y. Shi, C. Cheng, L. Lu, Y. Lin, H. Tang, M. Tsai, C. Chu, K. Wei, and J. He, *Science* **349**, 524 (2015).
- <sup>156</sup>Y. Gong, J. Lin, X. Wang, G. Shi, S. Lei, Z. Lin, X. Zou, G. Ye, R. Vajtai, B. I. Yakobson, H. Terrones, M. Terrones, B. K. Tay, J. Lou, S. T. Pantelides, Z. Liu, W. Zhou, and P. M. Ajayan, *Nat. Mater.* **13**, 1135 (2014).
- <sup>157</sup>C. Huang, S. Wu, A. M. Sanchez, J. J. P. Peters, R. Beanland, J. S. Ross, P. Rivera, W. Yao, D. H. Cobden, and X. Xu, *Nat. Mater.* **13**, 1096 (2014).
- <sup>158</sup>X. Duan, C. Wang, J. C. Shaw, R. Cheng, Y. Chen, H. Li, X. Wu, Y. Tang, Q. Zhang, A. Pan, J. Jiang, R. Yu, Y. Huang, and X. Duan, *Nat. Nanotechnol.* **9**, 1024 (2014).
- <sup>159</sup>K. Chen, X. Wan, W. Xie, J. Wen, Z. Kang, X. Zeng, H. Chen, and J. Xu, *Adv. Mater.* **27**, 6431 (2015).
- <sup>160</sup>A. Reina, H. Son, L. Jiao, B. Fan, M. S. Dresselhaus, Z. Liu, and J. Kong, *J. Phys. Chem. C* **112**, 17741 (2008).
- <sup>161</sup>A. Pirkle, J. Chan, A. Venugopal, D. Hinojos, C. W. Magnuson, S. McDonnell, L. Colombo, E. M. Vogel, R. S. Ruoff, and R. M. Wallace, *Appl. Phys. Lett.* **99**, 122108 (2011).
- <sup>162</sup>E. H. Lock, M. Baraket, M. Laskoski, S. P. Mulvaney, W. K. Lee, P. E. Sheehan, D. R. Hines, J. T. Robinson, J. Tosado, M. S. Fuhrer, S. C. Hernández, and S. G. Walton, *Nano Lett.* **12**, 102 (2012).
- <sup>163</sup>P. Zhang, L. Ma, F. Fan, Z. Zeng, C. Peng, P. E. Loya, Z. Liu, Y. Gong, J. Zhang, X. Zhang, P. M. Ajayan, T. Zhu, and J. Lou, *Nat. Commun.* **5**, 3782 (2014).
- <sup>164</sup>A. Castellanos-Gomez, M. Buscema, R. Molenaar, V. Singh, L. Janssen, H. S. J. van der Zant, and G. A. Steele, *2D Mater.* **1**, 011002 (2014).
- <sup>165</sup>F. Banhart, J. Kotakoski, and A. V. Krasheninnikov, *ACS Nano* **5**, 26 (2011).
- <sup>166</sup>A. Hashimoto, K. Suenaga, A. Glotter, K. Urita, and S. Iijima, *Nature* **430**, 870 (2004).
- <sup>167</sup>L. Li, S. Reich, and J. Robertson, *Phys. Rev. B* **72**, 184109 (2005).
- <sup>168</sup>J. C. Meyer, C. Kisielowski, R. Erni, M. D. Rossell, M. F. Crommie, and A. Zettl, *Nano Lett.* **8**, 3582 (2008).
- <sup>169</sup>A. A. El-Barbary, R. H. Telling, C. P. Ewels, M. I. Heggie, and P. R. Briddon, *Phys. Rev. B* **68**, 144107 (2003).
- <sup>170</sup>J. Kotakoski, A. V. Krasheninnikov, U. Kaiser, and J. C. Meyer, *Phys. Rev. Lett.* **106**, 105505 (2011).
- <sup>171</sup>W. Zhou, X. Zou, S. Najmaei, Z. Liu, Y. Shi, J. Kong, J. Lou, P. M. Ajayan, B. I. Yakobson, and J. Idrobo, *Nano Lett.* **13**, 2615 (2013).
- <sup>172</sup>P. O. Lehtinen, A. S. Foster, A. Ayuela, A. Krasheninnikov, K. Nordlund, and R. M. Nieminen, *Phys. Rev. Lett.* **91**, 017202 (2003).
- <sup>173</sup>F. Schedin, A. K. Geim, S. V. Morozov, E. W. Hill, P. Blake, M. I. Katsnelson, and K. S. Novoselov, *Nat. Mater.* **6**, 652 (2007).
- <sup>174</sup>D. C. Elias, R. R. Nair, T. M. G. Mohiuddin, S. V. Morozov, P. Blake, M. P. Halsall, A. C. Ferrari, D. W. Boukhvalov, M. I. Katsnelson, A. K. Geim, and K. S. Novoselov, *Science* **323**, 610 (2009).
- <sup>175</sup>R. Balog, B. Jorgensen, L. Nilsson, M. Andersen, E. Riems, M. Bianchi, M. Fanetti, E. Laegsgaard, A. Baraldi, S. Lizzit, Z. Sljivancanin, F. Besenbacher, B. Hammer, T. G. Pedersen, P. Hofmann, and L. Hornekaer, *Nat. Mater.* **9**, 315 (2010).
- <sup>176</sup>J. T. Robinson, J. S. Burgess, C. E. Junkermeier, S. C. Badescu, T. L. Reinecke, F. K. Perkins, M. K. Zalalutdinov, J. W. Baldwin, J. C. Culbertson, P. E. Sheehan, and E. S. Snow, *Nano Lett.* **10**, 3001 (2010).
- <sup>177</sup>T. Cui, R. Lv, Z. Huang, S. Chen, Z. Zhang, X. Gan, Y. Jia, X. Li, K. Wang, D. Wu, and F. Kang, *J. Mater. Chem. A* **1**, 5736 (2013).
- <sup>178</sup>A. V. Krasheninnikov, P. O. Lehtinen, A. S. Foster, P. Pykkö, and R. M. Nieminen, *Phys. Rev. Lett.* **102**, 126807 (2009).
- <sup>179</sup>P. Y. Huang, C. S. Ruiz-Vargas, A. M. van der Zande, W. S. Whitney, M. P. Levendorf, J. W. Kevek, S. Garg, J. S. Alden, C. J. Hustedt, Y. Zhu, J. Park, P. L. McEuen, and D. A. Muller, *Nature* **469**, 389 (2011).
- <sup>180</sup>O. V. Yazyev, and S. G. Louie, *Nat. Mater.* **9**, 806 (2010).
- <sup>181</sup>Q. Yu, L. A. Jauregui, W. Wu, R. Colby, J. Tian, Z. Su, H. Cao, Z. Liu, D. Pandey, D. Wei, T. F. Chung, P. Peng, N. P. Guisinger, E. A. Stach, J. Bao, S. Pei, and Y. P. Chen, *Nat. Mater.* **10**, 443 (2011).
- <sup>182</sup>A. W. Tsen, L. Brown, M. P. Levendorf, F. Ghahari, P. Y. Huang, R. W. Havener, C. S. Ruiz-Vargas, D. A. Muller, P. Kim, and J. Park, *Science* **336**, 1143 (2012).
- <sup>183</sup>S. Najmaei, M. Amani, M. L. Chin, Z. Liu, A. G. Birdwell, T. P. O'Regan, P. M. Ajayan, M. Dubey, and J. Lou, *ACS Nano* **8**, 7930 (2014).
- <sup>184</sup>O. V. Yazyev and S. G. Louie, *Phys. Rev. B* **81**, 195420 (2010).
- <sup>185</sup>L. Zhao, R. He, K. T. Rim, T. Schiros, K. S. Kim, H. Zhou, C. Gutierrez, S. P. Chockalingam, C. J. Arguello, L. Pálová, D. Nordlund, M. S. Hybertsen, D. R. Reichman, T. F. Heinz, P. Kim, A. Pinczuk, G. W. Flynn, and A. N. Pasupathy, *Science* **333**, 999 (2011).
- <sup>186</sup>D. Wei, Y. Liu, Y. Wang, H. Zhang, L. Huang, and G. Yu, *Nano Lett.* **9**, 1752 (2009).
- <sup>187</sup>A. L. M. Reddy, A. Srivastava, S. R. Gowda, H. Gullapalli, M. Dubey, and P. M. Ajayan, *ACS Nano* **4**, 6337 (2010).
- <sup>188</sup>Z. Jin, J. Yao, C. Kittrell, and J. M. Tour, *ACS Nano* **5**, 4112 (2011).
- <sup>189</sup>H. M. Jeong, J. W. Lee, W. H. Shin, Y. J. Choi, H. J. Shin, J. K. Kang, and J. W. Choi, *Nano Lett.* **11**, 2472 (2011).
- <sup>190</sup>X. Wang, X. Li, L. Zhang, Y. Yoon, P. K. Weber, H. Wang, J. Guo, and H. Dai, *Science* **324**, 768 (2009).
- <sup>191</sup>L. S. Panchakarla, K. S. Subrahmanyam, S. K. Saha, A. Govindaraj, H. R. Krishnamurthy, U. V. Waghmare, and C. N. R. Rao, *Adv. Mater.* **21**, 4726 (2009).
- <sup>192</sup>C. Zhang, N. Mahmood, H. Yin, F. Liu, and Y. Hou, *Adv. Mater.* **25**, 4932 (2013).
- <sup>193</sup>R. Lv, M. Cristina dos Santos, C. Antonelli, S. Feng, K. Fujisawa, A. Berkdemir, R. Cruz-Silva, A. L. Elías, N. Perea-Lopez, F. López-Urías, H. Terrones, and M. Terrones, *Adv. Mater.* **26**, 7593 (2014).
- <sup>194</sup>Z. Yang, Z. Yao, G. Li, G. Fang, H. Nie, Z. Liu, X. Zhou, X. Chen, and S. Huang, *ACS Nano* **6**, 205 (2012).
- <sup>195</sup>Y. Gong, Z. Liu, A. R. Lupini, G. Shi, J. Lin, S. Najmaei, Z. Lin, A. L. Elías, A. Berkdemir, G. You, H. Terrones, M. Terrones, R. Vajtai, S. T. Pantelides, S. J. Pennycook, J. Lou, W. Zhou, and P. M. Ajayan, *Nano Lett.* **14**, 442 (2014).
- <sup>196</sup>J. Gao, Y. D. Kim, L. Liang, J. C. Idrobo, P. Chow, J. Tan, B. Li, L. Li, B. G. Sumpter, T. Lu, V. Meunier, J. Hone, and N. Koratkar, *Adv. Mater.* **28**, 9735 (2016).
- <sup>197</sup>K. Zhang, S. Feng, J. Wang, A. Azcatl, N. Lu, R. Addou, N. Wang, C. Zhou, J. Lerach, V. Bojan, M. J. Kim, L. Chen, R. M. Wallace, M. Terrones, J. Zhu, and J. A. Robinson, *Nano Lett.* **15**, 6586 (2015).
- <sup>198</sup>E. Kim, C. Ko, K. Kim, Y. Chen, J. Suh, S. Ryu, K. Wu, X. Meng, A. Suslu, S. Tongay, J. Wu, and C. P. Grigoropoulos, *Adv. Mater.* **28**, 341 (2016).
- <sup>199</sup>X. Wang, J. Xu, W. Xie, and J. Du, *J. Phys. Chem. C* **115**, 7596 (2011).
- <sup>200</sup>N. Jung, N. Kim, S. Jockusch, N. J. Turro, P. Kim, and L. Brus, *Nano Lett.* **9**, 4133 (2009).
- <sup>201</sup>D. B. Farmer, R. Golizadeh-Mojarad, V. Perebeinos, Y. Lin, G. S. Tulevski, J. C. Tsang, and P. Avouris, *Nano Lett.* **9**, 388 (2009).
- <sup>202</sup>J. Wu, L. Xie, Y. Li, H. Wang, Y. Ouyang, J. Guo, and H. Dai, *J. Am. Chem. Soc.* **133**, 19668 (2011).
- <sup>203</sup>B. Li, L. Zhou, D. Wu, H. Peng, K. Yan, Y. Zhou, and Z. Liu, *ACS Nano* **5**, 5957 (2011).
- <sup>204</sup>F. Varchon, R. Feng, J. Hass, X. Li, B. N. Nguyen, C. Naud, P. Mallet, J. Y. Veuillem, C. Berger, E. H. Conrad, and L. Magaud, *Phys. Rev. Lett.* **99**, 126805 (2007).
- <sup>205</sup>Y. Kang, J. Kang, and K. J. Chang, *Phys. Rev. B* **78**, 115404 (2008).

- <sup>206</sup>G. Giovannetti, P. A. Khomyakov, G. Brocks, V. M. Karpan, J. van den Brink, and P. J. Kelly, *Phys. Rev. Lett.* **101**, 026803 (2008).
- <sup>207</sup>H. Fang, M. Tosun, G. Seol, T.-C. Chang, K. Takei, J. Guo, and A. Javey, *Nano Lett.* **13**, 1991 (2013).
- <sup>208</sup>D. Kiriyama, M. Tosun, P. Zhao, J. S. Kang, and A. Javey, *J. Am. Chem. Soc.* **136**, 7853 (2014).
- <sup>209</sup>M. Amani, D. Lien, D. Kiriyama, J. Xiao, A. Azcatl, J. Noh, S. R. Madhvapathy, R. Addou, S. Kc, M. Dubey, K. Cho, R. M. Wallace, S. Lee, J. He, J. W. Ager, X. Zhang, E. Yablonovitch, and A. Javey, *Science* **350**, 1065 (2015).
- <sup>210</sup>H. Nan, Z. Wang, W. Wang, Z. Liang, Y. Lu, Q. Chen, D. He, P. Tan, F. Miao, X. Wang, J. Wang, and Z. Ni, *ACS Nano* **8**, 5738 (2014).
- <sup>211</sup>S. Tongay, J. Zhou, C. Ataca, J. Liu, J. S. Kang, T. S. Matthews, L. You, J. Li, J. C. Grossman, and J. Wu, *Nano Lett.* **13**, 2831 (2013).
- <sup>212</sup>H. Fang, S. Chuang, T. C. Chang, K. Takei, T. Takahashi, and A. Javey, *Nano Lett.* **12**, 3788 (2012).
- <sup>213</sup>S. P. Koenig, R. A. Doganov, L. Seixas, A. Carvalho, J. Y. Tan, K. Watanabe, T. Taniguchi, N. Yakovlev, A. H. Castro Neto, and B. Özyilmaz, *Nano Lett.* **16**, 2145 (2016).
- <sup>214</sup>D. Xiang, C. Han, J. Wu, S. Zhong, Y. Liu, J. Lin, X. Zhang, W. P. Hu, B. Özyilmaz, A. H. Castro Neto, A. T. S. Wee, and W. Chen, *Nat. Commun.* **6**, 6485 (2015).
- <sup>215</sup>L. Ci, L. Song, C. Jin, D. Jariwala, D. Wu, Y. Li, A. Srivastava, Z. F. Wang, K. Storr, L. Balicas, F. Liu, and P. M. Ajayan, *Nat. Mater.* **9**, 430 (2010).
- <sup>216</sup>H. P. Komsa and A. V. Krasheninnikov, *J. Phys. Chem. Lett.* **3**, 3652 (2012).
- <sup>217</sup>H. Li, X. Duan, X. Wu, X. Zhuang, H. Zhou, Q. Zhang, X. Zhu, W. Hu, P. Ren, P. Guo, L. Ma, X. Fan, X. Wang, J. Xu, A. Pan, and X. Duan, *J. Am. Chem. Soc.* **136**, 3756 (2014).
- <sup>218</sup>Y. Chen, J. Xi, D. O. Dumicenco, Z. Liu, K. Suenaga, D. Wang, Z. Shuai, Y. Huang, and L. Xie, *ACS Nano* **7**, 4610 (2013).
- <sup>219</sup>X. Duan, C. Wang, Z. Fan, G. Hao, L. Kou, U. Halim, H. Li, X. Wu, Y. Wang, J. Jiang, A. Pan, Y. Huang, R. Yu, and X. Duan, *Nano Lett.* **16**, 264 (2016).
- <sup>220</sup>C. Zhang, S. Kc, Y. Nie, C. Liang, W. G. Vandenberghe, R. C. Longo, Y. Zheng, F. Kong, S. Hong, R. M. Wallace, and K. Cho, *ACS Nano* **10**, 7370 (2016).
- <sup>221</sup>S. J. Sandoval, D. Yang, R. F. Frindt, and J. C. Irwin, *Phys. Rev. B* **44**, 3955 (1991).
- <sup>222</sup>A. Nourbakhsh, A. Zubair, R. N. Sajjad, A. Tavakkoli, K. G. W. Chen, S. Fang, X. Ling, J. Kong, M. S. Dresselhaus, E. Kaxiras, K. K. Berggren, D. Antoniadis, and T. Palacios, *Nano Lett.* **16**, 7798 (2016).
- <sup>223</sup>R. Kappera, D. Voiry, S. E. Yalcin, B. Branch, G. Gupta, A. D. Mohite, and M. Chhowalla, *Nat. Mater.* **13**, 1128 (2014).
- <sup>224</sup>Y. Ma, B. Liu, A. Zhang, L. Chen, M. Fathi, C. Shen, A. N. Abbas, M. Ge, M. Mecklenburg, and C. Zhou, *ACS Nano* **9**, 7383 (2015).
- <sup>225</sup>D. Voiry, A. Goswami, R. Kappera, C. de Carvalho Castro e Silva, D. Kaplan, T. Fujita, M. Chen, T. Asefa, and M. Chhowalla, *Nat. Chem.* **7**, 45 (2015).
- <sup>226</sup>S. J. R. Tan, I. Abdelwahab, Z. Ding, X. Zhao, T. Yang, G. Z. J. Loke, H. Lin, I. Verzhbitskiy, S. M. Poh, H. Xu, C. T. Nai, W. Zhou, G. Eda, B. Jia, and K. P. Loh, *J. Am. Chem. Soc.* **139**, 2504 (2017).
- <sup>227</sup>Y. Kang, S. Najmaei, Z. Liu, Y. Bao, Y. Wang, X. Zhu, N. J. Halas, P. Nordlander, P. M. Ajayan, J. Lou, and Z. Fang, *Adv. Mater.* **26**, 6467 (2014).
- <sup>228</sup>D. Teweldebrhan and A. A. Balandin, *Appl. Phys. Lett.* **94**, 013101 (2009).
- <sup>229</sup>L. Tao, C. Qiu, F. Yu, H. Yang, M. Chen, G. Wang, and L. Sun, *J. Phys. Chem. C* **117**, 10079 (2013).
- <sup>230</sup>Y. Katagiri, T. Nakamura, A. Ishii, C. Ohata, M. Hasegawa, S. Katsumoto, T. Cusati, A. Fortunelli, G. Iannaccone, G. Fiori, S. Roche, and J. Haruyama, *Nano Lett.* **16**, 3788 (2016).
- <sup>231</sup>S. Song, D. H. Keum, S. Cho, D. Perello, Y. Kim, and Y. H. Lee, *Nano Lett.* **16**, 188 (2016).
- <sup>232</sup>K. S. Novoselov, E. McCann, S. V. Morozov, V. I. Fal'ko, M. I. Katsnelson, U. Zeitler, D. Jiang, F. Schedin, and A. K. Geim, *Nat. Phys.* **2**, 177 (2006).
- <sup>233</sup>E. McCann and V. I. Fal'ko, *Phys. Rev. Lett.* **96**, 086805 (2006).
- <sup>234</sup>A. Splendiani, L. Sun, Y. Zhang, T. Li, J. Kim, C. Chim, G. Galli, and F. Wang, *Nano Lett.* **10**, 1271 (2010).
- <sup>235</sup>K. F. Mak, C. Lee, J. Hone, J. Shan, and T. F. Heinz, *Phys. Rev. Lett.* **105**, 136805 (2010).
- <sup>236</sup>A. Ramasubramaniam, D. Naveh, and E. Towe, *Phys. Rev. B* **84**, 205325 (2011).
- <sup>237</sup>T. Chu, H. Ilatikhameneh, G. Klimeck, R. Rahman, and Z. Chen, *Nano Lett.* **15**, 8000 (2015).
- <sup>238</sup>C. Lee, H. Yan, L. E. Brus, T. F. Heinz, J. Hone, and S. Pyu, *ACS Nano* **4**, 2695 (2010).
- <sup>239</sup>J. Yang, R. Xu, J. Pei, Y. W. Myint, F. Wang, Z. Wang, S. Zhang, Z. Yu, and Y. Lu, *Light: Sci. Appl.* **4**, e312 (2015).
- <sup>240</sup>S. Tongay, H. Sahin, C. Ko, A. Luce, W. Fan, K. Liu, J. Zhou, Y. Huang, C. Ho, J. Yan, D. F. Ogletree, S. Aloni, J. Ji, S. Li, J. Li, F. M. Peeters, and J. Wu, *Nat. Commun.* **5**, 3252 (2014).
- <sup>241</sup>D. Jena, *Proc. IEEE* **101**, 1585 (2013).
- <sup>242</sup>C. Lee, X. Wei, J. W. Kysar, and J. Hone, *Science* **321**, 385 (2008).
- <sup>243</sup>S. Bertolazzi, J. Brivio, and A. Kis, *ACS Nano* **5**, 9703 (2011).
- <sup>244</sup>F. Ding, H. Ji, Y. Chen, A. Herklotz, K. Dorr, Y. Mei, A. Rastelli, and O. G. Schmidt, *Nano Lett.* **10**, 3453 (2010).
- <sup>245</sup>Y. Hui, X. Liu, W. Jie, N. Y. Chan, J. Hao, Y. Hsu, L. Li, W. Guo, and S. P. Lau, *ACS Nano* **7**, 7126 (2013).
- <sup>246</sup>W. Wu, L. Wang, Y. Li, F. Zhang, L. Lin, S. Niu, D. Chenet, X. Zhang, Y. Hao, and T. F. Heinz, *Nature* **514**, 470 (2014).
- <sup>247</sup>J. K. Lee, S. Yamazaki, H. Yun, J. Park, G. P. Kennedy, G. T. Kim, O. Pietzsch, R. Wiesendanger, S. Lee, S. Hong, U. Dettlaff-Weglikowska, and S. Roth, *Nano Lett.* **13**, 3494 (2013).
- <sup>248</sup>H. J. Conley, B. Wang, J. L. Ziegler, R. F. Haglund, S. T. Pantelides, and K. I. Bolotin, *Nano Lett.* **13**, 3626 (2013).
- <sup>249</sup>T. M. G. Mohiuddin, A. Lombardo, R. R. Nair, A. Bonetti, G. Savini, R. Jalil, N. Bonini, D. M. Basko, C. Gallois, N. Marzari, K. S. Novoselov, A. K. Geim, and A. C. Ferrari, *Phys. Rev. B* **79**, 205433 (2009).
- <sup>250</sup>H. Peelaerts and C. G. Van de Walle, *Phys. Rev. B* **86**, 241401(R) (2012).
- <sup>251</sup>Z. Liu, M. Amani, S. Najmaei, Q. Xu, X. Zou, W. Zhou, T. Yu, C. Qiu, A. G. Birdwell, F. J. Crowne, R. Vajtai, B. I. Yakobson, Z. Xia, M. Dubey, P. M. Ajayan, and J. Lou, *Nat. Commun.* **5**, 5246 (2014).
- <sup>252</sup>J. C. Meyer, A. K. Geim, M. I. Katsnelson, K. S. Novoselov, T. J. Booth, and S. Roth, *Nature* **446**, 60 (2007).
- <sup>253</sup>A. Fasolino, J. H. Los, and M. I. Katsnelson, *Nat. Mater.* **6**, 858 (2007).
- <sup>254</sup>V. B. Shenoy, C. D. Reddy, A. Ramasubramaniam, and Y. W. Zhang, *Phys. Rev. Lett.* **101**, 245501 (2008).
- <sup>255</sup>L. Tapaszto, T. Dumitrica, S. J. Kim, P. Nemes-Incze, C. Hwang, and L. P. Biro, *Nat. Phys.* **8**, 739 (2012).
- <sup>256</sup>X. Li, T. Zhao, K. Wang, Y. Yang, J. Wei, F. Kang, D. Wu, and H. Zhu, *Langmuir* **27**, 12164 (2011).
- <sup>257</sup>W. Bao, F. Miao, Z. Chen, H. Zhang, W. Jang, C. Dames, and C. N. Lau, *Nat. Nanotechnol.* **4**, 562 (2009).
- <sup>258</sup>D. Yoon, Y. Son, and H. Cheong, *Nano Lett.* **11**, 3227 (2011).
- <sup>259</sup>V. E. Calado, G. F. Schneider, A. M. M. G. Theulings, C. Dekker, and L. M. K. Vandersypen, *Appl. Phys. Lett.* **101**, 103116 (2012).
- <sup>260</sup>L. Gao, G. Ni, Y. Liu, B. Liu, A. H. Castro Neto, and K. P. Loh, *Nature* **505**, 190 (2014).
- <sup>261</sup>J. Hong, Y. C. Shin, A. Zubair, Y. Mao, T. Palacios, M. S. Dresselhaus, S. H. Kim, and J. Kong, *Adv. Mater.* **28**, 2382 (2016).
- <sup>262</sup>A. Castellanos-Gomez, R. Roldán, E. Cappelluti, M. Buscema, F. Guinea, H. S. J. van der Zant, and G. A. Steele, *Nano Lett.* **13**, 5361 (2013).
- <sup>263</sup>X. Li, H. Zhu, K. Wang, A. Cao, J. Wei, C. Li, Y. Jia, Z. Li, X. Li, and D. Wu, *Adv. Mater.* **22**, 2743 (2010).
- <sup>264</sup>H. Yang, J. Heo, S. Park, H. J. Song, D. H. Seo, K. Byun, P. Kim, I. Yoo, H. Chung, and K. Kim, *Science* **336**, 1140 (2012).
- <sup>265</sup>W. J. Yu, Z. Li, H. Zhou, Y. Chen, Y. Wang, Y. Huang, and X. Duan, *Nat. Mater.* **12**, 246 (2013).
- <sup>266</sup>T. Georgiou, R. Jalil, B. D. Belle, L. Britnell, R. V. Gorbachev, S. V. Morozov, Y. Kim, A. Gholinia, S. J. Haigh, O. Makarovsky, L. Eaves, L. A. Ponomarenko, A. K. Geim, K. S. Novoselov, and A. Mishchenko, *Nat. Nanotechnol.* **8**, 100 (2013).
- <sup>267</sup>D. Sinha and J. U. Lee, *Nano Lett.* **14**, 4660 (2014).
- <sup>268</sup>S. Das, H. Chen, A. Verma Penumatcha, and J. Appenzeller, *Nano Lett.* **13**, 100 (2013).
- <sup>269</sup>W. Liu, J. Kang, D. Sarkar, Y. Khatami, D. Jena, and K. Banerjee, *Nano Lett.* **13**, 1983 (2013).
- <sup>270</sup>S. Das and J. Appenzeller, *Appl. Phys. Lett.* **103**, 103501 (2013).
- <sup>271</sup>X. Cui, G. Lee, Y. D. Kim, G. Arefe, P. Y. Huang, C. Lee, D. A. Chenet, X. Zhang, L. Wang, F. Ye, F. Pizzocchero, B. S. Jessen, K. Watanabe, T. Taniguchi, D. A. Muller, T. Low, P. Kim, and J. Hone, *Nat. Nanotechnol.* **10**, 534 (2015).
- <sup>272</sup>S. Chuang, C. Battaglia, A. Azcatl, S. McDonnell, J. S. Kang, X. Yin, M. Tosun, R. Kapadia, H. Fang, R. M. Wallace, and A. Javey, *Nano Lett.* **14**, 1337 (2014).
- <sup>273</sup>S. Lee, A. Tang, S. Aloni, and H. S. P. Wong, *Nano Lett.* **16**, 276 (2016).

- <sup>274</sup>O. Lopez-Sanchez, E. A. Llado, V. Koman, A. F. Morral, A. Radenovic, and A. Kis, *ACS Nano* **8**, 3042 (2014).
- <sup>275</sup>M. R. Esmaeili-Rad and S. Salahuddin, *Sci. Rep.* **3**, 2345 (2013).
- <sup>276</sup>D. Sarkar, X. Xie, W. Liu, W. Cao, J. Kang, Y. Gong, S. Kraemer, P. M. Ajayan, and K. Banerjee, *Nature* **526**, 91 (2015).
- <sup>277</sup>D. Ruzmetov, K. Zhang, G. Stan, B. Kalanyan, G. R. Bhimanapati, S. M. Eichfeld, R. A. Burke, P. B. Shah, T. P. O'Regan, F. J. Crowne, A. Glen Birdwell, J. A. Robinson, A. V. Davydov, and T. G. Ivanov, *ACS Nano* **10**, 3580 (2016).
- <sup>278</sup>C. Lee, G. Lee, A. M. van der Zande, W. Chen, Y. Li, M. Han, X. Cui, G. Arefe, C. Nuckolls, T. F. Heinz, J. Guo, J. Hone, and P. Kim, *Nat. Nanotechnol.* **9**, 676 (2014).
- <sup>279</sup>C. Gong, H. Zhang, W. Wang, L. Colombo, R. M. Wallace, and K. Cho, *Appl. Phys. Lett.* **103**, 053513 (2013).
- <sup>280</sup>J. Kang, S. Tongay, J. Zhou, J. Li, and J. Wu, *Appl. Phys. Lett.* **102**, 012111 (2013).
- <sup>281</sup>M. Chiu, C. Zhang, H. Shiu, C. Chu, C. Chen, C. S. Chang, C. Chen, M. Chou, C. Shih, and L. Li, *Nat. Commun.* **6**, 7666 (2015).
- <sup>282</sup>X. Hong, J. Kim, S. Shi, Y. Zhang, C. Jin, Y. Sun, S. Tongay, J. Wu, Y. Zhang, and F. Wang, *Nat. Nanotechnol.* **9**, 682 (2014).
- <sup>283</sup>H. Chen, X. Wen, J. Zhang, T. Wu, Y. Gong, X. Zhang, J. Yuan, C. Yi, J. Lou, P. M. Ajayan, W. Zhuang, G. Zhang, and J. Zheng, *Nat. Commun.* **7**, 12512 (2016).
- <sup>284</sup>P. Rivera, J. R. Schaibley, A. M. Jones, J. S. Ross, S. Wu, G. Aivazian, P. Klement, K. Seyler, G. Clark, N. J. Ghimire, J. Yan, D. F. Mandrus, W. Yao, and X. Xu, *Nat. Commun.* **6**, 6242 (2015).
- <sup>285</sup>H. Fang, C. Battaglia, C. Carraro, S. Nemsak, B. Ozdol, J. S. Kang, H. A. Bechtel, S. B. Desai, F. Kronast, and A. A. Unal, *Proc. Natl. Acad. Sci. U.S.A.* **111**, 6198 (2014).
- <sup>286</sup>K. Zhang, T. Zhang, G. Cheng, T. Li, S. Wang, W. Wei, X. Zhou, W. Yu, Y. Sun, P. Wang, D. Zhang, C. Zeng, X. Wang, W. Hu, H. Fan, G. Shen, X. Chen, X. Duan, K. Chang, and N. Dai, *ACS Nano* **10**, 3852 (2016).
- <sup>287</sup>A. Nourbakhsh, A. Zubair, M. S. Dresselhaus, and T. Palacios, *Nano Lett.* **16**, 1359 (2016).
- <sup>288</sup>D. Jariwala, V. K. Sangwan, C. Wu, P. L. Prabhumirashi, M. L. Geier, T. J. Marks, L. J. Lauhon, and M. C. Hersam, *Proc. Natl. Acad. Sci. U.S.A.* **110**, 18076 (2013).
- <sup>289</sup>F. Wang, L. Yin, Z. X. Wang, K. Xu, F. M. Wang, T. A. Shifa, Y. Huang, C. Jiang, and J. He, *Adv. Funct. Mater.* **26**, 5499 (2016).
- <sup>290</sup>R. Yan, S. Fathipour, Y. Han, B. Song, S. Xiao, M. Li, N. Ma, V. Protasenko, D. A. Muller, D. Jena, and H. G. Xing, *Nano Lett.* **15**, 5791 (2015).
- <sup>291</sup>T. Roy, M. Tosun, X. Cao, H. Fang, D. Lien, P. Zhao, Y. Chen, Y. Chueh, J. Guo, and A. Javey, *ACS Nano* **9**, 2071 (2015).
- <sup>292</sup>M. Mahjouri-Samani, M. Lin, K. Wang, A. R. Lupini, J. Lee, L. Basile, A. Boulesbaa, C. M. Rouleau, A. A. Puretzky, I. N. Ivanov, K. Xiao, M. Yoon, and D. B. Geohegan, *Nat. Commun.* **6**, 7749 (2015).
- <sup>293</sup>B. W. Baugher, H. O. H. Churchill, Y. Yang, and P. Jarillo-Herrero, *Nat. Nanotechnol.* **9**, 262 (2014).
- <sup>294</sup>Y. He, A. Sobhani, S. Lei, Z. Zhang, Y. Gong, Z. Jin, W. Zhou, Y. Yang, Y. Zhang, X. Wang, B. Yakobson, R. Vajtai, N. J. Halas, B. Li, E. Xie, and P. Ajayan, *Adv. Mater.* **28**, 5126 (2016).
- <sup>295</sup>M. S. Choi, D. Qu, D. Lee, X. Liu, K. Watanabe, T. Taniguchi, and W. J. Yoo, *ACS Nano* **8**, 9332 (2014).
- <sup>296</sup>N. M. Gabor, J. C. W. Song, Q. Ma, N. L. Nair, T. Taychatanapat, K. Watanabe, T. Taniguchi, L. S. Levitov, and P. Jarillo-Herrero, *Science* **334**, 648 (2011).
- <sup>297</sup>J. C. W. Song, M. S. Rudner, C. M. Marcus, and L. S. Levitov, *Nano Lett.* **11**, 4688 (2011).
- <sup>298</sup>G. Lee, G. Park, and H. Lee, *Nat. Phys.* **11**, 925 (2015).
- <sup>299</sup>Y. Lin, A. Valdes-Garcia, S. Han, D. B. Farmer, I. Meric, Y. Sun, Y. Wu, C. Dimitrakopoulos, A. Grill, P. Avouris, and K. A. Jenkins, *Science* **332**, 1294 (2011).
- <sup>300</sup>Y.-M. Lin, C. Dimitrakopoulos, K. A. Jenkins, D. B. Farmer, H.-Y. Chiu, A. Grill, and Ph. Avouris, *Science* **327**, 662 (2010).
- <sup>301</sup>M. C. Lemme, T. J. Echtermeyer, M. Baus, and H. Kurz, *IEEE Electron Devices Lett.* **28**, 282 (2007).
- <sup>302</sup>T. Palacios, A. Hsu, and H. Wang, *IEEE Commun. Mag.* **48**, 122 (2010).
- <sup>303</sup>S. B. Desai, S. R. Madhvapathy, A. B. Sachid, J. P. Llinas, Q. Wang, G. H. Ahn, G. Pitner, M. J. Kim, J. Bokor, C. Hu, H.-S. P. Wong, and A. Javey, *Science* **354**, 99 (2016).
- <sup>304</sup>B. Radisavljevic, A. Radenovic, J. Brivio, V. Giacometti, and A. Kis, *Nat. Nanotechnol.* **6**, 147 (2011).
- <sup>305</sup>A. Allain and A. Kis, *ACS Nano* **8**, 7180 (2014).
- <sup>306</sup>W. S. Hwang, M. Remskar, R. Yan, V. Protasenko, K. Tahy, S. D. Chae, P. Zhao, A. Konar, H. Xing, A. Seabaugh, and D. Jena, *Appl. Phys. Lett.* **101**, 013107 (2012).
- <sup>307</sup>S. Larentis, B. Fallahazad, and E. Tutuc, *Appl. Phys. Lett.* **101**, 223104 (2012).
- <sup>308</sup>X. Lu, M. I. Utama, J. Lin, X. Gong, J. Zhang, Y. Zhao, S. T. Pantelides, J. Wang, Z. Dong, Z. Liu, W. Zhou, and Q. Xiong, *Nano Lett.* **14**, 2419 (2014).
- <sup>309</sup>D. A. Bandurin, A. V. Tyurnina, G. L. Yu, A. Mishchenko, V. Zolyomi, S. V. Morozov, R. K. Kumar, R. V. Gorbachev, Z. R. Kudrynskyi, S. Pezzini, Z. D. Kovalyuk, U. Zeitler, K. S. Novoselov, A. Patanè, L. Eaves, I. V. Grigorieva, V. I. Fal'ko, A. K. Geim, and Y. Cao, *Nat. Nanotechnol.* **12**, 223 (2017).
- <sup>310</sup>S. P. Koenig, R. A. Doganov, H. Schmidt, A. H. Castro Neto, and B. Özyilmaz, *Appl. Phys. Lett.* **104**, 103106 (2014).
- <sup>311</sup>A. J. Mannix, B. Kiraly, M. C. Hersam, and N. P. Guisinger, *Nat. Rev. Chem.* **1**, 0014 (2017).
- <sup>312</sup>K. H. Lee, H. Shin, J. Lee, I. Lee, G. Kim, J. Choi, and S. Kim, *Nano Lett.* **12**, 714 (2012).
- <sup>313</sup>S. Das, R. Gulotty, A. V. Sumant, and A. Roelofs, *Nano Lett.* **14**, 2861 (2014).
- <sup>314</sup>G. Fiori, F. Bonaccorso, G. Iannaccone, T. Palacios, D. Neumaier, A. Seabaugh, S. K. Banerjee, and L. Colombo, *Nat. Nanotechnol.* **9**, 768 (2014).
- <sup>315</sup>Y. Du, H. Liu, Y. Deng, and P. D. Ye, *ACS Nano* **8**, 10035 (2014).
- <sup>316</sup>N. R. Pradhan, D. Rhodes, S. Feng, Y. Xin, S. Memaran, B. Moon, H. Terrones, M. Terrones, and L. Balicas, *ACS Nano* **8**, 5911 (2014).
- <sup>317</sup>W. Wu, D. De, S. Chang, Y. Wang, H. Peng, J. Bao, and S. Pei, *Appl. Phys. Lett.* **102**, 142106 (2013).
- <sup>318</sup>A. Das, S. Pisana, B. Chakraborty, S. Pisanec, S. K. Saha, U. V. Waghmare, K. S. Novoselov, H. R. Krishnamurthy, A. K. Geim, A. C. Ferrari, and A. K. Sood, *Nat. Nanotechnol.* **3**, 210 (2008).
- <sup>319</sup>F. Xia, T. Mueller, Y. Lin, A. Valdes-Garcia, and P. Avouris, *Nat. Nanotechnol.* **4**, 839 (2009).
- <sup>320</sup>F. H. L. Koppens, T. Mueller, P. Avouris, A. C. Ferrari, M. S. Vitiello, and M. Polini, *Nat. Nanotechnol.* **9**, 780 (2014).
- <sup>321</sup>O. Lopez-Sanchez, D. Lembke, M. Kayci, A. Radenovic, and A. Kis, *Nat. Nanotechnol.* **8**, 497 (2013).
- <sup>322</sup>K. F. Mak and J. Shan, *Nat. Photonics* **10**, 216 (2016).
- <sup>323</sup>G. Su, V. G. Hadjiev, P. E. Loya, J. Zhang, S. Lei, S. Maharjan, P. Dong, P. M. Ajayan, J. Lou, and H. Peng, *Nano Lett.* **15**, 506 (2015).
- <sup>324</sup>X. Zhou, L. Gan, W. Tian, Q. Zhang, S. Jin, H. Li, Y. Bando, D. Golberg, and T. Zhai, *Adv. Mater.* **27**, 8035 (2015).
- <sup>325</sup>J. Wu, Z. Hu, Z. Jin, S. Lei, H. Guo, K. Chatterjee, J. Zhang, Y. Yang, B. Li, Y. Liu, J. Lai, R. Vajtai, B. Yakobson, M. Tang, J. Lou, and P. M. Ajayan, *Adv. Mater. Interfaces* **3**, 1600383 (2016).
- <sup>326</sup>Q. Guo, A. Pospischil, M. Bhuiyan, H. Jiang, H. Tian, D. Farmer, B. Deng, C. Li, S. Han, H. Wang, Q. Xia, T. Ma, T. Mueller, and F. Xia, *Nano Lett.* **16**, 4648 (2016).
- <sup>327</sup>G. Konstantatos, M. Badioli, L. Gaudreau, J. Osmond, M. Bernechea, F. P. G. de Arquer, F. Gatti, and F. H. L. Koppens, *Nat. Nanotechnol.* **7**, 363 (2012).
- <sup>328</sup>Z. Sun, Z. Liu, J. Li, G. Tai, S. Lau, and F. Yan, *Adv. Mater.* **24**, 5878 (2012).
- <sup>329</sup>C. Liu, Y. Chang, T. B. Norris, and Z. Zhong, *Nat. Nanotechnol.* **9**, 273 (2014).
- <sup>330</sup>Z. Chen, Z. Cheng, J. Wang, X. Wan, C. Shu, H. K. Tsang, H. P. Ho, and J. Xu, *Adv. Opt. Mater.* **3**, 1207 (2015).
- <sup>331</sup>Z. Chen, X. Li, J. Wang, L. Tao, M. Long, S. Liang, L. K. Ang, C. Shu, H. K. Tsang, and J. Xu, *ACS Nano* **11**, 430 (2017).
- <sup>332</sup>Y. Liu, R. Cheng, L. Liao, H. Zhou, J. Bai, G. Liu, L. Liu, Y. Huang, and X. Duan, *Nat. Commun.* **2**, 579 (2011).
- <sup>333</sup>Z. Fang, Z. Liu, Y. Wang, P. M. Ajayan, P. Nordlander, and N. J. Halas, *Nano Lett.* **12**, 3808 (2012).
- <sup>334</sup>X. Gan, K. F. Mak, Y. Gao, Y. You, F. Hatami, J. Hone, T. F. Heinz, and D. Englund, *Nano Lett.* **12**, 5626 (2012).
- <sup>335</sup>M. Furchi, A. Uriach, A. Pospischil, G. Lilley, K. Unterrainer, H. Detz, P. Klang, A. M. Andrews, W. Schrenk, G. Strasser, and T. Mueller, *Nano Lett.* **12**, 2773 (2012).
- <sup>336</sup>X. Gan, R. Shiue, Y. Gao, I. Meric, T. F. Heinz, K. Shepard, J. Hone, S. Assefa, and D. Englund, *Nat. Photonics* **7**, 883 (2013).
- <sup>337</sup>A. Pospischil, M. Humer, M. M. Furchi, D. Bachmann, R. Guider, T. Fromherz, and T. Mueller, *Nat. Photonics* **7**, 892 (2013).
- <sup>338</sup>N. Youngblood, C. Chen, S. J. Koester, and M. Li, *Nat. Photonics* **9**, 247 (2015).

- <sup>339</sup>S. Schuler, D. Schall, D. Neumaier, L. Dobusch, O. Bethge, B. Schwarz, M. Krall, and T. Mueller, *Nano Lett.* **16**, 7107 (2016).
- <sup>340</sup>R. Cheng, D. Li, H. Zhou, C. Wang, A. Yin, S. Jiang, Y. Liu, Y. Chen, Y. Huang, and X. Duan, *Nano Lett.* **14**, 5590 (2014).
- <sup>341</sup>Y. Deng, Z. Luo, N. J. Conrad, H. Liu, Y. Gong, S. Najmaei, P. M. Ajayan, J. Lou, X. Xu, and P. D. Ye, *ACS Nano* **8**, 8292 (2014).
- <sup>342</sup>M. Massicotte, P. Schmidt, F. Vialla, K. G. Schädler, A. R. Planete, K. Watanabe, T. Taniguchi, K. J. Tielrooij, and F. H. L. Koppens, *Nat. Nanotechnol.* **11**, 42 (2016).
- <sup>343</sup>L. Britnell, R. M. Ribeiro, A. Eckmann, R. Jalil, B. D. Belle, A. Mishchenko, Y.-J. Kim, R. V. Gorbachev, T. Georgiou, S. V. Morozov, A. N. Grigorenko, A. K. Geim, C. Casiraghi, A. H. Castro Neto, and K. S. Novoselov, *Science* **340**, 1311 (2013).
- <sup>344</sup>W. J. Yu, Y. Liu, H. Zhou, A. Yin, Z. Li, Y. Huang, and X. Duan, *Nat. Nanotechnol.* **8**, 952 (2013).
- <sup>345</sup>W. J. Yu, Q. A. Vu, H. Oh, H. G. Nam, H. Zhou, S. Cha, J. Kim, A. Carvalho, M. Jeong, H. Choi, A. H. Castro Neto, Y. H. Lee, and X. Duan, *Nat. Commun.* **7**, 13278 (2016).
- <sup>346</sup>X. Li, M. Zhu, M. Du, Z. Lv, L. Zhang, Y. Li, Y. Yang, T. Yang, X. Li, K. Wang, H. Zhu, and Y. Fang, *Small* **12**, 595 (2016).
- <sup>347</sup>M. Zhu, L. Zhang, X. Li, Y. He, X. Li, F. Guo, X. Zang, K. Wang, D. Xie, X. Li, B. Wei, and H. Zhu, *J. Mater. Chem. A* **3**, 8133 (2015).
- <sup>348</sup>M. Zhu, X. Li, S. Chung, L. Zhao, X. Li, X. Zang, K. Wang, J. Wei, M. Zhong, K. Zhou, D. Xie, and H. Zhu, *Carbon* **84**, 138 (2015).
- <sup>349</sup>M. Zhu, X. Li, Y. Guo, X. Li, P. Sun, X. Zang, K. Wang, M. Zhong, D. Wu, and H. Zhu, *Nanoscale* **6**, 4909 (2014).
- <sup>350</sup>M. Zhu, X. Li, X. Li, X. Zang, Z. Zhen, D. Xie, Y. Fang, and H. Zhu, *J. Appl. Phys.* **119**, 124303 (2016).
- <sup>351</sup>X. An, F. Liu, Y. J. Jung, and S. Kar, *Nano Lett.* **13**, 909 (2013).
- <sup>352</sup>X. Wang, Z. Z. Cheng, K. Xu, H. K. Tsang, and J. Xu, *Nat. Photonics* **7**, 888 (2013).
- <sup>353</sup>I. Goykhman, U. Sassi, B. Desiatov, N. Mazurski, S. Milana, D. de Fazio, A. Eiden, J. Khurgin, J. Shappir, U. Levy, and A. C. Ferrari, *Nano Lett.* **16**, 3005 (2016).
- <sup>354</sup>M. Massicotte, P. Schmidt, F. Vialla, K. Watanabe, T. Taniguchi, K. J. Tielrooij, and F. H. L. Koppens, *Nat. Commun.* **7**, 12174 (2016).
- <sup>355</sup>J. F. Rodriguez-Nieva, M. S. Dresselhaus, and J. C. W. Song, *Nano Lett.* **16**, 6036 (2016).
- <sup>356</sup>R. Urcuyo, D. L. Duong, P. Sailer, M. Burghard, and K. Kern, *Nano Lett.* **16**, 6761 (2016).
- <sup>357</sup>L. Zhang, L. Fan, Z. Li, E. Shi, X. Li, H. Li, C. Ji, Y. Jia, J. Wei, K. Wang, H. Zhu, D. Wu, and A. Cao, *Nano Res.* **4**, 891 (2011).
- <sup>358</sup>X. Li, C. Li, H. Zhu, K. Wang, J. Wei, X. Li, E. Xu, Z. Li, S. Luo, Y. Lei, and D. Wu, *Chem. Commun.* **46**, 3502 (2010).
- <sup>359</sup>G. Fan, H. Zhu, K. Wang, J. Wei, X. Li, Q. Shu, N. Guo, and D. Wu, *ACS Appl. Mater. Interfaces* **3**, 721 (2011).
- <sup>360</sup>Y. Lin, X. Li, D. Xie, T. Feng, Y. Chen, R. Song, H. Tian, T. Ren, M. Zhong, K. Wang, and H. Zhu, *Energy Environ. Sci.* **6**, 108 (2013).
- <sup>361</sup>Y. Song, X. Li, C. Mackin, X. Zhang, W. Fang, T. Palacios, H. Zhu, and J. Kong, *Nano Lett.* **15**, 2104 (2015).
- <sup>362</sup>X. Miao, S. Tongay, M. K. Pettersen, K. Berke, A. G. Rinzler, B. R. Appleton, and A. F. Hebard, *Nano Lett.* **12**, 2745 (2012).
- <sup>363</sup>X. Li, D. Xie, H. Park, M. Zhu, T. H. Zeng, K. Wang, J. Wei, D. Wu, J. Kong, and H. Zhu, *Nanoscale* **5**, 1945 (2013).
- <sup>364</sup>Z. Kang, X. Tan, X. Li, T. Xiao, L. Zhang, J. Lao, X. Li, S. Cheng, D. Xie, and H. Zhu, *Phys. Chem. Chem. Phys.* **18**, 1992 (2016).
- <sup>365</sup>X. Li, X. Zang, X. Li, M. Zhu, Q. Chen, K. Wang, M. Zhong, J. Wei, D. Wu, and H. Zhu, *Adv. Energy Mater.* **4**, 1400224 (2014).
- <sup>366</sup>X. Li, D. Xie, H. Park, T. H. Zeng, K. Wang, J. Wei, M. Zhong, D. Wu, J. Kong, and H. Zhu, *Adv. Energy Mater.* **3**, 1029 (2013).
- <sup>367</sup>E. Shi, H. Li, L. Yang, L. Zhang, Z. Li, P. Li, Y. Shang, S. Wu, X. Li, J. Wei, K. Wang, H. Zhu, D. Wu, Y. Fang, and A. Cao, *Nano Lett.* **13**, 1776 (2013).
- <sup>368</sup>M. Furchi, A. Pospischil, F. Libisch, J. Burgdörfer, and T. Mueller, *Nano Lett.* **14**, 4785 (2014).
- <sup>369</sup>R. S. Sundaram, M. Engel, A. Lombardo, R. Krupke, A. C. Ferrari, P. Avouris, and M. Steiner, *Nano Lett.* **13**, 1416 (2013).
- <sup>370</sup>A. Pospischil, M. M. Furchi, and T. Mueller, *Nat. Nanotechnol.* **9**, 257 (2014).
- <sup>371</sup>J. S. Ross, P. Klement, A. M. Jones, N. J. Ghimire, J. Yan, D. G. Mandrus, T. Taniguchi, K. Watanabe, K. Kitamura, W. Yao, D. H. Cobden, and X. Xu, *Nat. Nanotechnol.* **9**, 268 (2014).
- <sup>372</sup>F. Withers, O. Del Pozo-Zamudio, A. Mishchenko, A. P. Rooney, A. Gholinia, K. Watanabe, T. Taniguchi, S. J. Haigh, A. K. Geim, A. I. Tartakovskii, and K. S. Novoselov, *Nat. Mater.* **14**, 301 (2015).
- <sup>373</sup>D. Li, R. Cheng, H. Zhou, C. Wang, A. Yin, Y. Chen, N. O. Weiss, Y. Huang, and X. Duan, *Nat. Commun.* **6**, 7509 (2015).
- <sup>374</sup>M. Koperski, K. Nogajewski, A. Arora, V. Cherkez, P. Mallet, J. Y. Veullien, J. Marcus, P. Kossacki, and M. Potemski, *Nat. Nanotechnol.* **10**, 503 (2015).
- <sup>375</sup>Y. He, C. Genevieve, R. SchaibleyJohn, Y. He, C. Cheng, W. Jia, D. Xing, Q. Zhang, W. Yao, X. Xu, C. Lu, and J. Pan, *Nat. Nanotechnol.* **10**, 497 (2015).
- <sup>376</sup>C. Palacios-Berraquero, M. Barbone, D. M. Kara, X. Chen, I. Goykhman, D. Yoon, A. K. Ott, J. Beitner, K. Watanabe, T. Taniguchi, A. C. Ferrari, and M. Atatüre, *Nat. Commun.* **7**, 12978 (2016).
- <sup>377</sup>S. Wu, S. Buckley, J. R. Schaibley, L. Feng, J. Yan, D. G. Mandrus, F. Hatami, W. Yao, J. Vuckovic, A. Majumdar, and X. Xu, *Nature* **520**, 69 (2015).
- <sup>378</sup>M. Liu, X. Yin, E. Ulin-Avila, B. Geng, T. Zentgraf, L. Ju, F. Wang, and X. Zhang, *Nature* **474**, 64 (2011).
- <sup>379</sup>J. Kim, H. Son, D. J. Cho, B. Geng, W. Regan, S. Shi, K. Kim, A. Zettl, Y. Shen, and F. Wang, *Nano Lett.* **12**, 5598 (2012).
- <sup>380</sup>A. Majumdar, J. Kim, J. Vuckovic, and F. Wang, *Nano Lett.* **13**, 515 (2013).
- <sup>381</sup>Z. Fang, Y. Wang, A. E. Schlather, Z. Liu, P. M. Ajayan, F. Javier García de Abajo, P. Nordlander, X. Zhu, and N. J. Halas, *Nano Lett.* **14**, 299 (2014).
- <sup>382</sup>S. Hosseini Mousavi, I. Kholmanov, K. B. Alici, D. Purtseladze, N. Arju, K. Tatar, D. Y. Fozdar, J. W. Suk, Y. Hao, A. B. Khanikaev, R. S. Ruoff, and G. Shvets, *Nano Lett.* **13**, 1111 (2013).
- <sup>383</sup>N. Dabidian, I. Kholmanov, A. B. Khanikaev, K. Tatar, S. Trendafilov, S. Hosseini Mousavi, C. Magnuson, R. S. Ruoff, and G. Shvets, *ACS Photonics* **2**, 216 (2015).
- <sup>384</sup>Y. Yao, R. Shankar, M. A. Kats, Y. Song, J. Kong, M. Loncar, and F. Capasso, *Nano Lett.* **14**, 6526 (2014).
- <sup>385</sup>O. Solgaard, F. Ho, J. I. Thackara, and D. M. Bloom, *Appl. Phys. Lett.* **61**, 2500 (1992).
- <sup>386</sup>C. Zeng, J. Guo, and X. Liu, *Appl. Phys. Lett.* **105**, 121103 (2014).
- <sup>387</sup>S. H. Lee, M. Choi, T. Kim, S. Lee, M. Liu, X. Yin, H. K. Choi, S. S. Lee, C. Choi, S. Choi, X. Zhang, and B. Min, *Nat. Mater.* **11**, 936 (2012).
- <sup>388</sup>B. Sensale-Rodriguez, R. Yan, M. Zhu, D. Jena, L. Liu, and H. Xing, *Appl. Phys. Lett.* **101**, 261115 (2012).
- <sup>389</sup>A. C. Ferrari *et al.*, *Nanoscale* **7**, 4598 (2015).
- <sup>390</sup>K. S. Novoselov, V. I. Fal'ko, L. Colombo, P. R. Gellert, M. G. Schwab, and K. Kim, *Nature* **490**, 192 (2012).